A Study of Kimberlitic Eclogites and Mafic Granulites from the Southern Adelaide Fold Belt

Geology Honours

David Segui

May, 2010

Abstract

A xenolith suite recovered from a Jurassic, diatreme facies kimberlite pipe located near Angaston is the subject of this thesis. This kimberlite is the southern-most occurrence in a province of xenolith-bearing kimberlites that intrudes the Adelaide Fold Belt (mainly as thin dykes), as far north as Port Augusta. The majority of the xenoliths, which range up ~5 kgs, are mafic garnet-clinopyroxene granulites, kyanite bearing granulites, kyanite bearing eclogites and amphibole bearing eclogites. Mineral assemblages include; gar-cpx-ky-rutile, gar-hb-cpx-ky and gar-cpx-plag. The use of garnet-clinopyroxene Fe-Mg exchange geothermometers and clinopyroxene site occupancy (Ganguly *et al.* 1998), together with the use of *THERMOCALC* (Powell *et al.* 1998) suggests the xenoliths span a pressure range between ~10 and 30 kbar with temperatures in the range 800 – 1020 ºC. These mafic granulites and eclogites are mildly silica under saturated mafic rocks with compositions dominated by normative olivine, plagioclase and clinopyroxene. They have SiO_2 contents between 40-50 wt% coupled with Mg# (calculated with total Fe) ranging from 0.4 up 0.85. They display positive correlations between Mg# vs. MgO, Fe_2O_3 (total), CaO, Al_2O_3, Cr, Sc and Ni and negative correlation between TiO_2, V and potentially incompatible trace elements Zr, Nb, Y and REE. Their composition and trends are like those of Neoproterozoic basalts that were erupted at rifts in SE Gondwana (including the Gairdner dykes and Wooltana basalts). In detail they share the closest similarities with late Neoproterozoic basalts from NW Tasmania and King Island. The xenoliths apparent magmatic trend is defined by plagioclase-pyroxene crystallisation suggesting initial intrusion at or close to the Moho. The Angaston xenoliths also share MORB-like initial $^{143}Nd/^{144}Nd$ isotopic compositions with the Tasmanian Basalts with an isochron-like array yielding a ~580 Ma age. Garnet-clinopyroxene pairs gave a well-defined Early Jurassic internal Sm-Nd isochron (~206Ma). This is interpreted as an eruption age. Two models are proposed for the formation of these eclogites. They may either be relicts of oceanic lithosphere subducted in the Cambrian, or they may be (perhaps more likely) the delaminated remains of Moho-depth mafic under plates intruded during Rodinian rift-drift and then delaminated at the end of the Delamerian Orogeny to become distributed amongst the mantle peridotite that subsequently cooled to form the present (and Jurassic) lithospheric mantle.

Table of Contents

1 Introduction

Kimberlites are volatile rich, highly potassic ultramafic rocks which originate deep in the mantle (> 150 km) and travel quickly to the surface (~4 - 20 m/s) (Sparks *et al.* 2006). The deep source of this volcanism coupled with high transport velocity leads the kimberlites to sample and transport xenoliths and xenocrysts from a wide range of usually inaccessible upper mantle and lower crustal rocks. This makes samples available for direct geological analysis complementing the normal indirect geophysical analysis. The rapid transport of the xenoliths also means they do not have time to re-equilibrate to lower pressure and temperature conditions thus freezing the mineral assemblages formed at their previous depths. Eclogite is one of the common xenolith types transported by kimberlite. Eclogite is a high pressure metamorphic rock generally of mafic bulk composition. They have garnet-clinopyroxene dominated mineralogy. Plagioclase is absent as they are formed about the albite-jadite transition pressure, but are known to sometimes contain; coesite (converted to quartz), ilmenite, rutile, sanidine, orthopyroxene, diamond, graphite, kyanite, corundum, apatite, zircon and sulphides (Haüy 1822, Coleman *et al.* 1965, Jacob 2004). Eclogites were also the first rocks recognised as diamond host rocks (Bonney 1899), thus extensive research over the years has been undertaken to better understand their nature and origins.

Kimberlitic eclogites are inferred to have experienced higher temperatures and pressures than eclogites occurring as layers or lenses within crustal migmatite gneissic terrains or those contained within glaucophane schist terrains (Coleman *et al.* 1965). These kimberlitic eclogites are referred to as HT/UHP eclogites Carswell (1990) which are characterised by having experienced T > 900 ºC which under ambient T conditions (40 mWm^{-2} continental geotherm), occurs at P > 36 kbar (115 km depth). These temperature estimates are determined through the exchange of Fe^{2+} – Mg between garnet – clinopyroxene pairs at set pressures, developed by Ellis and Green (1979) which was further refined by Krogh (1998) however geobarometry is a problem in eclogites because the simple bimineralic garnet - clinopyroxene assemblage does not provide pressure-sensitive exchange reactions (Ghent *et al.* 2004, Jacob 2004). However work carried out by Nimis (1995, 1998) and Nimis and Taylor (2000) have quantified for the pressure dependency of some site occupations in clinopyroxene, including Cr-substitution, providing a source of some pressure estimates.

The original protoliths to these xenolith eclogites are the source of debate. The clinopyroxene, garnet assemblage has a wide stability field and can form from a wide variety of initial bulk rock compositions, which Jacob (2004) states "this fact enough alone to show a single origin for all eclogites found in the Earth's mantle is not justified." There are 3 main theories for the origin of kimberlitic eclogites. Each of these probably occur:

1) A high pressure cumulate magmatic origin (mantle hypothesis)
2) Mafic-magmatic under-plating at the Moho forming gabbro which eventually cools, first into the garnet granulite field and then into the eclogite facies.
3) Oceanic crust subducted at a convergent margin and converted to eclogite.

The latter model is favoured by many authors based on the MORB-like geochemistry of some xenoliths and on their oxygen isotope compositions. Garnet trace element patterns which display flat HREE patterns along with positive Eu anomalies, combined with whole rock patterns that have positive Sr and Eu anomalies are used as evidence of the prograde metamorphic reaction from plagioclase to garnet (Jacob *et al.* 2003, Jacob 2004). According to Jacob (2004) mid ocean ridge basalts which crystallises at low pressures and hence is plagioclase-phyric thus providing a potential source for prograde garnet forming reactions. However, almost any tholeiitic basaltic magma will potentially crystallise plagioclase and a dry tholeiitic basalt magma will potentially crystallise it up to ~20 kbars (with clinopyroxene and garnet where P > ~15 kbar (Green 1982). The second line of evidence used is that provided by oxygen isotope compositions. Some eclogite xenoliths have low $\delta^{18}O$ values and these can these can only be caused close to the earth's surface by hydrothermal alteration, e.g. by hydrothermal circulation of seawater at mid ocean ridges. Many eclogites display variable $\delta^{18}O$ values with some lower than that of mantle $\delta^{18}O$ values (5.5 ± 0.4‰ (Mattey *et al.* 1994)) which they attribute to this hydrothermal alteration.

Within South Australia work has been carried out on the xenolith suites from south-eastern Australia which represents the Eastern Margin of the Australian Craton (EMAC) during the Proterozoic. Kimberlitic xenolith suites thus give insight into the geological history of the accretion of eastern Australia (Ferguson *et al.* 1979, McCulloch *et al.* 1982, Arculus *et al.* 1988, Pearson & O'Reilly 1991, Pearson *et al.* 1991).

The Angaston kimberlite is located in the southern part of the Adelaide Fold belt approximately 230 km southeast of the mid north kimberlite occurrences (Figure 1). These xenoliths include mafic granulites, kyanite granulites, kyanite eclogites and amphibole eclogites which are typical of those seen in the EMAC xenolith suite. These xenoliths represent the most southern sampling of the EMAC to date and offer the rare insight into the lower crust to unravel its secrets.

The aim of this thesis is to give initial petrological, geochemical (major, trace and radiogenic), thermal history and age data of the Angaston xenolith suite. Hand specimen and petrographical descriptions, major and trace element geochemistry's both on *in situ* minerals as well as whole rock samples was undertaken. This data is then used to estimate *P-T* conditions of metamorphism experienced by the xenoliths through a combination of conventional thermobarometry and calculated phase diagram analysis. Radiogenic (Sm/Nd) isotopic work was also undertaken on both whole rock and garnet-clinopyroxene mineral seperate samples to determine protolith formation ages aswell as the age of metamorphism. From this data models of how this xenolith suite could have formed are then proposed.

2 Geological Setting and Previous Work of the EMAC

2.1 Kimberlites of EMAC in South Australia

Kimberlites are located in the northern Flinders Ranges at Pt Augusta (El Alamein), Eurelia, Terowie (Calcutteroo and Pine Creek), Orroroo and in the Adelaide Hills which are both part of the Adelaide Fold Belt (Figure 1). They intrude the lower sequences of the Adelaidean sedimentary rocks (Burra and Umberatana Groups) which are or Proterozoic age (Colchester 1972, McCulloch *et al.* 1982). The mid north kimberlites are diamondiferous but contain below economic grades thus several studies have been undertaken investigating their nature and occurrence whereas little work has been carried out on the southern kimberlites due to their barren nature and more recent discovery (Tappert *et al.* 2009).

The EMAC xenolith suite ranges in composition from felspathoid rocks through to ultramafic xenoliths. The ultramafics xenoliths are garnet-spinel lherzolites which are interpreted to represent mantle wall rock to the kimberlite emplacement which imparts important information on the depth of the crust-mantle boundary (Cull *et al.* 1991, Pearson *et al.* 1991). Mafic xenoliths are reported as the dominant xenolith type from South Australian kimberlites (Cull *et al.* 1991, Pearson & O'Reilly 1991, Pearson *et al.* 1991) which range from nepheline through olivine-hypersphene through to quartz normative whole rock compositions (Ferguson *et al.* 1979, Pearson *et al.* 1991).

Within the mafic xenolith suite a wide range rock mineralogies are displayed consisting of garnet pyroxenites, various mafic granulites including two pyroxene (garnet absent), garnet two pyroxene and garnet-clinopyroxene granulites, kyanite bearing mafic granulites which are unique to the EMAC (Pearson *et al.* 1991), as well as eclogites. The minerals of these mafic xenoliths are found to share similar chemical characteristics regardless of their rock type. Garnets of the mafic xenoliths display a range of solid solutions of pyrope (prp), almandine (alm) and grossular (gr), with minor spessartine. The eclogites and garnet-clinopyroxene granulites plot towards higher almandine compositions whereas the kyanite bearing mafic granulites plot towards more pyropic compositions. Clinopyroxene is characterised by high diopside (Di) + hedenbergite (Hd), jadeite (Jd) + Tshermakite (Ts) and acmite (am) compositions. Coarse, equilibrated amphiboles have been described from many samples and are of hornblende-pargasite composition and micas range from phlogopite to biotite. Feldspars

compositions of equilibrated plagioclase grains range from An_{72-15} with orthoclase contents generally being low (<10 mole %) with some secondary potash feldspar (Or_{90-75}) being reported (Ferguson *et al.* 1979).

P-T estimates from these xenoliths display overlap between eclogite and granulite samples indicating that the conditions at which conversion takes place is controlled by the bulk rock compositions and not just *P-T* conditions (Pearson *et al.* 1991). These *P-T* estimates represent a vertical profile through the upper mantle and lower crust at the time of kimberlite emplacement and are used to construct palaeogeotherms. Work carried out by Pearson *et al.* (1991) on the EMAC xenolith suites calculated a curved palaeogeotherm (Figure 1) during the Jurassic of 150 ºC lower than the geotherm identified in South Eastern Australia (SEA) (O'Reilly & Griffin 1985) but is still 300 - 400 ºC hotter than a cratonic geotherm (40 mWm^{-2}). The SEA geotherm is also curved with the shape being attributed to magmatic under-plating of a basalt slab at a rate 900 m/Ma by Cull *et al.* (1991). A model determined by Griffin and O'Reilly (1987) predicts that the ambient geotherm will retain the curvature imposed upon it by advective heat transfer after 10 Ma of cooling from a SEA-type geotherm. So Pearson *et al.* (1991) state that the EMAC geotherm could represent a similar mechanism of magmatic under-plating but with lower rates of magma supply indicated by the lower temperature or that cooling has occurred from a SEA type geotherm. This indicates that the protoliths to the mafic xenoliths of South Australia are basaltic magmatic under plates.

Radiogenic isotopic work carried out on South Australian kimberlitic xenoliths has been undertaken by McCulloch *et al.* (1982) and Arculus *et al.* (1988). McCulloch *et al.* (1982) determined Sm-Nd and Sr-Rb whole rock compositions for garnet clinopyroxenite, garnet granulite and felsic garnetiferous gneiss xenoliths from the Calcutteroo kimberlite. These samples produced initial $^{143}Nd/^{144}Nd$ ratios of 0.5090 ± 4 which correspond to ε_{Nd} (T) =+4 ± 2 and initial $^{87}Sr/^{86}Sr$ ratios of 0.7062 ± 14 which gave dates of 2350 ± 400 Ma and 2470 ± 60 Ma respectively. They attributed these ages to a major chemical fractionation event which occurred within the crust due to the high initial isotope compositions which are greater than those representative within the mantle (McCulloch *et al.* 1982). Younger ages have been presented by Rudnick *et al.* (1986) who suggested ages of 1300 Ma for the mafic xenoliths, determined through the back calculation of Nd and Sr isotopic ratios to a time where they conform to a mixing curve on εNd vs. $^{87}Sr/^{86}Sr$ (Pearson *et al.* 1991).

The kimberlite of the mid north occurs as pipes (up to 6.35 Ha) and NW-NE trending dykes (mm - m thick, striking for 100 m's to km) that are heavily weathered and are Jurassic in age (164 – 174 Ma) (Stracke *et al.* 1979). The pipes contain a brecciated form of kimberlite containing variable numbers of xenoliths set in the clast supported matrix whereas the dykes possess a more massive nature (Colchester 1972). Colchester (1972) describes the kimberlite rock as having an olive green colour, containing serpentinised euhedral olivine phenocrysts (1 mm) which are psuedomorphed by chlorite and carbonate and have abundant micas with platy, phlogopite phenocrysts (up to 2 mm). These are set in a finer grained groundmass composed of phlogopite, magnesite, opaques and in some cases brown spinel and perovskite (Ferguson *et al.* 1979). Additional minerals found are chrome pyrope, picroilmenite and chrome diopside (Colchester 1972, Scott Smith *et al.* 1984). The xenoliths contained in the kimberlite pipes are a mixture of heterolithic country rock nodules as well as autolithic nodules ranging from ultramafics to felsic nodules derived from the lower crust and upper mantle (Colchester 1972, Ferguson *et al.* 1979).

2.2 Angaston Kimberlite

The Angaston kimberlite is located 7.5 km east-south east from the town of Angaston (80 km northeast of Adelaide), in the eastern part of the Adelaide Fold Belt (Figure 2). The rocks of the Adelaide Hills consist of metamorphosed Neoproterozoic Adelaidean sediments along with younger Cambrian sediments from the Kanmantoo trough (Howard 2003). The basement of the area consists of five Mesoproterozoic inliers (Houghton, Warren, Aldgate, Oakbank, Myponga) which are collectively known as the Barossa Complex (Drexel *et al.* 1993). These rocks were originally upper amphibolite facies metamorphics, possibly equivalent to those seen within the Gawler and Willyama Cratons but due to subsequent deformation during the Delamerian Orogeny have retrogressed to greenschist facies metamorphic rocks.

The Angaston kimberlite itself was discovered by Rio Tinto between 1995 - 1997 through drilling of a magnetic anomaly (Figure 3) located adjacent to a mineral catchment containing kimberlite indicator mineral (chrome diopside, pyrope garnets, chromite, picroilmenite). It gives a 2000 nT ground magnetic response and is approximately 150 m by 300 m large. Drilling core contained diatreme kimberlite facies (breccia facies) composed of phlogopite, red-orange pyrope garnet and serpentinised olivine with the core being cross cut by calcite veins (Howard

2003). This kimberlite was then trenched in 2005 by John Howard of then Flinders Diamonds Ltd with the first trench targeting the main body (MB) of the kimberlite as well as a smaller magnetic anomaly NW of the main body which was also kimberlite (AHT 34). Trenching revealed xenolith rich, brecciated diatreme facies which included eclogites with a 30 cm sample being sent away for thin sectioning (Howard 2005). Retrenching of the Angaston kimberlite in 2009 by Flinders Mines Ltd allowed the collection of 177 xenolith samples, 33 of which have been analysed as work undertaken for this study.

3 Petrography of the Angaston Xenolith Suite

3.1 The Angaston Xenolith Suite

A total of 177 mafic xenoliths were recovered from the Angaston kimberlite displaying a large range of hand specimen characteristics presented in Table 1 with all samples displaying variable external weathering. The xenolith suite is divided into 6 different classes based on their mineral assemblages including mafic granulite, kyanite granulite, kyanite eclogite, amphibole eclogite, amphibolites and carbonate rocks with their major and minor mineralogy's as well as their textures presented in Table 2. The amphibolites and carbonate rich rocks are not considered within this study.

3.2 Petrology

18 samples were thin sectioned, selected to represent the entire range of the Angaston xenolith suite and thus be used for petrological and analytical work. 540 µm thick thin sections were produced rather than the usual 230 µm to allow combined microprobe and LA-ICPMS analysis.

3.2.1 Granulites

They possess coarse to medium grained minerals forming equi-to sub granular interlocking textures. The clinopyroxene of the samples are large, subhedral dark green grains sharing straight boundaries with plagioclase and more curved boundaries with garnet. Plagioclase exists as large, elongate grains displaying twinning and surrounds the garnet of the sample (Figure 4). Garnets exist as subhedral dark red-orange grains possessing kelyphytic rims. Coarse grained subhedral rutile forms straight boundaries with garnet and smaller clinopyroxene grains but wavy boundaries with plagioclase. The rutile grains contain dark ilmenite exsolution lamellae, ilmenites dominant existence with respect to rutile; however in sample MB 2.6 ilmenite exist as coarse, black – dark brown anhedral grains (Figure 5) with small rutile inclusions of the pre-described nature. Hornblende inferred to have equilibrated with the mineral assemblages are coarse, dark brown– lighter brown grains (Figure 6) indicating they may by primary in origin through possible metasomatism occurring in the mantle (Appleyard *et al.* 2007).

Accessory minerals include quartz found in sample MB 2.9, existing as a medium (1 mm) rounded grain of blocky nature, and a single sample was found to contain fluoro-apatite (MB 1.5) existing as groups of small (<1 mm), rounded, opaque, interlocking grains of a white colour. Retrograde minerals include amphibole, biotite, zeolite, pumpellyite and carbonate with the retrogressive amphiboles occurring as smaller anhedral grains. Biotite occurs as larger (>.5 mm - 2 mm) xenomorphic grains displaying dark brown colours and a strong single cleavage, appearing to fill the gaps between garnet, clinopyroxene and plagioclase. Zeolite and pumpellyite exists as brown overprinting on the plagioclase and carbonate is present as cross cutting veins and around grain boundaries.

3.2.2 Kyanite Granulite

This xenolith is characterised by having a bimodal mineral size as well as a bimodal texture. The first texture occurs at either ends of the thin section where equigranular garnet-rich and clinopyroxene rich layering alternates. The grains are slightly larger than the fine grained central area. The central section has a bimodal nature consisting of a very fine grained matrix of angular mineral fragments, displaying extensive undulose extinction which surrounds larger mineral grains with corroded boundaries as well as remnant areas displaying the alternating bands of the garnet and clinopyroxene (Figure 7, 8). This fine-grained matrix is composed of kyanite, corundum and second-generation clinopyroxene and garnet. The coarse-grained minerals are plagioclase indicated through their display of twinning in thin section.

Spinel exists within the sample as small, translucent dark green meaning low (≤1 Fe_2O_3 wt%) iron, rounded, grains which only occurs included within garnet grains and appear only at the ends of the sample and not within the mylonitic zone. Black opaques occur at the joints between garnet and clinopyroxene as rounded blobs.

3.2.3 Kyanite Eclogites

These xenoliths are characterised by the presence of kyanite and clinopyroxene symplectites surrounding xenoblastic garnet grains (Figure 9), seperating coarse garnets from coarse first generation clinopyroxenes. The garnets and clinopyroxenes display very light colours under plane polarised light similar to the kyanite granulite sample. In areas away from symplectite growth, garnet grains possesses kelyphytic rims and shares equilibrated boundaries with

clinopyroxene forming granoblastic textures. One kyanite eclogite (34 5.2) sample displays complete re-equilibration with kyanite existing as porphyritic idioblasts (Figure 10), with only one small symplectite occurrence being found within the sample indicating a possible extended residence at higher pressure than the other samples. A darker blue kyanite also exists which was identified as Cr rich kyanite grains. All samples also contain sulphides and rutile occurring as miniscule (<.2 mm) interstitial blebs. Hornblende is observed in samples 34 1.5, 34 1.5, 34 5.2 occurring as medium, light yellow, idiomorphic grains which appear to share equilibration boundaries with garnet and clinopyroxene, therefore being interpreted as of primary origin (Figure 11). The retrograde minerals observed within the kyanite eclogites are biotite, clinozoisite, K-feldspar, sulphides and carbonates. The smallest sample 34 4.3 has experienced the highest observed alteration with fine grained retrogression minerals occurring over the entire assemblage.

3.2.4 Amphibole Eclogites

The garnets and clinopyroxenes have darker colours (Figure 12); similar to those of the granulites and form a sub-granular texture with coarse, light to dark brown, subhedral amphibole (Figure 13). Garnet grains possess kelyphytic rims. Rutile exists as coarse xenomorphic grains, occurring at the joints of clinopyroxene and garnet and contain coarse ilmenite exsolution similar to that displayed by the rutile grains in the granulite xenoliths. Plagioclase when present occurs as small, xenoblastic grains appearing to fill in spaces rather than dictate grain boundary placement. Retrograde minerals include fine grained amphibole overprinting and pumpellyite and mica formation Biotite also exists in 2 samples (MB 1.5 and 2.6) as platy xenomorphic grains forming straight boundaries against garnet and clinopyroxene. Carbonate within the samples is a strong indicator that these xenoliths have been influenced by the kimberlite magma during transport.

4 Methods

4.2 Sample Preparation

Whole rock and mineral separate preparation for radiogenic isotope and XRF work was carried out in the Mawson Laboratories at Adelaide University. This involved the removal of weathered and metasomatised surfaces from samples using a diamond saw to produce blocks ~ 5 - 7 cm^3. These blocks were then crushed to gravel in a stainless steel jaw crusher which was cleaned in-between each sample. These crushed samples were then divided into thirds ensuring each fraction contained representative amounts of both fine and coarse material. A third was set aside for future work/reference whereas the other 2/3 were then further processed for whole rock and isotope work. Samples selected for whole rock XRF work were then milled down to a fine powder in a tungsten carbide mill through 3 minutes of working.

Samples selected for mineral separation work were then crushed further in a small ceramic crusher and sieved to a size fraction between $100 \leq x \leq 425$ µm diameter. Fractions were then magnetically separated into garnet and clinopyroxene using a Franz separator with extensive cleaning occurring in between samples. Final hand separation using a microscope resulted in ~200 mg aliquots of pure garnet and clinopyroxene grain fragments that were free of inclusions, possessed a clear uniform colour and had fresh unaltered surfaces.

4.3 Major Element Geochemistry

Major, minor and trace element analysis was carried out *in situ* on mineral grains in the thin sections. Major and minor element results were collected on the Cameca SX 51 microprobe located at the University of Adelaide using a 5 µm focused beam produced by a 15 kV accelerating voltage and a 20 nA beam current. Calibration of the machine was carried out during and before analysis using Astimex Mineral Mount MINM25-53 standards with data being PAP corrected.

Whole rock major element analysis involved the production of fused glass disks for XRF work. 6 g of the sample powder was heated at 130 ºC for 4 hours to remove water from the sample. Samples were then transferred into ceramic crucibles and weighed in a Toledo balance before being ignited at 960 ºC for 3 hours. Loss on ignition was calculated. 1 g of this ignited powder was then mixed with 4 g of lithium borate flux and fused in Pt/Au crucibles and molds producing the fused disks. XRF Analysis was carried out on a Philips PW 1480 X-ray Fluorescence

Spectrometer running a dual-anode (Sc-Mo) X-ray tube, operating at 40 kV, 75 mA. The results were calculated using an analysis program calibrated against several international and local standards.

Total FeO was determined for 5 whole rock samples by Amdel using a procedure involving digestion of sample in HCl in the presence of CO_2 with the solution then being titrated using potassium di-chromate with BADS as an indicator.

4.4 Trace Element Geochemistry

In situ trace element data was obtained through laser ablation inductively coupled plasma mass spectrometry (LA-ICP-MS) located at Adelaide University using a New Wave UP213 laser ablation system coupled to an Agilent 7500cx ICPMS. The data was collected using an initial 40 s background trace measure with a further 60 s ablation measure. Ten standards in total were run before and after individual mineral analysis, consisting of eight NIST 612 and two NIST 614 analyses. The data was then processed through the program GLITTER with individual minerals being normalised using Ca electron microprobe data for garnets, clinopyroxene, amphibole and plagioclase and Ti electron microprobe data for rutile.

Whole rock trace element analysis was carried out on pressed pellets using the same XRF procedure as the major elements. Pressed pellets were made by mixing 6 g of whole rock powder with ~.8 mL of EtOH/PVA binder and compacted with a hydraulic press. Whole rock trace element analysis was also carried out by Amdel using a by dissolving 0.5 g powder in HF/multiple acids which is then analysed on an ICP-MS.

4.5 Radiogenic Isotope Geochemistry

Radiogenic isotope work was carried out on 6 mineral seperates, 5 whole rock powders, a standard (BCR2) and a blank initially being weighed and spiked into cleaned 15 mL Teflonware PFA vials using a Mettler Toledo AT201 balance. The samples were spiked using Nd-Sm spike F (calculated at the additions of 0.2 g Sm-Nd spike F per 1 µg Nd) at estimations of 4 ppm for the whole rocks and 10 ppm for the mineral seperates with the standard known to be 25 ppm spiked accordingly.

The samples are dissolved through a process involving 2 doses of HF, and a final dissolution in HCl with 7M HNO_3 being added at crucial stages to retard the formation of insoluble fluorides. Samples are then centrifuged and loaded onto Biorad Poly Prep seperating columns (2 mL AG50W X8 200 - 400 mesh Biorad cation exchange resin) for initial REE separation and then loaded onto the Sm-Nd seperating columns (2 mL Teflon powder impregnated with HDEHP) separating the Nd and Sm. Second dissolution involved the addition of 15M HNO3 along with ~2 mL .01 µg/g H_3BO_3 in 6M HCl with the samples being capped and boiled for 3 days after no aqua regia was observed. Ultra sounding was also undertaken in an attempt to ensure complete dissolution of samples.

Nd and Sm were subsequently dried and loaded onto double Re filaments for Thermal Ionisation Mass Spectrometer (TIMS) analysis. Nd and Sm analysis was carried out on a Finnigan MAT 262 TIMS at the University of Adelaide using dynamic measurement for $^{143}Nd/^{144}Nd$ and static measurement for $^{150}Nd/^{144}Nd$, $^{147}Sm/^{149}Sm$ and $^{152}Sm/^{149}Sm$. The blank contained <200 pg $^{150}Nd/^{144}Nd$ and <150 pg Sm. The international standard JNDi-1produced $^{144}Nd/^{143}Nd$ measurements of 0.512074 ± 27 (n=2) and the BCR2 basalt standard produced results of $^{144}Nd/^{143}Nd$ 0.512662 ± 41 (n=1). $^{143}Nd/^{144}Nd$ and $^{147}Sm/^{144}Nd$ values were calculated using depleted mantle values taken from Goldstein *et al.* (1984).

5 Major and Trace Mineral Geochemistry

Representative garnet and clinopyroxene analysis major and trace results are in Tables 3 to 6 respectively however due to time constraints not all samples were analysed for trace elements.

5.2 Garnet

The majority of garnet grains are homogeneous with few samples displaying chemical heterogeneity between rim and core analyses. Figure 14 displays the garnets plotted in the compositional triangle diagram based on the Fe, Mg and Ca end members of garnet. The kyanite bearing xenoliths plot towards the pyrope end member whereas the granulite and amphibole eclogites plot towards the almandine end member. There is also a positive correlation within the garnets of increasing Mg# and Cr2O3 wt% content (Figure 15) with the kyanite bearing samples having the highest values. Garnet trace element patterns display depleted LREE with flat to slightly curved HREE patterns. Garnet displays strong depletions in Ti and Sr and the alkali earths (Ce, K) coupled with positive Eu anomalies (Eu* 1.07 - 2.41), and strong U and Pb enrichments. Sample 34 5.0 displays an inverse pattern possessing much higher REE contents (Figures 16, 17, 18). Ti depletions are attributed to rutile being present in the samples (Barth *et al.* 2001) which takes up Ti in its crystal lattice but also has high positive partition coefficients for the high field strength elements (HFSE) of Nb, Ta, Zr and Hf (Jacob 2004).

5.3 Clinopyroxene

The clinopyroxenes were also found to be homogeneous having high Ca (diopside/hedenbergite) contents and similar Fe-Mg affinities as seen in garnets from the same xenolith types (Figure 14). No omphacite compositions were recorded in these xenoliths. A plot of jadeite vs. Mg# (Figure 19) displays a negative correlation indicating that the higher Mg# clinopyroxene samples have experienced higher pressures, due to fact that jadeite is converted to omphacite during prograde metamorphism (Deer *et al.* 1966). Trace element patterns display convex REE patterns of flat to slightly curved increasing LREE with the HREE displaying consistent depletion with increasing incompatibility. They also posses positive Eu* (1.1 - 2.8) and positive Sr*, coupled with variable enriched/depleted LREE Nd (Nd* .01 - 22) as well as variable U, Pb, Ti and P enrichment/depletion (Figures 20, 21, 22).

5.4 Other minerals

The majority of plagioclase compositions fall between albite and anorthite compositions with only a single analyses recording higher orthoclase content (Figure 23). The majority of amphiboles analysed of the Angaston xenolith suite plot as pargasite with a few samples straddling hornblende, edinite compositions (Figure 24) The ilmenites of the samples contain minor geikielite ($MgTiO_2$) compositions being recorded (~1 - 3wt%).

6 Whole rock Geochemistry of the Angaston xenolith Suite

The whole rock data results were determined through a combination of work carried out at Adelaide University (XRF major and trace) and by Amdel laboratories (ICP-MS trace) (see methods for description of analytical procedures) with both datasets being combined and presented as major elements in Tables 7 and 8, and as trace elements in Tables 9 and 10. The whole rock data is presented as spidergrams generated through Geoplot (Zhou & Li 2006) (normalised using Sun and McDonough (1989) values), and Harker and modified Harker diagrams through IgPet (Carr 2002) to display the geochemical nature of the Angaston xenolith suite. The Angaston xenolith data (red circles) has been plotted along with South Australian Adelaidean and Cambrian Basalts (Gairdner dykes and Wooltana basalts) (grey crosses) and Tasmanian Neoproterozoic Basalts (King Island Basalts) (blue circles) with Tasmanian olivine + orthopyroxene rich cumulates (black stars) (J. Foden unpubl. data).

The Angaston xenolith suite is composed of mafic rocks (eclogites and mafic granulites). They are mildly silica under saturated with bulk rock compositions being dominated by normative olivine, plagioclase and clinopyroxene. They have SiO_2 contents between 40-50 wt% coupled with Mg# (calculated with total Fe) ranging from 0.4 up 0.85. The suite has Al_2O_3 values ranging for 14 - 21 Wt%. Variations in MgO, Fe_2O_3 (total), CaO, Al_2O_3, Cr, Sc and Ni all show positive correlation with Mg#. TiO_2, V and potentially incompatible trace elements such as Zr, Nb, Y and REE all show negative correlations with Mg#. Their trace element patterns are characterised by wavy LREE patterns showing variable depletion and enrichment coupled with flat HREE patterns (Figures 25 to 28). All samples display positive Sr and Eu anomalies along with huge alkali earth enrichments and positive U and Pb anomalies (except for sample 34 5.0 U 200 ppm).This is coupled with Nb depletions.

Overall the major element trends suggest that the suite is potentially co-magmatic, controlled by the fractionation and accumulation of olivine - clinopyroxene – plagioclase (Figure 29, 30). The positive correlation between Al_2O_3 and MgO implies that plagioclase together with Fe-Mg silicates are involved in the entire suite protoliths (Figure 31). Positive Sr and Eu whole rock anomalies also support this interpretation (Figure 25 to 28). The most magnesian, apparently cumulative rocks are also the most aluminous. The strong depletion of Cr, Ni and Sc with decreasing Mg# also implies the role of olivine and clinopyroxene within the protolith mineral assemblage (Figures 32, 33). The low negative correlation between TiO_2 and Mg# (Figure 34)

indicates that little crustal contamination has occurred (34 5.0 exception?). There is no apparent control of garnet. Therefore an important conclusion drawn here is that in spite of the widely varying metamorphic mineralogy of the rocks seen today, the whole suite seems to have common igneous protoliths forming within the plagioclase stability field. This would imply pressures less than ~20 kbar in garnet absent crystallisation (Green 1982). As is illustrated in Figures 35 and 36, there is no apparent correlation between the apparent pressure of metamorphism of individual samples and its position in the igneous differentiation trend.

6.1 Secondary Geochemical Influences

The huge alkali concentrations (Ba_N ranging between 100 to 500 times mantle concentrations, Figures 30 to 33) are attributed to a second-order process representing the influence of the kimberlite magma interacting with the samples during their transport to the surface. Kimberlite magma is enriched in highly incompatible LREE's (Ba, Cs, Nb, La, Ce, U, Th)(Jacob 2004). Several other studies report that passing metasomatic fluids/partial peridotite melts associated with kimberlite emplacement can also increase the incompatible LREE concentrations of xenoliths (Zinder & Jagoutz 1988, Ireland *et al.* 1994). Work carried out by Barth *et al.* (2001) displayed that the differences between measured and reconstructed whole rock could be accounted for by an addition of ~5 - 10% kimberlite.

7 Thermobarometry

P-T work carried out on the Angaston xenolith suite involved the calculation of a pseudosection and individual *P-T estimations* using geothermometers/barometers. The pseudosection was calculated using the program THERMOCALC (Powell *et al.* 1998) using sample 34 1.5 whole rock XRF data combined with total Fe^{3+} data, determined by Fe_2O_3Tot (XRF) – FeO (Amdel) (see methods for FeO analysis procedure). Sample 34 1.5 is a kyanite eclogite sample composed of the mineral assemblage garnet, clinopyroxene, kyanite, hornblende, rutile (Figures 9 and 11) with textures dominated by kyanite + clinopyroxene symplectites forming around coarse xenomorphic garnets. The kyanite eclogite clinopyroxene compositions are characterised by diopside not omphacite.

The pseudosection (Figure 37) displays the calculated boundaries of mineral stability and assemblages that can occur for the composition of sample 34 1.5. Two major mineral transitions are displayed in the diagram with: 1) the transformation of plagioclase into kyanite as pressure increases; and 2) the conversion of hornblende to fluid and finally quartz as temperature increases. The actual mineral stability field for 34 1.5 is the field which corresponds to its current mineral assemblage, being the "g cpx ky hb ru fl" stability field ('1' on Figure 34). Due to the broad range of pressures and temperatures over which this field spans it does not give an exact *P-T* estimate.

Individual xenolith temperature estimates were generated using the Ellis and Green (1979) and the Krogh (1998) Fe-Mg garnet-clinopyroxene thermometers. These temperatures were calculated using P estimates determined by the Nimis (1995) clinopyroxene barometer. Averaged microprobe data of adjacent garnet and clinopyroxene grains with all Fe assumed to be Fe^{2+} was used in the calculations (Figures 35, 36). The assumption of no Fe^{3+} within the samples results in lower temperature estimates by the Ellis and Green (1979) thermometer which are generally still higher the Krogh (1998) thermometer except at greater pressures. The range of temperatures and pressures produced are presented in Table 11 with most displaying small ranges in values except for the lower temperature samples which generally have larger T ranges. The fact that the T estimations fall within tight ranges despite being generated from separate P estimates using a separate barometer indicates that these samples are likely to reflect the actual conditions of metamorphism experienced by the rocks. This is further supported by the fact that the estimated *P-T* range of sample 34 1.5 falls largely within the low

P-high T area of its mineral stability field (range displayed on Figure 34) thus providing further evidence the individual *P-T* estimates are valid.

A comparison of the average compositions of garnet and clinopyroxene used in the geothermometery calculations is displayed in Figures 35 and 36. Figure 36 is individual plots of the garnet and clinopyroxene compositions used in the calculation of pressure and temperature. Note that some display crossed lines indicating that some of the xenoliths still poses compositional remnants of the higher temperature conditions with one individual sample T ranges up to 300 ºC (34 5.1 on Figure 36). Figure 35 displays the nature of the geothermometer where increasing Mg correlates to higher temperature estimates.

The samples display an overall range between 11 to 30 kbar and between 800 to 1130 ºC (Table 11) with the samples showing no correlation of xenolith type with a specific *P-T* area indicating composition of the whole rock controlled metamorphism more so than *P-T* conditions. This data is then plotted in Figure 38 along with other kimberlite xenolith *P-T* data from EMAC xenoliths (Pearson *et al.* 1991) (red squares) and Monk's Hill kimberlite to the east of Peterborough (J Foden unpubl. data) (red circles). The Angaston *P-T* estimates fall in-between the two plotted data sets with the majority of the samples recording higher P/lower T than the EMAC data and similar T at lower P when compared to the Monks Hill data, appearing to align more so with the Monks Hill data than the EMAC data.

8 Radiogenic Isotopes of the Angaston Xenoliths

Sm-Nd work was carried out to determine relative ages of the xenolith samples as well as determine their radiogenic compositions. Samples 34 3.2 (amphibole eclogite), 34 5.2 (kyanite eclogite) and MB 2.9 (granulite) were chosen as representative samples for combined mineral seperate and whole rock work, with samples 34 4.9 (amphibolite) and MB 2.4 (kyanite eclogite) selected for whole rock work. The combined mineral separate and whole rock samples were selected to represent the three main xenolith groups. The samples were prepared and analysed using the techniques described in the methods section however several mineral seperates failed initial analysis and were found to contain significant mineral residue. The samples were subsequently re-dissolved and reanalysed. Sample MB 2.9 CP was spilt during separation but subsequent analysis has revealed concordant $^{143}Nd/^{144}Nd$ values with the rest of the analysed samples. All Sm-Nd data is recorded in Table 12.

The majority of the analysed samples (whole rock and mineral seperate) results display a tight range in negative $^{147}Sm/^{144}Nd$ ratios coupled with the high $^{143}Nd/^{144}Nd$ ratios when compared to bulk earth $^{143}Nd/^{144}Nd = 0.51265$ (Philpotts & Ague 2009). Garnet $^{143}Nd/^{144}Nd$ is higher than its coexisting clinopyroxene relating to the higher Sm/Nd of garnet. The majority of samples also display positive εNd values. These two facts indicate a possible mantle source for the Angaston xenoliths.

The isochrons plotted with Isoplot 3.6 (Ludwig 2008) give two different ages when the whole rock and mineral data are considered separately. The isochrons calculated from the five whole rock samples and 6 mineral seperates have large errors and require further radiogenic work on more samples to reduce these errors. The whole rock isochron gives an age of Late Neoproterozoic (568 ± 230 Ma) whereas the mineral separates report an Early Jurassic age (206 ± 44 Ma). When the Angaston data is plotted with Sm-Nd data from the Tasmanian basalts used in the WR geochemistry section it is found they both possess similar isotopic compositions. They have positive εNd values, and, interestingly, the initial εNd values are the same with both displaying MORB isotopic ratios at 580 Ma (Figure 39). This probably indicates they have come from a similar source within the mantle during the Late Neoproterozoic (isochron gives 594 ± 71 Ma (Figure 40)). The Angaston samples also display little crustal contamination as indicated by Figure 39 which plots the Sm/Nd ratios from Cambrian Kanmantoo sediments as blue diamonds. The line has 5% crustal increments plotted on it with

the Angaston samples plotting at the 0% end of the line. This lack of crustal contamination possibly indicates the Angaston xenoliths did not penetrate the crust which would indicate a deeper origin for cooling.

The Early Jurassic ages recorded in the mineral seperates isochron of 206 ± 44 Ma (Figure 41) probably represents the time when the minerals of the rocks cooled below the closure temperatue (T_c) of Sm-Nd diffusion into garnet and clinopyroxene. The exact temperature at which this happens is highly debated ranging from <500 ºC to above 800 ºC (Mezger *et al.* 1992, Hensen & Zhou 1995, Dutch & Hand 2010) and is influenced by a number of other variables.

9 Discussion

The aim of this study is to gain insight into the origins and history of the mafic xenoliths from the Angaston kimberlite. This study represents the first investigation of a xenolith suite from this part of the Adelaide Fold Belt. The geoanalytical work undertaken in this study gives an insight to the possible protoliths and origins of the rocks existing at this depth on which no previous information exists. This section interprets and discusses the dataset compiled on the Angaston xenoliths through this study. The nature and possible origins of the xenoliths are discussed which leads into theories of their initial formation and subsequent metamorphism and final exhumation within the erupting kimberlite.

9.1 Protolith

The whole rock ages determined for the Angaston xenoliths when plotted with Tasmanian basalt samples give Late Neoproterozoic ages. As can be seen in the Harker diagrams (Figures 29 to 34) the Angaston xenoliths have similar whole rock compositions and follow a similar trend as other mafic rocks in South Australia (Gairdner dykes and Wooltana basalts) and Tasmania. The Angaston xenoliths display a continuous range of results with a small group consistently plotting at very high Mg#, Ni and Cr values (Figures 32 to 34) coupled with low incompatible element concentrations which could possibly be early cumulates (Wilson 1989) from partial melting of a olivine rich mantle rock. The remainder of the samples fall on a trend of increasing incompatible elements (Y and TiO_2) with decreasing Mg#, Ni and Cr which could represent the residual melts from the mantle source. This could indicate that the xenoliths are possibly part of a co-magmatic suite representing cumulates and residual melts from the partial melting of an olivine rich, mantle source rock.

Figures 29 to 31 appear to indicate that the initial mineral assemblage controlling crystallisation within the Angaston protolith rocks was being controlled by plagioclase, clinopyroxene and olivine without orthopyroxene. In Figures 29 to 31, the trend of the Angaston xenoliths appear to plot away from olivine and orthopyroxene controlled crystallisation rather more towards plagioclase and clinopyroxene controlled crystallisation. The Angaston xenolith suite whole rock REE data displays positive Sr and Eu anomalies and flat HREE patterns (Figures 25 to 28). The presence of positive Sr and Eu anomalies provides strong evidence for the crystallisation of plagioclase (Jacob *et al.* 2003, Jacob 2004) and flat whole rock HREE patterns may indicate the lack of garnet as a controlling mineral of crystallisation.

So it appears that plagioclase along with clinopyroxene in the absence of garnet and orthopyroxene was part of the initial mineralogy controlling crystallisation. Olivine would also have to be part of this initial mineralogy as it is one of the dominant minerals within the mantle and these protoliths are inferred to represent a co-magmatic suite possibly originating from the partial melting of mantle rock.

The fact that plagioclase appears to be present as one of the initial controlling minerals of crystallisation indicates the Angaston protoliths formed at shallow depths. As stated earlier almost any tholeiitic basaltic magma will potentially crystallise plagioclase and a dry tholeiitic basalt magma will potentially crystallise it up to ~20 kbars (with clinopyroxene and garnet where P > ~15kbar (Green 1982). 10 - 20 kbar is equivalent to a depth of 30-60 km, corresponding to the stable Moho for continental crust (Wilson 1989). The Angaston whole rock data combined with that of the Tasmanian basalt data appears to fall on a similar line which forms an isochron of 594 ± 71 Ma age (Figure 40) indicating that the Angaston protoliths probably formed during the Late Neoproterozoic. The fact that both the Angaston xenoliths and the Tasmanian basalts both have initial or primitive εNd values of MORB at 580 Ma may possibly infer that both samples came from a similar source. The fact that they both share a similar age and similar primitive εNd composition could infer they originated from the same tectonic event.

9.2 Metamorphism

Due to the fact that the Angaston xenolith suite is made up of mafic granulites and eclogites and not plagioclase bearing igneous rocks indicates that the xenoliths have experienced subsequent metamorphism. The individual *P-T* estimates generated through thermobarometry ranges from the Angaston xenoliths indicates they experienced pressures ranging from 11 - 30 kbar and temperatures from 800 - 1130 ºC. These values are then plotted in Figure 38 along with other kimberlite xenolith *P-T* data from EMAC xenoliths (Pearson *et al.* 1991) (red squares) and Monks Hill kimberlite xenoliths (Eurelia, South Australia) (J Foden unpubl. data) (red circles).

The EMAC xenolith suite are dated at ~1300 Ma (Rudnick *et al.* 1986) with their *P-T* estimates described as recording a palaeogeotherm which is 300 – 400 ºC hotter than a stable cratonic geotherm (40 mWm^{-2}) and displays a curved nature which is similar to the geotherm identified

in South Eastern Australia (SEA) (O'Reilly & Griffin 1985). The curve of the SEA geotherm is attributed to magmatic under-plating of a basalt slab at a rate 900 m/Ma (Cull *et al.* 1991). A model determined by Griffin and O'Reilly (1987) predicts that the ambient geotherm will retain the curvature imposed upon it by advective heat transfer after 10 Ma of cooling from a SEA-type geotherm. The Monks Hill samples are believed to record *T-P* conditions associated with cooling along an elevated cratonic geotherm displaying re-equilibration after increased *P-T* conditions possible caused by lithospheric delamination. This elevation of *P-T* conditions would have caused the samples to re-equilibrate and form new stable mineral assemblages. Once the area cooled the geotherms would relax to lower temperatures causing a new mineral assemblage to form as the rocks re-equilibrate to lower temperatures at similar pressures. Partial re-equilibration from higher *P-T* conditions associated with possible lithospheric delamination; to lower temperature/similar pressure post deformation conditions is suggested as to what the Angaston xenolith suite could be recording (Figure 42). Possible evidence of this is indicated through the Angaston xenoliths partially re-equilibrated petrological textures (e.g. symplectites and sub-granular grain boundaries) and in the large temperature ranges recorded by the lower pressure samples.

An age of 206 ± 44 Ma is given by the Sm-Nd isochron plotted for the mineral seperates however this age may not report the age of peak metamorphism experienced by the rocks but rather the age at which the minerals cooled through the Sm-Nd closure temperature (T_c). The determination of a T_c for any chemical system or mineral is critically dependent on a number of variables writes Dutch & Hand (2010) including grain size, cooling rates, peak temperature and the diffusion properties of species in garnet (Hensen & Zhou 1995, Ganguly *et al.* 1998, Zhang *et al.* 2001). In high pressure rocks such as eclogites the temperature may not be higher than the Sm-Nd T_c thus the minerals will not record that metamorphic event. Mezger *et al.* (1992) postulated that the bi-mineralic nature of eclogite may cause diffusion of Sm-Nd to be limited due to clinopyroxene possessing a higher Sm T_c (800 ºC) in slowly cooling rocks, thus closing diffusion to garnet at higher temperatures giving an age related to peak metamorphism if period of metamorphism is substantial, rather than a cooling age. Work carried out by van Orman *et al.* (2001, 2002) looked into the REE diffusion trends between high Ca clinopyroxene and pyrope garnet and found that at temperatures less than ~1500 ºC, Ca-rich clinopyroxenes controlled the exchange of Nd between minerals of the rock, including pyrope garnet. Thus diffusion would be controlled by clinopyroxene Sm T_c at 800 ºC suggested by Mezger *et al.* (1992). Work carried out by Dutch & Hand (2010) displayed that garnets of larger grain size (>8

mm) within an anhydrous, low-strain granite (Sir Isaac), accurately recorded age of formation after experiencing metamorphism at 750 ± 35 ºC at 10 kbar (Dutch *et al.* 2008) whereas the smaller garnets (7 to 2.5 mm) recorded progressively reset Sm-Nd ages of 35 to 100 Ma respectively. From this study not only is the importance of the garnet grain size highlighted but also that the garnets still retainined their Sm-Nd formation isotopic compositions despite experiencing metamorphic temperatures around ~750 ºC.

Most kimberlitic xenoliths however, usually reside at depths where the temperature is greater than 750 to 800 ºC (~T_c) thus once they are emplaced on the surface by kimberlite eruption and subsequently cool, the minerals will record the age of eruption rather than previous metamorphic events. In the case of the Angaston xenoliths this Early Jurassic age overlaps within error of the other ages given by South Australian kimberlites (167 - 179 Ma) (Stracke *et al.* 1979). Dating carried out by Ralf Tappert on the Angaston kimberlite also produced Jurassic ages (J. Foden unpubli. data). Thus the age recorded by the mineral seperates is believed to be age of eruption rather than the peak metamorphic conditions experienced during possible lithospheric delamination.

9.3 Models of Formation

I suggest that this sequence of events could have happened in two ways using models 2 (magmatic underplating) and 3 (subduction of MORB followed by slab rollback) given in the introduction.

Evidence to support model 2 is that the Angaston mafic xenolith suite appears to have similar isotopic characteristics and a similar age of formation as the Tasmanian Basalts, indicating that the two rock samples may have evolved from a similar tectonic event. The mechanism proposed for the formation of the Tasmanian basalts is a volcanic passive margin occurring in the SE of Gondwana in the Late Neoproterozoic (Direen & Crawford 2003, Meffre *et al.* 2004). These basalts are part of a larger sequence termed a seaward dipping reflector sequence which occur parallel to continent-ocean boundaries and overly highly thinned, normal faulted continental crust (Symonds *et al.* 1998). These sequences are strong indicators' of an active rift setting immediately prior to continental break-up writes Meffre (2004) thus the area was experiencing passive rifting at the time, thinning the crust which allows the primitive asthenosphere to up well and melt, possibly forming partial melts. These partial melts could then undergo further fractionation to form a co-magmatic suite composed of cumulate rocks

possessing high Mg#, Ni, Cr concentrations; and residual melt rocks possessing decreasing Mg# and increasing TiO_2 and Y concentrations. This co-magmatic suite could have then crystallised at shallow depths indicated by plagioclase appearing to be present as an initial mineral controlling crystallisation. As stated earlier plagioclase is stable between 10 - 20 kbar (30 - 60km) which is equivalent to the stable Moho beneath continental crust. Thus it is possible that this co-magmatic suite pooled at the Moho, forming magmatic under plates which over time could have cooled through the eclogite facies. A fact that supports this possible conclusion is displayed in the Angaston xenolith radiogenic compositions which appear to not have been influenced by crustal contamination thus providing possible evidence for a deep origin of cooling (Figure 39).

If the co-magmatic suite did cool through the eclogite facies and metamorphose into eclogites then the possible magmatic underplates which they were part of would have increased in density. This increase in density makes the magmatic underplates (lower lithosphere) heavier than the asthenosphere below which could allow possible delamination to occur. This possible delamination would result in the Angaston xenoliths experiencing initially higher pressures and then higher temperatures as the magmatic underplates descended into the asthenospheric mantle causing metamorphism to occur. The xenoliths from the Monks Hill kimberlite appear to record an elevated conductive geotherm which could have resulted from possible lithospheric delamination. The Angaston xenoliths *P-T* estimates could be recording palaeogeotherms relaxing back from high temperature conditions associated with this possible lithospheric delamination. Other evidence for possible delamination is seen in the rapid termination of the Delamerian Orogeny. For 24 Ma the Delamerian Orogeny was a compressional setting which formed the Adelaide Hills but rapidly terminated at the end of the Cambrian and became an extensional setting. This rapid termination and transformation from a compressional to extensional setting, coupled with the fact the area experienced post-tectonic uplift is used as evidence to support the exhumation being buoyancy driven and thus indicating possible delamination (Foden *et al.* 2006).

Thus metamorphism of the Angaston xenoliths is achieved are subsequently emplaced in the kimberlite and transported to the surface most likely during the Jurassic. However Foden *et al.* (2006) contributed this delamination as slab rollback of a subducted oceanic slab which had reached the middle mantle transition zone (650km) which leads into the second possible model of formation proposed for the Angaston xenolith suite.

A similar co-magmatic protolith rock suite could have formed at a mid ocean ridge and then subsequently been subducted as proposed by Foden *et al.* (2006). This subduction would have caused similar metamorphism as discussed in the magmatic underplates model forming dense eclogite but instead this time the high pressure and then high temperature metamorphism is attributed to slab roll back rather than lithospheric delamination. This model would predict much higher *P-T* conditions to be experienced by the oceanic slab (Angaston protoliths) than is seen today (e.g. >>than 11 - 30 kbar and 800 - 1130 ºC); due to slab rollback occurring after the slab has lost its negative buoyancy having reached the middle mantle transition zone (650 km!). It is possible that the Angaston xenoliths no longer record these high *P-T* conditions of metamorphism due to overprinting of lower *P-T* metamorphism through post-tectonic events. These xenoliths could then be entrained within the kimberlite and erupted. Oxygen and Sr isotope analysis of the Angaston xenolith suite would give a definitive answer to the origins of these xenoliths.

10 Conclusion

The aim of this thesis was to gain insight into the nature and possible origins of the Angaston kimberlite xenolith suite. The Angaston xenolith suite is dominantly composed of mafic rocks consisting of granulite and eclogite xenoliths. The mafic xenolith samples were subdivided on the basis of their present mineralogy into garnet-clinopyroxene granulites (granulite) and kyanite bearing granulites; and kyanite bearing eclogites and amphibole bearing eclogites. They displayed textures indicative of partial re-equilibration (symplectites and sub-granular grain boundaries).

Through whole rock major and trace element work several lines of evidence appear to exist for the presence of plagioclase along with clinopyroxene and olivine in the initial mineral assemblage controlling crystallisation of the Angaston xenolith protoliths. Whole rock Harker diagrams appear to display trends away from olivine and orthopyroxene controlled crystallisation and more so towards plagioclase and clinopyroxene controlled crystallisation. This coupled with whole rock spidergrams displaying positive Sr and Eu along with flat HREE infers that crystallisation probably involved plagioclase without garnet. The fact that olivine is the dominant mineralogy of the mantle indicates it was probably part of the initial mineralogy controlling crystallisation, along with clinopyroxene and plagioclase; but probably not garnet or orthopyroxene.

It also appears that the Angaston xenolith suite could be a co-magmatic suite composed of cumulate and residual melt rocks formed from the partial melting of an olivine rich source. This is inferred through the whole rock diagrams where the Angaston xenoliths appear to fall in a continuous trend ranging from possible cumulative rocks possessing high Mg#, high compatible/low incompatible concentrations through to possible residual melt samples displaying decreasing Mg#/ compatible elements and increasing incompatible elements.

The Angaston xenolith suite appears to have similar Sm-Nd compositions as those displayed by the Tasmanian basalts used in the WR geochemistry section. Both have positive εNd values, and, interestingly, the initial εNd values are the same with both displaying MORB isotopic ratios at 580 Ma. This probably indicates they have come from a similar source within the mantle during the Late Neoproterozoic (isochron gives 594 ± 71 Ma (Figure 39))

The Angaston xenoliths experienced subsequent metamorphism with their minerals recording pressures from 11-30 kbar and temperatures between 800 -1130 ºC and is thought to be the result of lithospheric delamination, as recorded by the xenoliths at Monks Hill. The exact age of this metamorphism is not recorded in the samples due to the mineral seperates isochron age of 206 ± 44 Ma believed to record the age at which the samples cooled below the Sm-Nd closure temperature. It has been suggested that this metamorphism might be related to the termination of the Delamerian Orogeny.

Two possible theories have been put forward as to how these xenoliths could have been formed. The first suggests that these protolith rocks possibly formed at a passive rift margin present in the Late Neoproterozoic responsible for the formation of the Tasmanian Basalts. The Angaston xenoliths could have possibly formed as magmatic under plates at Moho depths within the plagioclase stability field. As cooling occurred the rocks could have initially formed eclogite, which would cause an increase in the density and possibly result in the delamination of the magmatic underplates (lithosphere) from the lower crust. This would result in the magmatic underplates experiencing high pressure followed by high temperature metamorphism. This would eventually cool to form a thickened lithosphere with the xenoliths rocks possibly cooling along the prevailing geotherms forming granulite and eclogite assemblages before being entrained within the kimberlite and emplaced on the surface, probably during the Jurassic.

The second theory suggests that these rocks possibly formed at a mid ocean ridge which could have undergone subduction during the Delamerian. This possible subduction would cause low temperature/high pressure metamorphism of the plagioclase protoliths and form eclogites. This oceanic crust could delaminate through possible slab rollback processes due to a loss of negative buoyancy once the slab reaches the middle mantle (650 km). This would then plunge the lower lithospheric column into the upper mantle and cause high pressure and eventually high temperature metamorphism to occur. It would be expected to see higher *P-T* conditions under possible middle mantle depths proposed through this model however the present *P-T* conditions recorded by the Angaston xenoliths could be lower grade metamorphic overprinting.

Further work that can be carried out on the Angaston xenolith suite includes:

- Sr and oxygen isotope work to reveal origins of formation and to give better ages of the Angaston xenoliths by themselves.
- Further Sm-Nd work undertaken on whole rock and mineral seperate samples to reduce the errors associated with dates.
- Further THERMOCALC work to be carried out on the xenoliths which have experienced medium and low temperature metamorphism to better constrain the metamorphic pathway.
- Further investigation into the xenolith displaying contrary REE natures to see if they are from the same xenolith population or a represent a different source (i.e. 34 5.0)

11 Acknowledgments

I would like to thank Flinders Mines who supplied the funding for retrenching of the Angaston kimberlite as well as the land owner Mr John Angas for allowing us to carry out the excavation. In particular I would like to thank Lachlan Cole and Tracey Scroop from Flinders Mines who provided assistance with the trenching and subsequent maps provided in the text. I have also received an extensive amount of help from several different people during my analytical work that I would like to thank. From Adelaide Microscopy I thank Angus Netting and Ben Wade for advice and assistance during and after my time on the microprobe, LA-ICP-MS and XL20.

I would also like to thank Dave Kelsey for sharing his extensive knowledge of THERMOCALC and helping me to plot my pseudosection as well as Alec Walsh for helping me with my numerous THERMOCALC problems, and Martin Hand for giving advice on my microprobe data and thin section identification. I'd like to thank John Stanley and David Bruce for their extensive help throughout the preparation, analysis and subsequent questions involved with my XRF and radiogenic isotope work, as well as Justin Payne for his demonstration and assistance of sample preparation.

The 2010 honours geology group for the good times and my close friends at Aquinas for also supporting me throughout the year with special thanks going to Paolo Sossi for his frequent advice and help with my many geological questions and Vair Pointon for her support throughout the year.

To my family, Mum, Dad, Anthony and my girlfriend Sophie for being a constant support throughout the year.

My biggest thanks however has to go to John Foden for all of his patience and help throughout the year to expand my understanding of the geology and for the work and knowledge he contributed to the writing of this thesis.

12 References

APPLEYARD C. M., BELL D. R. & LE ROEX A. P. 2007. Petrology and geochemistry of eclogite xenoliths from the Rietfontein kimberlite, Northern Cape, South Africa. *Contributions to Mineralogy and Petrology* 154, 309-333.

ARCULUS R. J., FERGUSON J., CHAPPELL B. W., SMITH D., MCCULLOCH M. T., JACKSON I., HENSEL H. D., TAYLOR S. R., KNUTSON J. & GUST D. A. 1988. Trace element and isotopic characteristics of eclogites and other xenoliths from the lower continental crust of southeastern Australia and southwestern Colorado Plateau U.S.A *In:* Smith D. C. ed., *Eclogites and Eclogite-Facies Rocks*, pp 335-380, Elsevier, New York.

AVIGAD D. & GVIRTZMAN Z. 2009. Late Neoproterozoic rise and fall of the northern Arabian-Nubian shield: The role of lithospheric mantle delamination and subsequent thermal subsidence. *Tectonophysics* 477, 217-228.

BARTH M. G., RUDNICK R. L., HORN I., MCDONOUGH W. F., SPICUZZA M. J., VALLEY J. W. & HAGGERTY S. E. 2001. Geochemistry of xenolithic eclogites from West Africa, part 1: A link between low MgO eclogites and Archean crust formation. *Geochimica et Cosmochimica Acta* 65, 1499-1527.

BONNEY T. G. 1899. The parent rock of the diamond in South Africa. *Proceedings of the Royal Society of London* 65, 223-236.

CARR M. J. 2002. *IgPet for Windows*. Terra Softa Inc., Somerset, NJ.

COLCHESTER D. M. 1972. A preliminary note on kimberlite occurrences in South Australia. *Journal of the Geological Society of Australia* 19, 383-386.

COLEMAN R. G., LEE D. E., BEATTY L. B. & BRANNOCK W. W. 1965. Eclogites and Eclogites: Their Differences and Similarities. *Geological Society of America Bulletin* 76, 483-508.

CULL J. P., O'REILLY S. Y. & GRIFFIN W. L. 1991. Xenolith geotherms and crustal models in Eastern Australia. *Tectonophysics* 192, 359-366.

DEER W. A., HOWIE R. A. & ZUSSMAN J. 1966. *An Introduction To The Rock Forming Minerals* (2nd edition). Longman Group UK Limited, Harlow.

DIREEN N. G. & CRAWFORD A. J. 2003. Fossil seaward-dipping reflector sequences preserved in the southeastern Australia: a 600 Ma volcanic passive margin in eastern Gondwanaland. *Journal of the Geological Society London* 160, 985 -990.

DREXEL J. F., PREISS W. V. & PARKER A. J. 1993. *The geology of South Australia. Volume 1, The Precambrian* (Vol. 1). South Australia. Geological Survey, Bulletin 54.

DUTCH R. & HAND M. 2010. Retention of Sm-Nd isotopic ages in garnets subjected to high-grade thermal reworking: implications for diffusion rates of major and rare earth elements and the Sm-Nd closure temperature in garnet. *Contributions to Mineralogy and Petrology* 112, 93-112.

DUTCH R., HAND M. & KINNY P. D. 2008. High-grade Paleoproterozoic reworking in the southeastern Gawler Craton, South Australia. *Australian Journal of Earth Sciences* 55, 1063-1081.

ELLIS D. J. & GREEN D. H. 1979. An experimental study of the effect of Ca upon garnet - clinopyroxene Fe - Mg exchange equilibria. *Contributions to Mineralogy and Petrology* 71, 13 -22.

FERGUSON J., ARCULUS R. J. & JOYCE J. 1979. Kimberlite and kimberlitic intrusives of southeastern Australia: a review. *Journal of Australian Geology and Geophysics* 4, 227-241.

FODEN J., ELBURG M., DOUGHERTY-PAGE J. & BURTT A. 2006. The timing and Duration of the Delamerian Orogeny: Correlation with the Ross Orogen and Implications for Gondwana Assembly. *The Journal of Geology* 114, 182-210.

GANGULY J., TIRONE M. & HERVIG R. L. 1998. Diffusion Kinetics of Samarium and Neodymium in Garnet, and a Method for Determining Cooling Rates of Rocks. *Science* 281, 805-807.

GHENT E. D., DIPPLE G. M. & RUSSELL J. K. 2004. Thermodynamic models for eclogitic mantle lithosphere. *Earth and Planetary Science Letters* 218, 451-462.

GOLDSTEIN S. L., O'NIONS R. K. & HAMILTON P. J. 1984. A Sm-Nd isotopic study of atmospheric dusts and particulates from major river systems. *Earth and Planetary Science Letters* 70, 221 -236.

GREEN D. H. & RINGWOOD A. E. 1967. An experimental investigation of the gabbro-eclogite transformation and some geophysical implications. *Geochimica et Cosmochimica Acta* 31, 767-833.

GREEN T. H. 1982. Anatexis of mafic crust and high pressure crystallisation of andesite. *In:* Thorpe R. S. ed., *Andesites*, John Wiley, New York.

HAÜY R. J. 1822. *Traite de mineralogie* (2nd edition). (Vol. 2). Bachelier, Paris.

HENSEN B. J. & ZHOU B. 1995. Retention of isotopic memory in garnets partially broken down during an overprinting granulite-facies metamorphism: Implications for the Sm-Nd closure temperature. *Geology* 23, 225-228.

HOWARD J. P. 2003. Adelaide Hills Project : First Combined Annual Technical Report: For the year ending 15 May 2003. *Flinders Diamonds Limited*.

HOWARD J. P. 2005. Adelaide Hills Project: Third Annual Technical Report: For the year ending 15 May 2005. *Flinders Diamonds Limited*.

IRELAND T. R., RUDNICK R. L. & SPETSIUS Z. 1994. Trace elements in diamond inclusions from eclogites reveal link to Archean granites. *Earth and Planetary Science Letters* 128, 199-213.

JACOB D. E. 2004. Nature and origin of eclogite xenoliths from kimberlites. *Lithos* 77, 295-316.

JACOB D. E., SCHMICKLER B. & SCHULZE D. J. 2003. Trace element geochemisty of coesite-bearing eclogites from the Roberts Victor kimberlite, Kaapvaal craton. *Lithos* 71, 337-351.

LUDWIG K. R. 2008. Isoplot 3.6 A Geochronological Toolkit for Microsoft Excel. *Berkeley Geochronology Centre Special Publication No. 4*, 0-77.

MATTEY D., LOWRY D. & MACPHERSON C. 1994. Oxygen isotope composition of mantle peridotite. *Earth and Planetary Science Letters* 128, 231-241.

MCCULLOCH M. T., ARCULUS R. J., CHAPPELL B. W. & FERGUSON J. 1982. Isotopic and geochmical studies of nodules in kimberlite have implications for the lower crust. *Nature* 300, 166-169.

MEFFRE S., DIREEN N. G., CRAWFORD A. J. & KAMENETSKY V. 2004. Mafic volcanic rocks on King Island, Tasmania: evidence for the 579 Ma break-up in east Gondwana. *Precambrian Research* 135, 177-191.

MEZGER K., ESSENE E. J. & HALLIDAY A. N. 1992. Closure Temperatures of the Sm-Nd system in metamorphic garnets. *Earth and Planetary Science Letters* 113, 397-409.

NIMIS P. 1998. Clinopyroxene geobarometry of pyroxenitic xenoliths from Hyblean Plateau(SE Sicily, Italy). *European Journal of Mineralogy* 10, 521-533.

NIMIS P. & TAYLOR W. R. 2000. Single clinopyroxene thermobarometry for garnet peridotites. Part 1. Calibration and testing of a Cr-in-Cpx barometer and an enstatite-in-Cpx thermometer. *Contributions to Mineralogy and Petrology* 139, 541-554.

O'REILLY S. Y. & GRIFFIN W. L. 1985. A xenolith derived geotherm for southeastern Australia and its geophysical implications. *Tectonophysics* 111.

PEARSON N. J. & O'REILLY S. Y. 1991. Thermobarometry and P-T-t paths: the granulite to eclogite transition in lower crustal xenoliths from eastern Australia. *Journal of Metamorphic Geology* 9, 349-359.

PEARSON N. J., O'REILLY S. Y. & GRIFFIN W. L. 1991. The granulite to eclogite transition beneath the eastern margin of the Australian craton. *European Journal of Mineralogy* 3, 293-322.

PHILPOTTS A. R. & AGUE J. J. 2009. *Principle of Igneous and Metamorphic Petrology Second Edition*. Cambridge University Press, New York.

POWELL R., HOLLAND T. & WORLEY B. 1998. Calculating phase diagrams involving solid solutions via non-linear equations, with examples using THERMOCALC. *Metamorphic Geology* 16, 577-588.

RUDNICK R. L., MCDONOUGH W. F. & TAYLOR S. R. 1986. Lower crust xenoliths from Queensland, Australia: evidence for deep crustal assimilation and fractionation of continental basalt. *Geochimica et Cosmochimica Acta* 50, 1099-1115.

SCOTT SMITH B. H., DANCHIN R. V., HARRIS J. W. & STRACKE K. J. 1984. Kimberlites near Orroroo, South Australia. *In:* Kornprobst J. ed., *Kimberlites I: Kimberlites and Related Rocks*, pp 121-142, Elsevier, Amsterdam.

SPARKS R. S. J., BAKER L., BROWN R. J., FIELD M., SCHUMACHER J., STRIPP G. & WALTERS A. 2006. Dynamical constraints on kimberlite volcanism. *Journal of Volcanology and Geothermal Research* 155, 18-48.

STRACKE K. J., FERGUSON J. & BLACK L. P. 1979. Structural setting of kimberlites in southeastern Australia. *Kimberlites, Diatremes and Diamonds: their Geology, Petrology and Geochemistry, Proceedings of the 2nd international Kimberlite Conference,* Washington, D.C., pp. 71 -91. American Geophysical Union.

SUN S. S. & MCDONOUGH W. F. 1989. Chemical and isotopic systematics of oceanic basalts: implications for the mantle composition and processes. *In:* Saunders A. D. & Norry M. J. eds., *Magmatism in the Ocean Basins*, Vol. 42, pp 313-345, Geological Society, London, Special Publications.

SYMONDS P. A., PLANKE S., FREY O. & SKOGSEID J. 1998. Volcanic evolution of the Western Australian continental margin and its implications for basin development. The Sedimentary Basins of Western Australia 2. *In:* Purcell G. & Purcell R. R. eds., *Proceedings of Petroleum Exploration of Australia Symposium*, Perth, WA.

TAPPERT R., FODEN J., STACHEL T., MUEHLENBACHS K., TAPPERT M. & WILLS K. 2009. The diamonds of South Australia. *Lithos* 112, 806-821.

VAN ORMAN J. A., GROVE T. L. & SHIMIZU N. 2001. Rare earth element diffusion in diopside: influence of temperature, pressure, and ionic radius, and an elastic model for diffusion in silicates. *Contributions to Mineralogy and Petrology* 141, 687-703.

VAN ORMAN J. A., GROVE T. L., SHIMIZU N. & LAYNE G. D. 2002. Rare earth element diffusion in a natural pyrope single crystal at 2.8 GPa. *Contributions to Mineralogy and Petrology* 142, 416-424.

WILSON M. 1989. *Igneous Petrology*. Allen & Unwin, Sydney.

ZHANG J., ZHANG Z., XU Z., YANG J. & CUI J. 2001. Petrology and geochronology of eclogites from the western segment of the Altyn Tagh, northwestern China *Lithos* 56, 187-206.

ZHOU J. & LI X. 2006. GeoPlot: An Excel VBA program for geochemical data plotting. *Computers and Geosciences* 32, 554-560.

ZINDER A. & JAGOUTZ E. 1988. Manlte crytology. *Geochimica et Cosmochimica Acta* 52, 319-333.

13 Appendices

13.1 Appendix A – Table Captions

13.2 Appendix B – Tables

Lithology	Mineralogy	Thin Sections	Shape and Size	Surface Textures
Granulite	Grt+cpx+pl+Hb+Rt+Ilm	34 3.1, 34 .48, MB 1.5, MB 2.6, MB 2.9	Angular – sub angular nodules(5-10cm) - large(20-25cm) well rounded, spheroidal - ellipsoidal boulders	Smooth outer surface, caked by kimberlite of opaque green colour. Bare areas reveal specks of dark red-orange garnets, dark green clinopyroxene
Kyanite Granulite	Grt+cpx+Pl+Ky	MB 1.4	Small(<10cm)fine grained elongate blocks possessing rounded corners	Smooth outer face, no kimberlite coating, characterised by grass green and red-orange layers with central area having dark grey, light grey mylonitic appearance
Kyanite Eclogite	Grt+Clinopyroxene+Ky+Am+Rt	34 1.1, 34 1.5, 34 4.3, 34 5.2, MB 2.2	Very large rounded cobbles(10-15cm) - ellipsoid boulders(20 - 25cm)	Rough surface, light green/blue colour with pink-light red/orange garnets and light green clinopyroxene.
Amphibole Eclogite	Grt+Cpx+Am+Rt	34 3.2, 34 5.0, 34 5.1, MB 1.9, MB 2.8	Angular nodules(7 – 15cm)	Dark overall appearance, dark red-orange Grt, dark green Clinopyroxene, coarse Dark brown Am
Amphibolite	Am+Pl+Bt+Ilm	34 4.9	Single large (15cm) ellipsoid nodule	Rough surface of dark overall colour
Carbonate	CO_2	34 2.7	Rounded - ellipse nodules(5 - 20cm)	Smooth, green-beige outer surface with light purple – light grey crystalline grains

Table 1

Lithology	Major Mineralogy	Minor Mineralogy	Textures
Granulite	Grt, Cpx, Pl, Hb, Rt, Ilm	Qtz, Ap	Coarse to medium grained, granoblastic, coarse-grained rutile with ilmenite exsolution
Kyanite Granulite	Grt, Cpx, Pl, Ky	Crd, Sph	Fine grained, layered idioblastic Clinopyroxene and Grt, very fine grained angular Ky, Crd fragments surrounding anhedral Pl grains, overprinting of green Sphene on Grt
Kyanite Eclogite	Grt, Cpx, Ky, Hb, Rt	S	Equi-sub granular texture of Grt and Clinopyroxene in areas, whereas other areas xenoblastic garnet surrounded by Ky, Clinopyroxene symplectite, idioblastic Ky in one sample, garnet with kelyphytic rims
Amphibole Eclogite	Grt, Cpx, Hb, Rt, Ilm	Pmp, Bt, CO_2, S ,Ksp	Granoblastic texture of Grt, Clinopyroxene, Hb , coarse grained rutile exsolving ilmenite , kelyphytic garnets
Amphibolite	Am, Pl, Bt, Ilm	CO_2, S	Schist texture of platy Am and Bt grains anastamosing around large xenoblastic Pl, Il exists as fingerprint shaped exsolution surrounded by calcite(CO2)
Carbonate	CO_2		Large remnant carbonate grains filled with fine grained carbonate (<200μm), surrounded by interlocking carbonate grains (<1mm) with wavy grain boundaries.

Table 2

Sample	Spot	SiO_2	TiO_2	Al_2O_3	Cr_2O_3	FeO	MnO	MgO	CaO	Na_2O	K_2O	F	Cl	Total	Mg#
Granulites															
34 3.1	Core	39.76	0.02	21.47	0.07	21.79	0.44	8.53	8.97	0.02	0.00	0.16	0.01	101.25	0.41
34 4.8	Core	40.07	0.06	23.26	0.09	15.47	0.37	13.45	8.73	0.02	0.02	0.09	0.00	101.64	0.61
MB 1.5	Core	37.50	0.17	21.05	0.06	25.55	0.70	5.79	8.70	0.04	0.00	0.34	0.00	99.90	0.29
MB 2.6	Core	38.64	0.08	21.18	0.01	21.12	0.79	8.94	8.84	0.03	0.00	0.23	0.00	99.87	0.43
MB 2.9	Core	38.51	0.02	22.11	0.07	17.39	0.48	11.92	8.97	0.01	0.00	0.13	0.00	99.62	0.55
Kyanite Granulite															
MB 1.4	Rim	40.35	0.03	23.28	0.00	10.00	0.15	17.17	8.56	0.02	0.00	0.17	0.00	99.73	0.75
Kyanite Eclogites															
34 1.1	Rim	38.96	0.14	21.98	0.00	14.08	0.42	14.29	9.66	0.11	0.19	0.19	0.00	100.02	0.64
34 1.5	Rim	40.74	0.03	23.34	0.19	8.80	0.26	16.09	10.66	0.03	0.00	0.20	0.00	100.36	0.77
34 4.3	Rim	40.68	0.04	21.93	0.46	14.52	0.41	10.95	10.72	0.57	0.02	0.23	0.01	100.53	0.57
34 5.2	Core	41.26	0.06	23.75	0.01	10.12	0.28	17.85	8.09	0.00	0.00	0.15	0.00	101.56	0.76
MB 2.2	Core	40.60	0.00	23.47	0.22	9.03	0.24	18.34	7.78	0.00	0.01	0.23	0.01	99.94	0.78
Amphibole Eclogite															
34 3.2	Rim	37.45	0.08	20.87	0.04	25.12	0.57	6.50	8.89	0.01	0.00	0.25	0.00	99.79	0.32
34 5.0	Core	39.46	0.01	22.72	0.01	16.34	0.35	11.72	9.50	0.03	0.00	0.22	0.00	100.36	0.56
34 5.1	Core	39.88	0.05	21.64	0.05	20.25	0.34	11.48	6.11	0.03	0.02	0.12	0.01	99.98	0.50
MB 1.9	Rim	38.34	0.09	21.99	0.04	22.58	1.11	6.57	10.23	0.06	0.01	0.27	0.01	101.29	0.34
MB 2.8	Rim	39.89	0.00	22.31	0.14	14.59	0.83	11.18	10.89	0.04	0.00	0.21	0.00	100.09	0.58

Table 3

Sample	Spot	SiO_2	TiO_2	Al_2O_3	Cr_2O_3	FeO	MnO	MgO	CaO	Na_2O	K_2O	F	Cl	Total	Mg#
Granulites															
34 3.1	Core	52.32	0.48	7.26	0.00	7.03	0.01	10.71	18.39	3.53	0.00	0.15	0.00	99.87	0.73
34 4.8	Core	51.77	0.37	9.20	0.10	3.21	0.08	12.57	19.77	2.97	0.00	0.08	0.00	100.12	0.87
MB 1.5	Rim	51.88	0.71	9.17	0.03	10.07	0.05	8.02	14.70	5.34	0.02	0.18	0.00	100.16	0.59
MB 2.6	Core	50.63	0.54	8.24	0.00	9.08	0.08	9.79	18.06	3.50	0.01	0.27	0.00	100.21	0.66
MB 2.9	Core	51.81	0.47	9.55	0.05	3.82	0.05	11.58	19.20	3.37	0.00	0.13	0.00	100.03	0.84
Kyanite Granulite															
MB 1.4	Rim	52.31	0.07	12.13	0.00	1.71	0.00	11.34	17.94	4.25	0.02	0.08	0.01	99.88	0.92
Kyanite Eclogites															
34 1.1	Core	51.86	0.57	9.21	0.02	2.31	0.03	13.14	21.40	2.04	0.00	0.01	0.00	100.60	0.91
34 1.5	Rim	51.05	0.42	10.19	0.19	1.71	0.01	13.25	21.60	1.95	0.00	0.00	0.00	100.37	0.93
34 4.3	Core	52.42	0.48	11.15	0.25	3.47	0.00	10.87	18.58	3.63	0.02	0.11	0.01	100.99	0.85
34 5.2	Rim	52.38	0.22	9.45	0.08	1.84	0.02	13.21	19.88	2.95	0.00	0.13	0.02	100.17	0.93
MB 2.2	Core	51.59	0.14	11.62	0.17	1.61	0.03	11.95	19.78	3.03	0.01	0.05	0.01	100.00	0.93
Amphibole Eclogite															
34 3.2	Core	51.59	0.36	7.38	0.01	8.54	0.08	10.27	17.55	3.73	0.00	0.09	0.00	99.60	0.68
34 5.0	Core	52.25	0.44	9.95	0.08	4.23	0.00	11.30	18.24	3.60	0.01	0.06	0.00	100.15	0.83
34 5.1	Core	53.09	0.51	6.52	0.04	5.02	0.09	12.18	19.91	2.34	0.09	0.11	0.00	99.89	0.81
MB 1.9	Core	52.32	0.41	9.57	0.01	7.74	0.11	9.13	16.34	4.76	0.00	0.00	0.00	100.40	0.68
MB 2.8	Rim	52.17	0.10	11.46	0.18	3.21	0.12	10.90	17.78	3.97	0.02	0.18	0.00	100.10	0.86

Table 4

Xenolith Type	Granulite				Kyanite Eclogite			Amphibole Eclogite
Sample	MB 1.5	MB 2.9	34 1.1	34 5.2	34 3.2	34 5.0	34 5.1	MB 2.8
Spot	Core	Core	Rim	Core	Core	Rim	Rim	Core
P	161.1	109.9	106.0	18.3	141.4	65.8	139.0	52.3
K	0.0	0.0	142.6	0.0	96.1	0.0	111.0	9.0
Sc	22.9	77.1	51.9	4.7	76.2	284.1	250.9	437.9
Ti	1179.6	395.2	255.1	28.7	533.0	1193.5	1668.3	244.8
Mn	5376.9	3449.8	2355.1	293.2	3995.3	12357.7	9771.1	13921.4
Ni	0.7	26.6	6.4	1.9	2.3	1149.1	143.4	86.1
Ga	8.9	8.3	4.9	0.7	9.7	106.0	199.8	64.5
Sr	0.3	5.0	6.3	0.1	0.3	0.2	11.5	0.2
Y	66.1	21.0	11.5	1.3	82.0	897.6	933.3	793.5
Zr	7.8	1.4	0.5	0.5	2.5	61.4	538.0	35.8
Nb	0.0	0.0	0.0	0.0	0.0	0.0	3.7	1.7
La	0.0	0.1	0.0	0.0	0.0	0.5	24.6	0.6
Ce	0.2	0.2	0.0	0.0	0.1	2.7	40.9	1.2
Pr	0.2	0.0	0.0	0.0	0.1	1.7	8.1	0.0
Nd	3.4	0.2	0.0	0.0	1.2	29.4	22.4	0.0
Sm	5.6	0.4	0.0	0.1	2.1	41.3	39.6	9.2
Eu	5.4	0.4	0.1	0.1	1.4	40.0	23.3	7.9
Gd	13.1	1.6	0.8	0.1	6.3	152.3	87.9	38.2
Tb	2.3	0.4	0.2	0.0	1.6	30.6	25.6	15.2
Dy	14.8	3.5	2.3	0.3	13.5	179.4	166.3	131.5
Ho	2.9	0.8	0.5	0.1	3.3	36.6	44.4	33.7
Er	7.1	2.5	1.1	0.1	10.1	87.2	128.5	99.4
Yb	4.5	2.7	0.9	0.1	10.6	98.6	94.0	91.2
Lu	0.6	0.4	0.1	0.0	1.5	10.0	16.7	14.7
Hf	0.2	0.0	0.0	0.0	0.0	1.8	32.5	0.0
Pb	0.0	0.1	0.0	0.0	0.0	0.0	60.5	0.4
Th	0.0	0.1	0.0	0.0	0.0	0.0	7.2	0.0
U	0.0	0.1	0.0	0.0	0.0	0.0	127.1	0.2

Table 5

Xenolith Type	Granulite			Kyanite Eclogite				Amphibole Eclogite
Sample	MB 1.5	MB 2.9	34 1.1	34 5.2	34 3.2	34 5.0	34 5.1	MB 2.8
Spot	Rim	Core	Rim	Rim	Core	Rim	Core	Rim
P	35.3	49.1	48.8	21.2	25.1	29.4	59.8	26.7
K	81.8	219.0	43.7	225.7	0.0	0.0	32.2	22.6
Sc	20.9	39.7	23.5	2.8	43.3	117.1	231.3	160.6
Ti	5508.0	3022.7	2831.8	637.5	1906.6	9643.2	10970.6	1793.4
Mn	413.6	247.4	214.0	46.9	255.3	1045.5	1300.1	1058.4
Ni	14.0	129.5	101.7	66.0	33.6	18987.6	3768.6	1123.8
Ga	29.7	17.5	12.4	5.0	13.5	327.4	498.9	167.5
Sr	185.7	53.0	65.0	93.1	111.6	116.5	104.5	36.6
Y	1.3	1.1	0.9	0.1	2.0	35.4	72.7	31.6
Zr	27.3	9.8	4.0	2.9	17.7	229.8	709.2	74.8
Nb	0.0	0.2	0.3	0.0	0.0	2.8	21.6	13.7
La	3.1	0.2	0.3	0.5	1.0	62.4	264.1	0.0
Ce	13.2	0.8	0.6	1.5	3.9	182.4	868.8	108.1
Pr	2.7	0.2	0.1	0.2	0.9	32.6	118.8	0.6
Nd	16.2	1.2	0.5	1.0	5.8	164.3	630.3	6.0
Sm	4.4	0.6	0.0	0.2	1.9	62.1	145.0	3.1
Eu	2.0	0.4	0.1	0.1	0.6	21.9	49.3	2.4
Gd	2.7	0.8	0.3	0.2	1.6	39.1	77.1	9.2
Tb	0.2	0.1	0.0	0.0	0.2	4.0	8.6	1.3
Dy	0.5	0.4	0.3	0.0	0.6	12.0	33.8	6.7
Ho	0.1	0.0	0.1	0.0	0.1	1.4	2.4	1.1
Er	0.0	0.1	0.1	0.0	0.2	2.1	3.9	3.2
Yb	0.0	0.0	0.0	0.0	0.1	2.2	3.5	3.0
Lu	0.0	0.0	0.0	0.0	0.0	0.0	0.6	0.4
Hf	2.7	0.5	0.3	0.2	1.3	20.2	93.5	4.4
Pb	0.1	0.2	0.4	0.1	0.2	3.3	26.5	2.5
Th	0.0	0.0	0.1	0.0	0.0	1.0	30.2	0.0
U	0.0	0.0	0.3	0.0	0.0	2.1	70.8	0.5

Table 6

Sample	SiO_2	Al_2O_3	Fe_2O_3T	MnO	MgO	CaO	Na_2O	K_2O	TiO_2	P_2O_5	SO3	LOI	Total	Mg#
Granulites														
34 1.2	50.49	15.37	8.56	0.15	10.47	11.57	2.08	0.41	0.2	0.04	0.02	0.8	100.13	0.68
34 3.1	47.22	14.8	12.54	0.19	7.99	11.46	2.72	0.36	1.46	0.19	0.02	0.86	99.79	0.52
34 4.8	45.29	16.84	8.8	0.12	9.78	12.57	1.59	0.62	0.4	0.08	0.06	2.64	98.78	0.66
34 5.3	48.73	16.58	10.79	0.16	6.56	10.21	3.54	0.6	1.45	0.05	0.16	0.83	99.64	0.51
34 5.4	46.51	14.49	13.79	0.2	7.6	12.13	2.34	0.39	1.09	0.13	0.02	0.78	99.47	0.48
34 5.5	45.1	12.85	17.64	0.23	6.63	10.45	2.56	0.93	2.09	0.07	0.04	1.35	99.94	0.39
34 5.7	49.35	14.85	10.59	0.17	7.51	11.26	3.43	0.41	1.01	0.05	0.02	0.82	99.46	0.55
MB 1.3	45.58	17.51	10.29	0.18	7.19	12.33	2.93	1.09	1.27	0.34	0.11	1.22	100.02	0.54
MB 2.1	47.43	17.27	9.29	0.13	9.15	11.37	2.71	0.56	0.67	0.05	0.17	0.93	99.72	0.63
MB 2.6	39.58	10.55	21.11	0.22	7.18	12.64	1.9	0.56	4.81	0.62	0.03	0.65	99.84	0.37
MB 2.9	48.31	16.72	8.36	0.17	9.04	12.69	2.99	0.41	0.32	0.05	0.1	0.51	99.67	0.65
MB 3.2	46.35	16.8	10.4	0.14	9.61	11.6	2.31	0.54	0.91	0.04	0.18	0.9	99.77	0.61
Kyanite Granulites														
34 1.4	45.64	15.23	11.96	0.19	9.26	13.71	2.09	0.2	1.27	0.05	0.02	0.46	100.08	0.57
MB 3.0	44.81	23.96	4.14	0.06	10.6	12.79	2.48	0.1	0.09	0.04	0.02	0.74	99.83	0.81

Table 7

Sample	SiO_2	Al_2O_3	Fe_2O_3T	MnO	MgO	CaO	Na_2O	K_2O	TiO_2	P_2O_5	SO3	LOI	Total	Mg#
Kyanite Eclogites														
34 1.1	45.62	15.01	6.18	0.12	11.46	14.19	1.33	0.49	0.26	0.05	0.02	4.78	99.5	0.76
34 1.5	46.86	18.64	4.43	0.08	12.39	15.24	1.43	0.09	0.16	0.04	0.03	0.39	99.77	0.83
34 1.6	44.98	15.54	11.66	0.2	9.67	13.93	1.99	0.2	0.73	0.04	0.02	0.86	99.82	0.59
34 4.3	44.75	18.02	6.11	0.1	8.9	16.1	2.31	0.28	0.63	0.06	0.14	2.12	99.52	0.71
34 5.2	45.8	21.03	5	0.08	12.24	12.74	1.65	0.15	0.16	0.04	0.01	0.6	99.49	0.81
MB 2.2	47.55	17.01	4.5	0.09	12.83	14.83	1.92	0.1	0.12	0.04	0.04	0.73	99.76	0.83
MB 2.4	46.27	17.93	3.84	0.08	12.65	16.82	1.04	0.07	0.12	0.05	0.03	0.7	99.57	0.85
MB 3.0	44.81	23.96	4.14	0.06	10.6	12.79	2.48	0.1	0.09	0.04	0.02	0.74	99.83	0.81
Amphibole Eclogites														
34 3.2	44.15	13.05	15.54	0.21	8.9	13.17	1.9	0.29	1.81	0.05	0.02	1.05	100.13	0.49
34 5.0	42.8	17.57	11.31	0.16	10.48	11.41	2.11	0.59	0.73	0.1	0.14	1.32	98.7	0.61
MB 1.2	45.97	15.3	8.92	0.15	12.34	13.8	1.56	0.29	0.47	0.05	0.02	0.86	99.74	0.7
MB 1.9	45.14	13.19	12.85	0.23	8.67	12.51	3.49	0.83	0.91	0.11	0.03	1.76	99.75	0.54
MB 3.1	44.27	12.98	14.49	0.25	8.49	12.25	3.02	0.65	1.28	0.24	0.02	1.68	99.63	0.5

Table 8

Xenolith Type	Granulites												Kyanite Granulites	
Trench	34							MB					34	MB
Sample	1.2	3.1	4.8	5.3	5.4	5.5	5.7	1.3	2.1	2.6	2.9	3.2	1.4	3
V*	167	347	176.5	246	334	494	283	162	185	595	251	265	343	24
Cr*	758	182	705.5	157	227	39	124	203	384	58	412	314	331	317
Ni	245	105	300	40	70	165	95	75	115	365	95	130	120	75
Ga	14	17	15	20.5	18.5	22	16	15.5	17	10.5	28	17	16	15.5
Rb	4.1	10	20	8	8.5	25	11	13	5.5	1.2	11.5	6.5	2.5	4.7
Sr	140	365	365	1200	175	255	395	1300	850	395	170	700	280	460
Y	5	21	13.5	15	19	29.5	16	14	6.5	1.5	65	8	29	10
Zr*	5.5	63.5	33.1	37.4	57.4	63.2	37.8	65.6	21.1	361.6	17	20.4	31.2	9.5
Nb	0.5	3.5	8.5	1	1	1.5	1	3.5	0	0	4	1	0.5	5.5
Ba*	1392	3223	5270.5	2542	700	3470	3200	2895	2708	1881	2152	2483	1078	1091
La	2.5	10	9.5	5.5	5.5	9	5	18.5	3.5	0	19.5	3.5	2	2.5
Ce	3.5	23	12.5	10	13.5	12	13	36.5	6.5	0.5	55	7	6.5	4
Pr	0.4	3.4	1.4	1.5	2.1	2	2.1	4.9	0.9	0.1	10	1	1.4	0.5
Nd	1.6	16	6	7.5	10.5	10	10.5	21	3.9	0.6	50	4.1	7.5	1.9
Sm	0.6	4.2	2.4	2.6	2.9	3.8	3.1	4.6	1.4	0.3	14	1.4	2.8	0.9
Eu	0.4	1.5	1	1.2	1.1	1.4	1.3	1.9	0.6	0.2	3.9	0.7	1.1	0.5
Gd	0.7	4.3	2.6	3.1	3.5	5	3.2	4.3	1.4	0.3	16	1.6	4.2	1.3
Tb	0.1	0.7	0.4	0.5	0.6	0.9	0.5	0.6	0.2	0.1	2.6	0.3	0.8	0.3
Dy	0.9	4.1	2.3	3	3.7	5.5	3.2	3.2	1.4	0.3	14.5	1.6	5	1.8
Ho	0.2	0.8	0.4	0.6	0.7	1.2	0.6	0.5	0.3	0.1	2.6	0.3	1.1	0.4
Er	0.6	2.5	1.3	1.7	2.2	3.5	1.9	1.6	0.8	0.2	7.5	0.9	3.4	1.2
Tm	0.1	0.4	0.2	0.2	0.3	0.5	0.3	0.2	0.1	0	1	0.1	0.5	0.2
Yb	0.6	2.3	1.2	1.5	2.1	3.3	1.9	1.3	0.7	0.2	6	0.8	3.2	1.2
Lu	0.1	0.3	0.2	0.2	0.4	0.7	0.3	0.2	0.1	0	0.8	0.1	0.5	0.2
Pb	0.5	1.5	1	3	0.5	2	3	1.5	1	0	1	1	0	2
Th	0.2	0.4	0.6	1	0	0.8	0.2	1.7	0.2	0	0	0.2	0	0.7
U	0.3	0.3	0.5	0.5	0.1	0.5	0.2	0.4	0	0	0.1	0	0	0.2

Table 9

Xenolith Type	Kyanite Eclogites								Amphibole Eclogites				
Trench	34					MB			34		MB		
Sample	1.1	1.5	1.6	4.3	5.2	2.2	2.4	3	3.2	5	1.2	1.9	3.1
V*	175	114	288	195	53	116	121	24	677	270	191	294	356
Cr*	340	1228	569	1763	661	1090	1915	317	132	990.5	1218	107	57
Ni	130	300	85	175	230	230	250	75	70	220	215	65	50
Ga	11	9	16	15.5	10	9.5	9.5	15.5	17	17	13.5	15.5	16.5
Rb	8	1.1	7	7.5	2.3	0.8	0.2	4.7	12	8.5	4	10	12
Sr	305	260	260	950	330	395	650	460	275	650	335	335	375
Y	6.5	4.7	15.5	11.5	3.2	3.2	2.5	10	21	22.5	9.5	22.5	32
Zr*	10.5	15.2	21.2	42.9	16.9	11.9	14.4	9.5	26.9	27.2	16.4	28.5	46
Nb	2.5	0.5	3.5	1.5	0.5	0.5	0	5.5	1	3.5	0.5	10.5	6.5
Ba*	1658	895	1840	1459	489	1656	1913	1091	2894	3096	1384	2300	2818
La	4	1	1	2.5	3	1	1	2.5	3	420	2	3.5	5
Ce	5	2	2	5	5.5	1.5	1	4	6.5	600	5	7	11.5
Pr	0.7	0.3	0.5	0.9	0.7	0.2	0.2	0.5	1.1	65	0.8	1.1	2
Nd	2.7	1.4	2.8	4.6	2.4	1	0.9	1.9	6	205	4.2	5.5	10.5
Sm	1	0.6	1.5	1.7	0.6	0.5	0.5	0.9	2.5	26	1.5	2.5	3.7
Eu	0.4	0.3	0.7	0.7	0.3	0.2	0.2	0.5	1	6.5	0.6	1.1	1.4
Gd	1.1	0.8	2.3	2.1	0.6	0.5	0.5	1.3	3.3	16.5	1.8	3.5	5
Tb	0.2	0.1	0.4	0.4	0.1	0.1	0.1	0.3	0.6	1.6	0.3	0.7	1
Dy	1.2	0.9	2.9	2.3	0.6	0.6	0.5	1.8	4	5.5	1.9	4.3	6.5
Ho	0.3	0.2	0.6	0.4	0.1	0.1	0.1	0.4	0.8	0.9	0.4	0.9	1.3
Er	0.8	0.6	1.8	1.4	0.4	0.4	0.3	1.2	2.6	2.5	1.1	2.8	4.1
Tm	0.1	0.1	0.3	0.2	0	0.1	0	0.2	0.4	0.3	0.2	0.4	0.6
Yb	0.8	0.5	1.7	1.2	0.4	0.4	0.3	1.2	2.4	2	1	2.8	4
Lu	0.1	0.1	0.3	0.2	0.1	0.1	0.1	0.2	0.4	0.3	0.2	0.4	0.6
Pb	0.5	0	0.5	2.5	0.5	0	0	2	1	3	0.5	1.5	1.5
Th	0.3	0	0	0.5	0.3	0.2	0	0.7	0.4	55	0.4	0.4	0.3
U	0.2	0	0.1	0.3	0.1	0	0	0.2	0.5	4.2	0	0.2	0.2

Table 10

Sample	T_{EG79}		T_{K88}		P_{N95}	
	Min	Max	Min	Max	Min	Max
Granulite						
34 3.1	898	940	870	918		17
34 4.8	866	888	833	860		20
MB 2.6	1098	1170	1117	1212		16
MB 2.9	891	923	868	906		21
Kyanite Granulite						
MB 1.4	860	1003	825	988	15	30
Kyanite Eclogite						
34 1.1	806	875	775	854		14
34 1.5	866	977	844	976		18
34 4.3	958	1015	952	1019		25
34 5.2	893	929	855	898		21
MB 2.2	842	892	797	857		20
Amphibole Eclogites						
34 3.2	887	938	910	920	18	20
34 5.0	958	1041	946	1051		22
34 5.1	793	1129	726	1118		11
MB 1.9	976	991	972	990		25
MB 2.8	969	1002	948	989		27

Table 11

Sample	Sm(ppm)	Nd(ppm)	$^{147}Sm/^{144}Nd$	$^{144}Nd/^{143}Nd$	1 SD	εNd
Garnet						
34 3.2 G	12.39	8.14	0.920	0.513944	± 83	25
34 5.2 G	0.34	0.32	0.649	0.513470	± 2624	16
MB 2.9 G	0.39	0.16	1.457	0.514501	± 224*	36
Clinopyroxene						
34 3.2 CP	2.27	7.97	0.172	0.513013	± 74	7
34 5.2 CP	0.60	3.21	0.113	0.512499	± 72	-3
MB 2.9 CP	0.58	1.15	0.303	0.513038	± 98	8
Whole Rock						
34 3.2 WR	2.15	2.15	0.219	0.513053	± 53	8
34 4.9 WR	3.53	12.52	0.170	0.512892	± 62	5
34 5.2 WR	0.37	1.72	0.130	0.512614	± 97	0
MB 2.4 WR	0.25	0.80	0.187	0.512835	± 76	4
MB 2.9 WR	0.66	2.20	0.180	0.512798	± 106	3

Table 12

13.3 Appendix C – Figure Captions

.

13.4 Appendix D – Figures

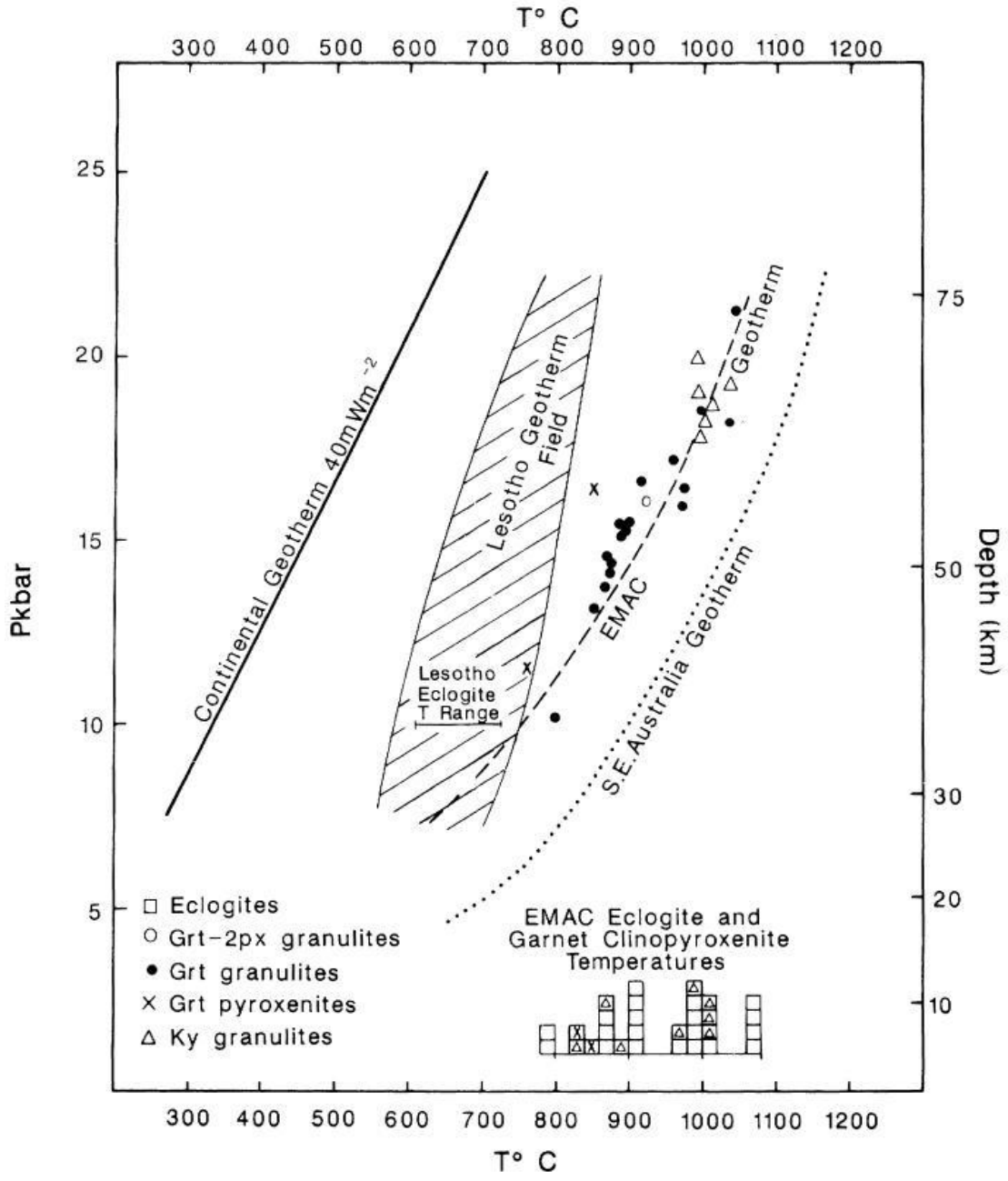
T° C
300 400 500 600 700 800 900 1000 1100 1200
25
20
15
10
5
Pkbar
75
50
30
20
10
Depth (km)
Continental Geotherm 40mWm⁻²
Lesotho Geotherm Field
Lesotho Eclogite T Range
EMAC
Geotherm
S.E. Australia Geotherm
□ Eclogites
○ Grt–2px granulites
• Grt granulites
× Grt pyroxenites
△ Ky granulites
EMAC Eclogite and Garnet Clinopyroxenite Temperatures
300 400 500 600 700 800 900 1000 1100 1200
T° C

Figure 1

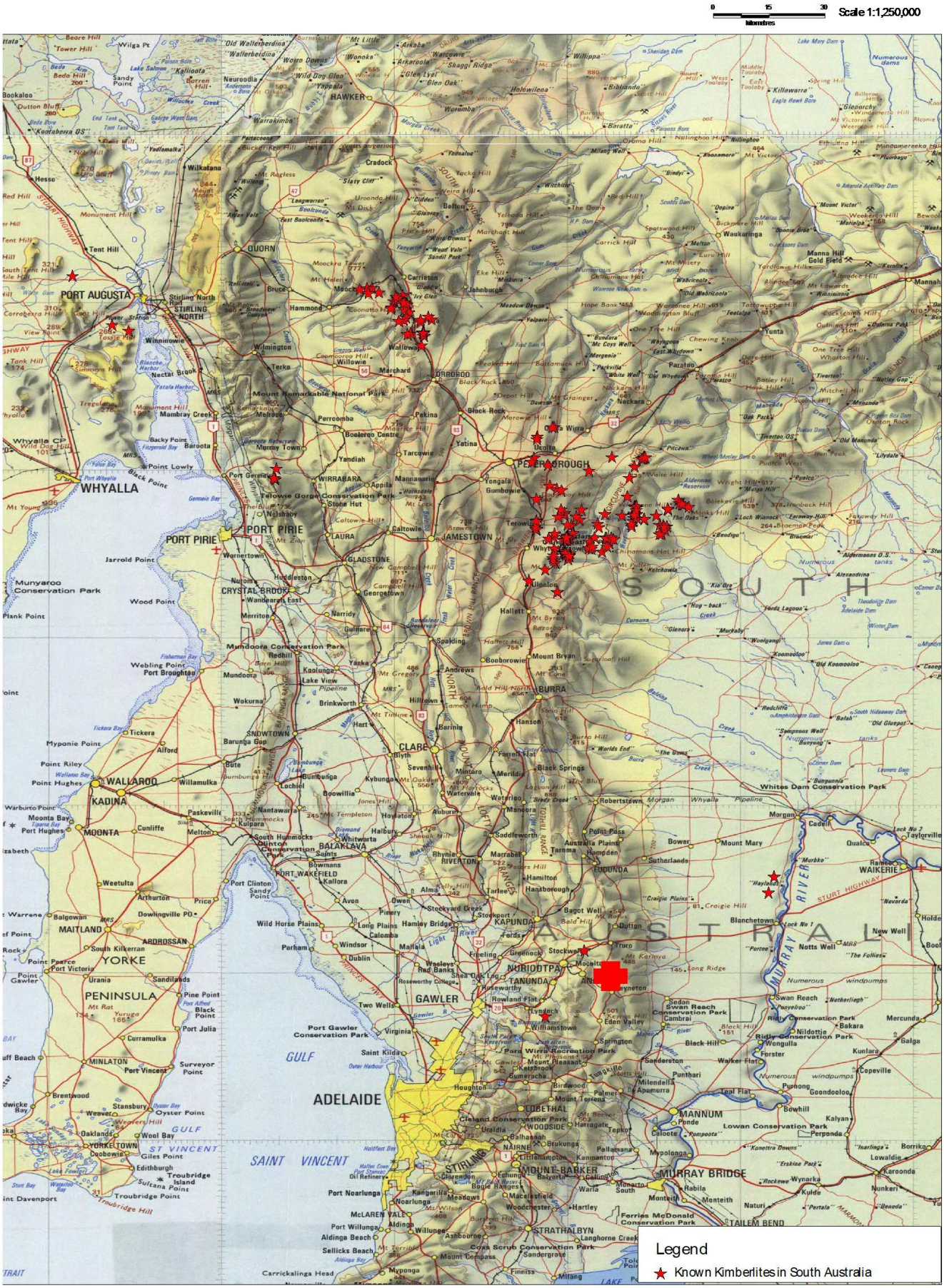
Scale 1:1,250,000
Legend
Known Kimberlites in South Australia
PORT AUGUSTA
WHYALLA
PORT PIRIE
PETERBOROUGH
JAMESTOWN
BURRA
CLARE
WALLAROO
KADINA
MOONTA
MAITLAND
YORKE
PENINSULA
GAWLER
ADELAIDE
MURRAY BRIDGE
MANNUM
NURIOOTPA
TANUNDA
KAPUNDA
STRATHALBYN
MOUNT BARKER
GULF
SAINT VINCENT
SOUTH AUSTRALIA

Figure 2

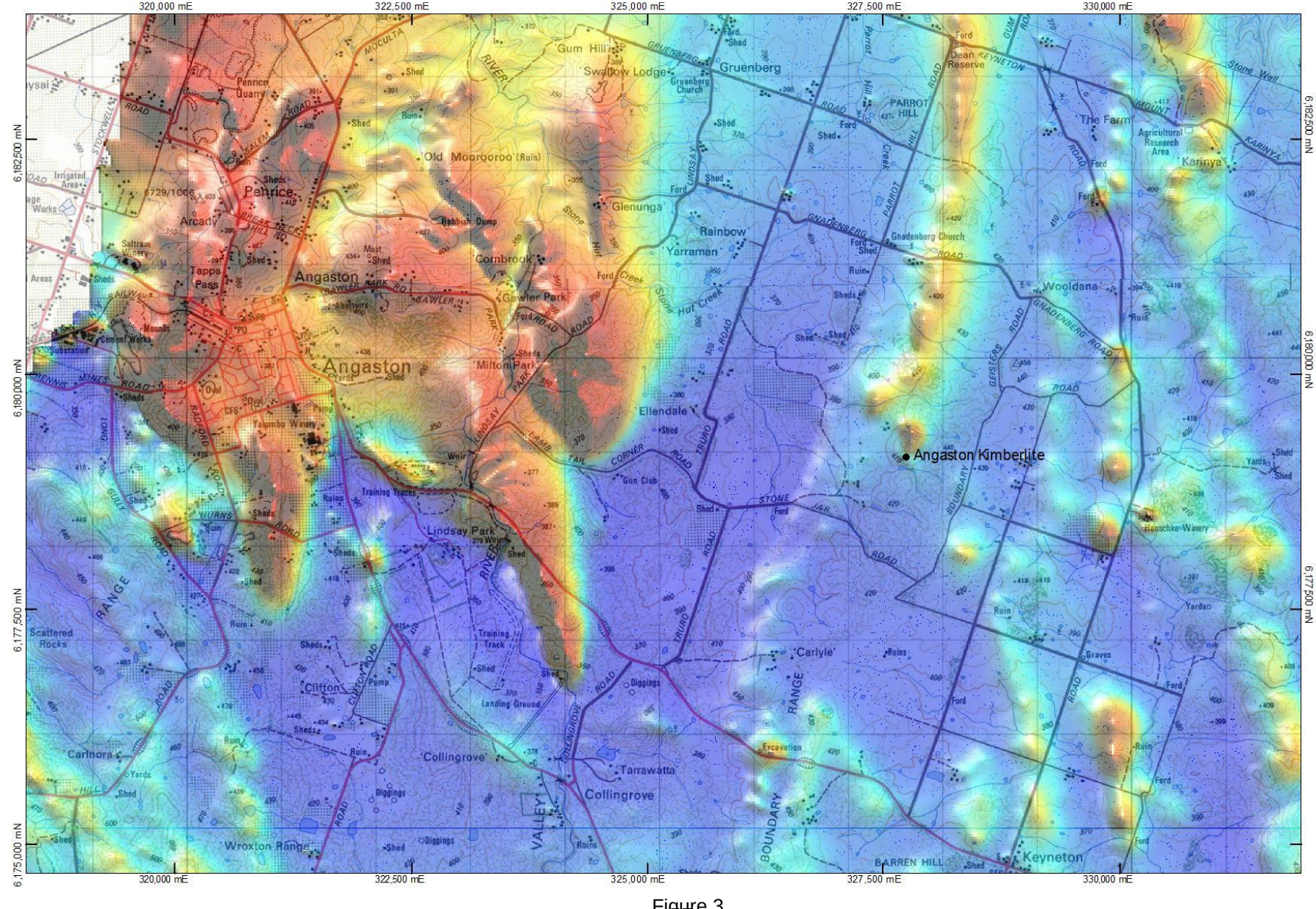
320,000 mE
322,500 mE
325,000 mE
327,500 mE
330,000 mE
6,182,500 mN
6,180,000 mN
6,177,500 mN
6,175,000 mN
Angaston Kimberlite
Angaston
Penrice
Penrice Quarry
Old Mooroorroo (Ruin)
Arcady
Tappa Pass
Cornbrook
Gawler Park
Milton Park
Lindsay Park
Ellendale
Gruenberg
Gum Hill
Swallow Lodge
Dean Reserve
PARROT HILL
The Farm
Karinya
Glenunga
Rainbow
Yarraman
Gnadenberg Church
Wooldana
Henschke Winery
Carlyle
Clifton
Carlnora
Collingrove
Tarrawatta
Wroxton Range
Keyneton
BARREN HILL
Scattered Rocks
Gun Club
Training Tracks
Landing Ground
Excavation
Diggings
Rubbish Dump
Saltram Winery
Yalumba Winery
Cement Works
Substation
Irrigated Area
Agricultural Research Area
Stone Hut Creek
Ford Creek
Graves
Ruins

Figure 3

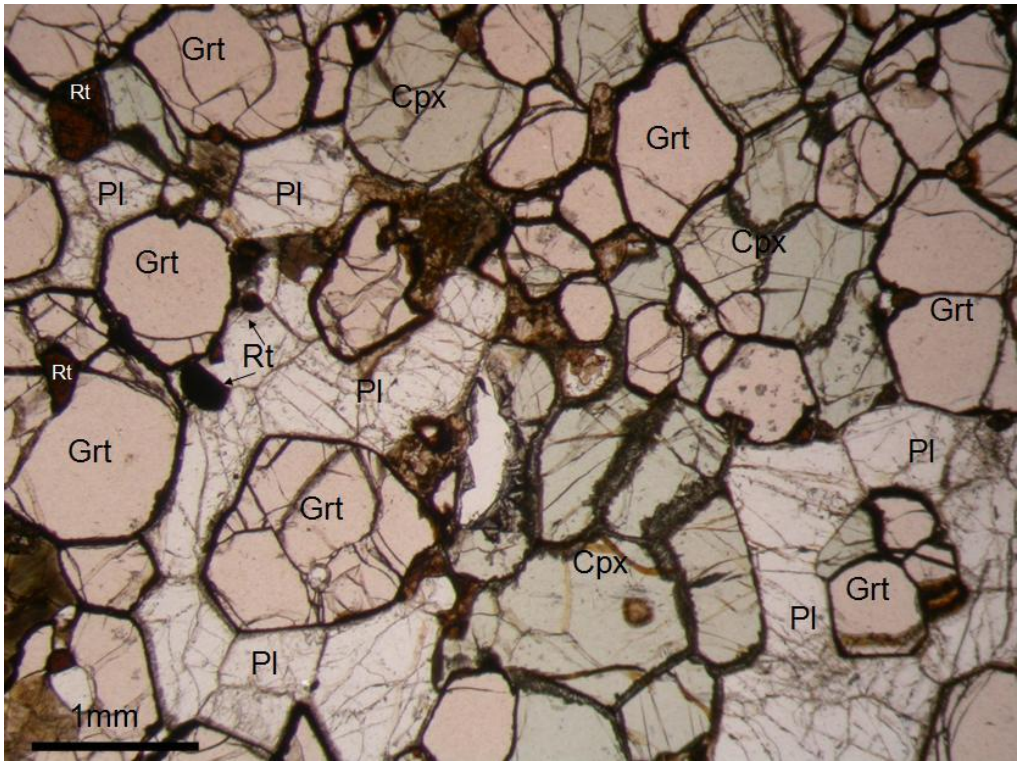

Figure 4

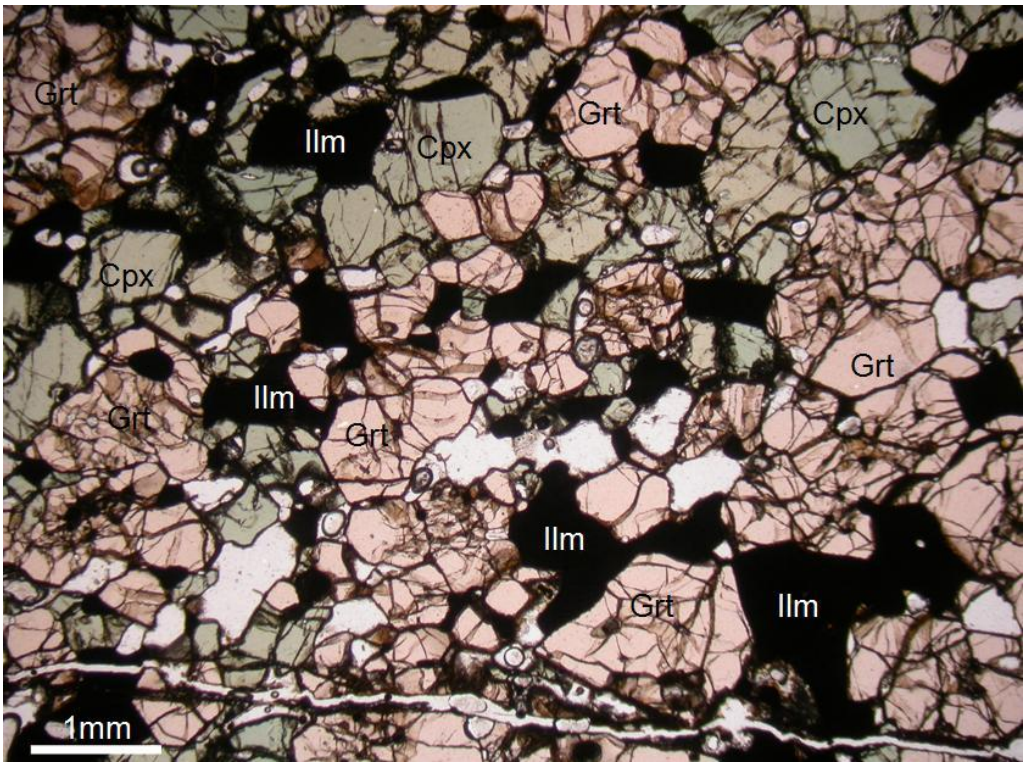

Figure 5

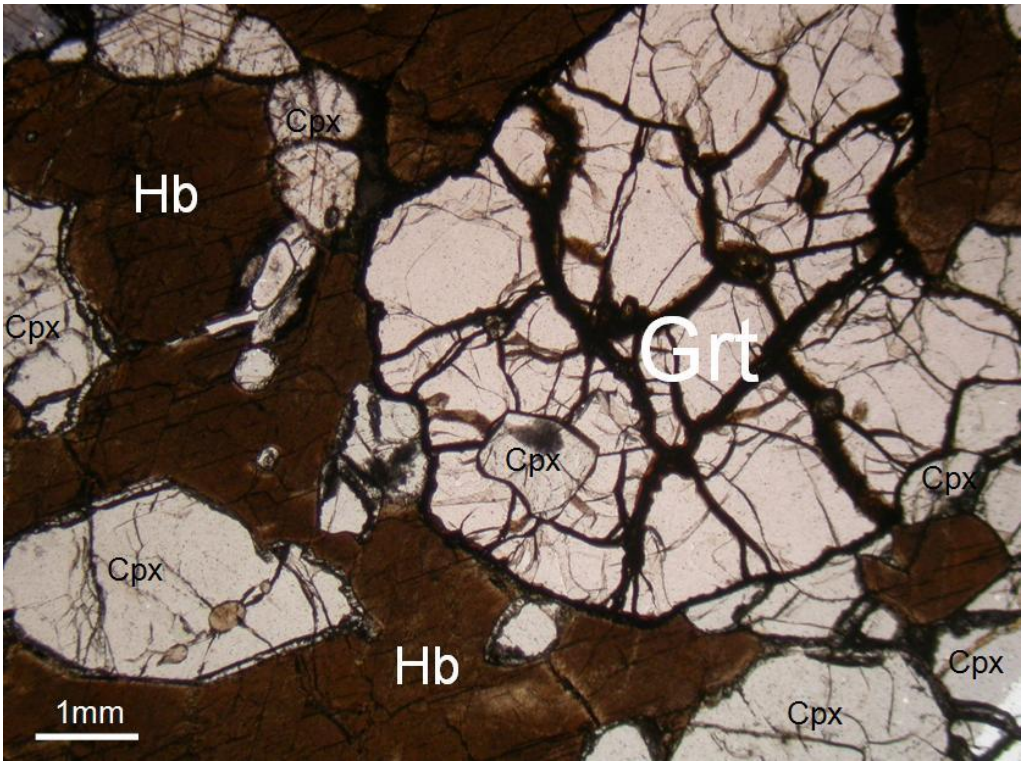

Figure 6

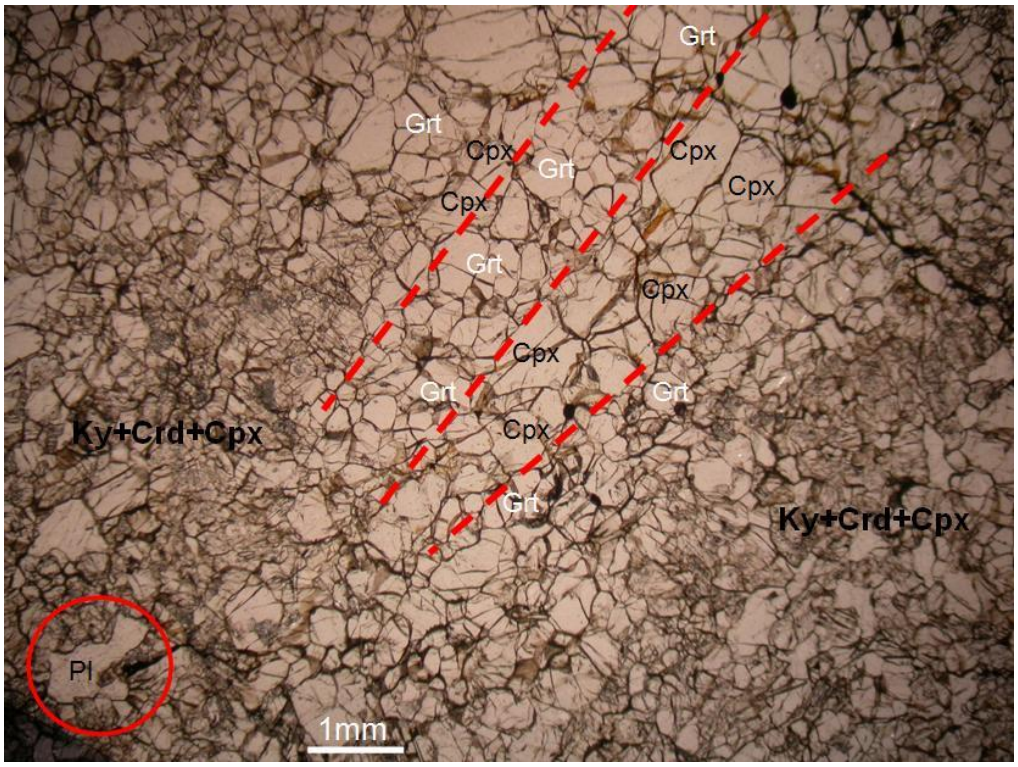

Figure 7

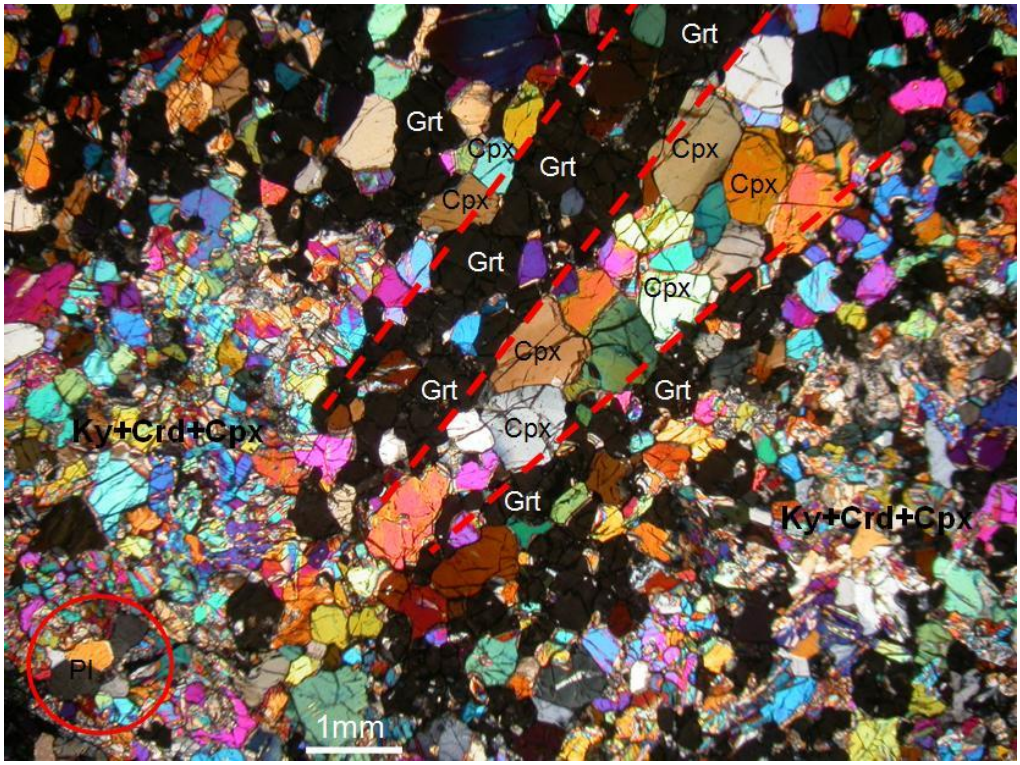

Figure 8

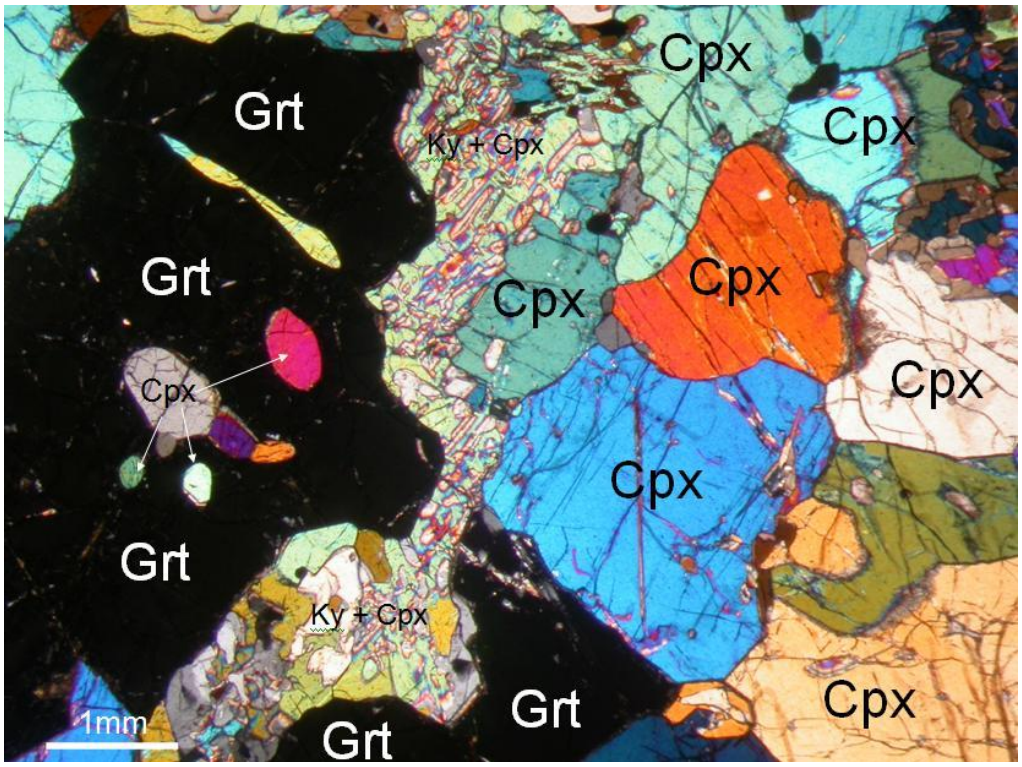

Figure 9

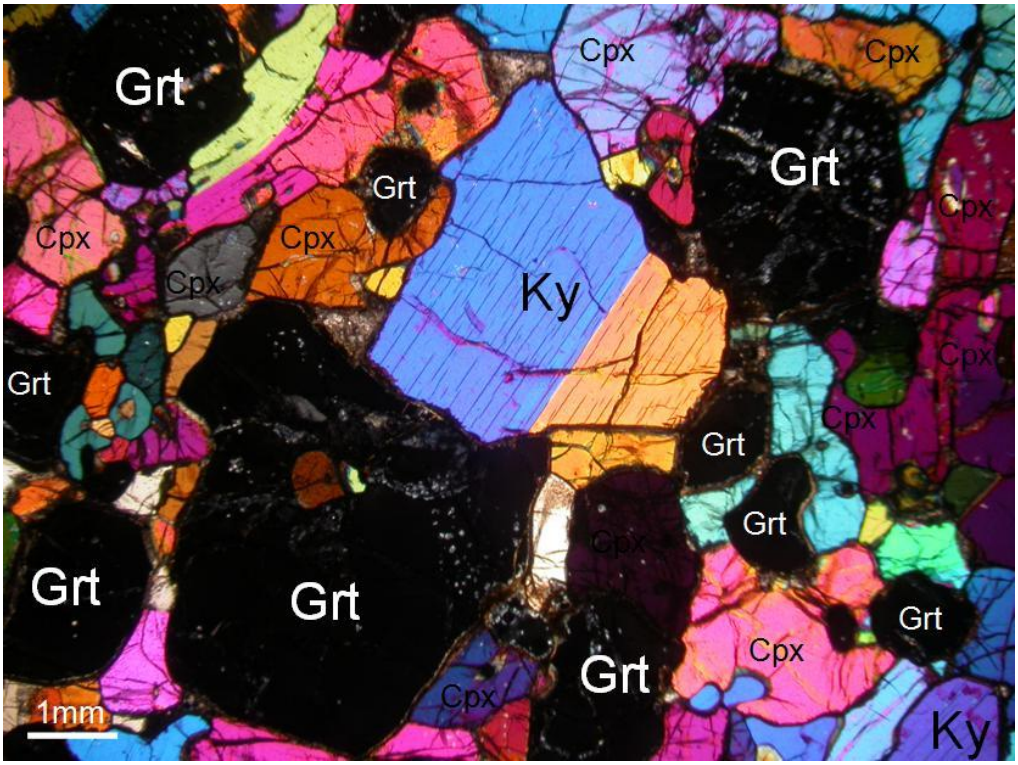

Figure 10

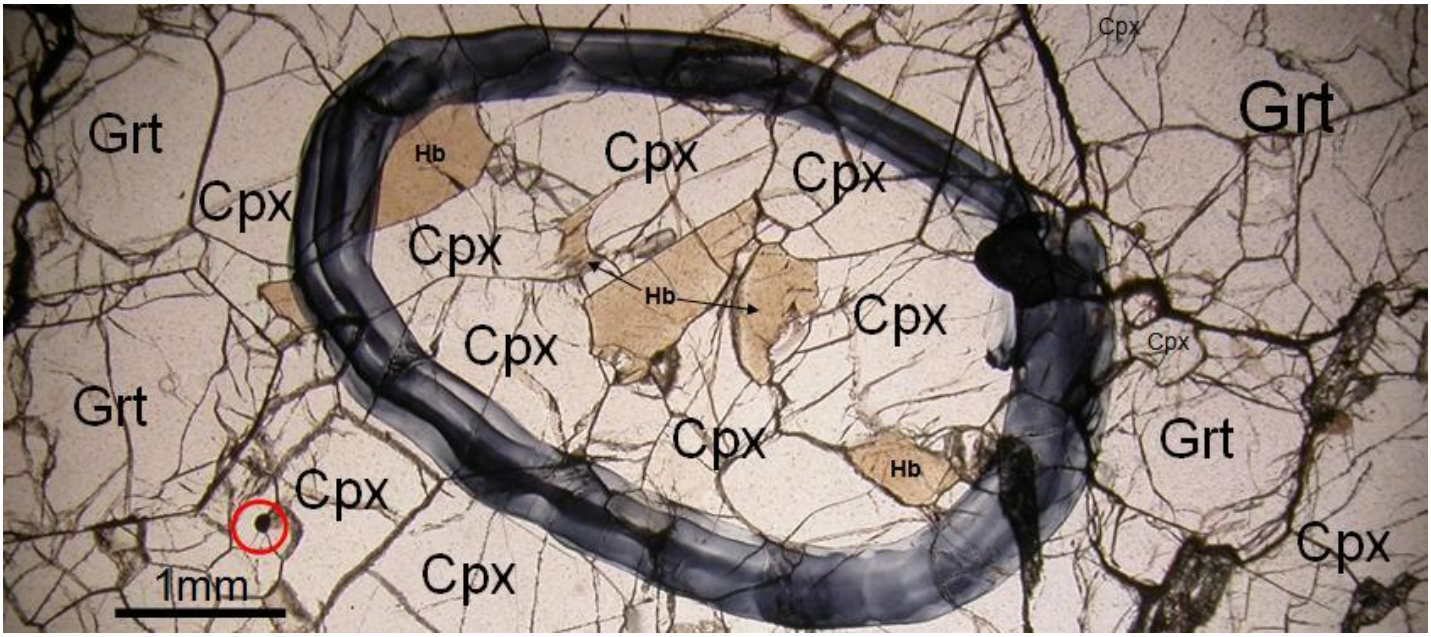

Figure 11

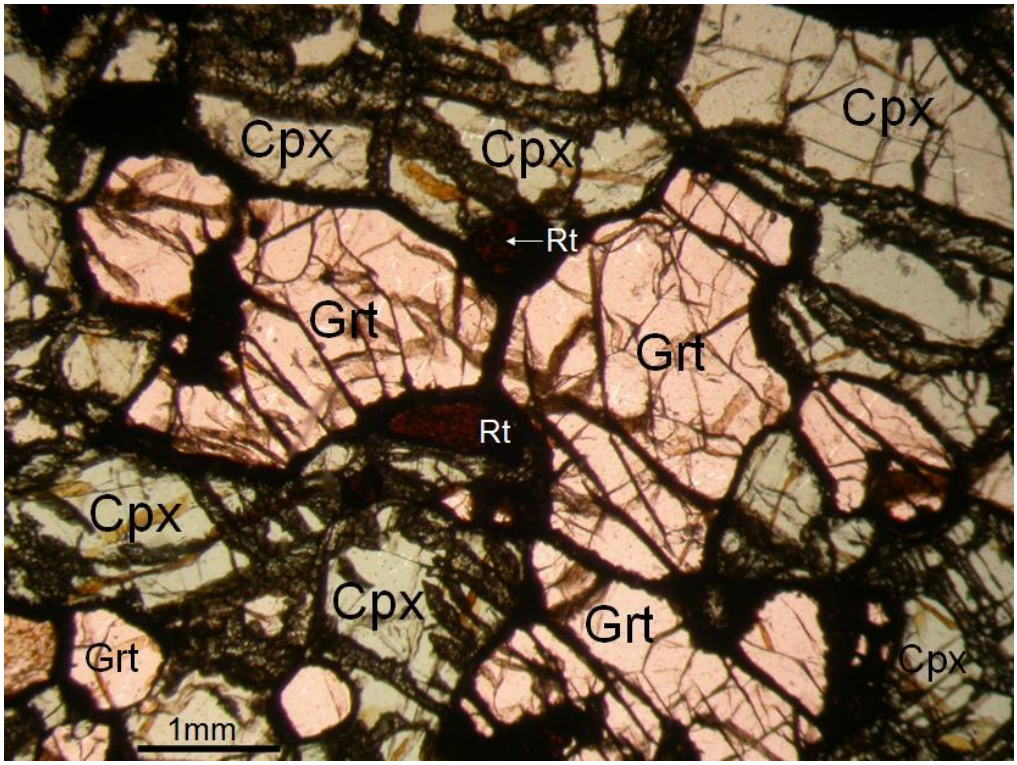

Figure 12

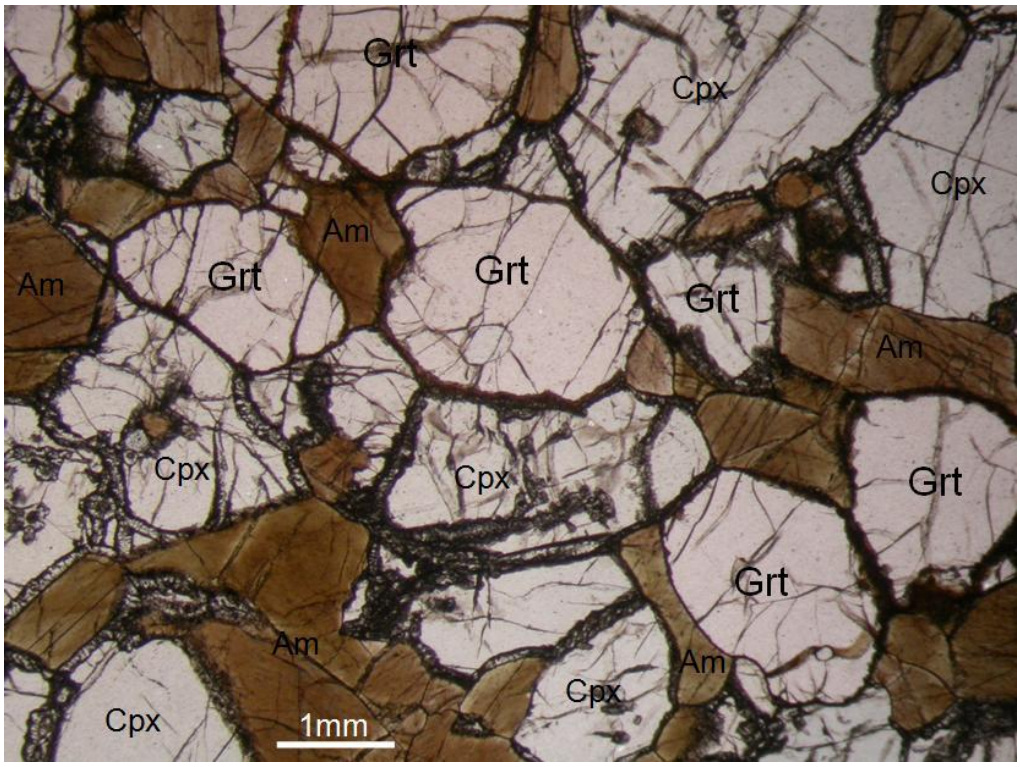

Figure 13

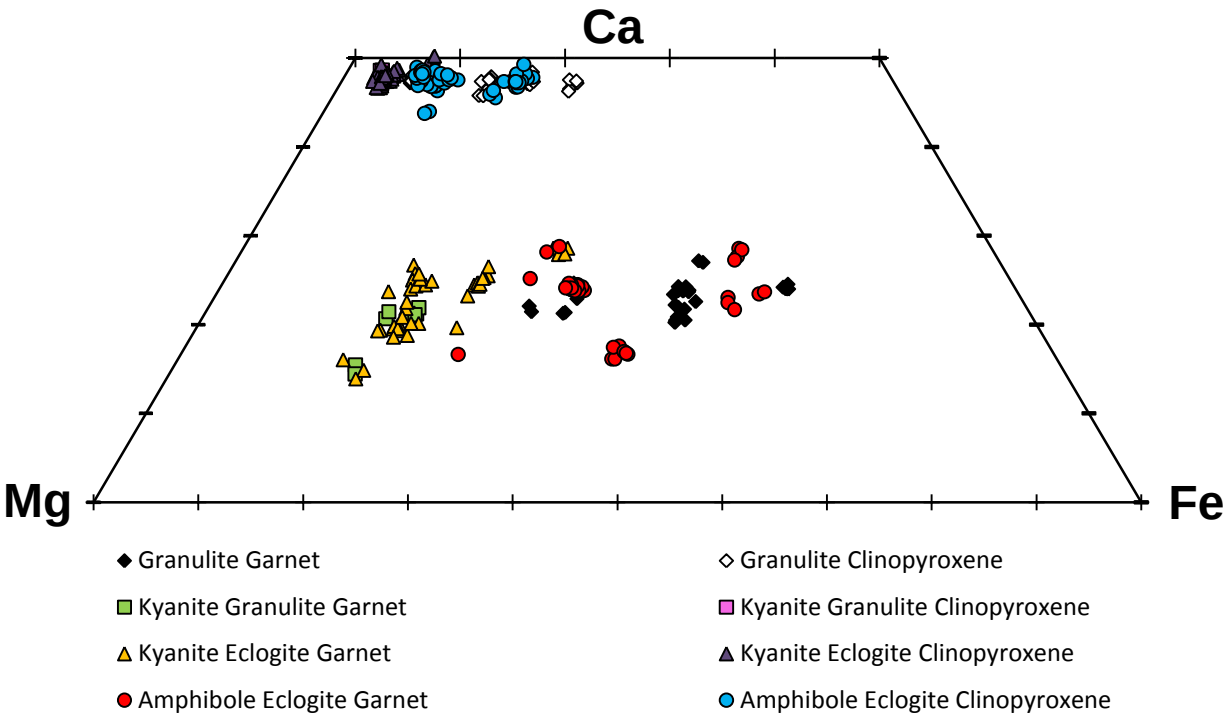

Figure 14

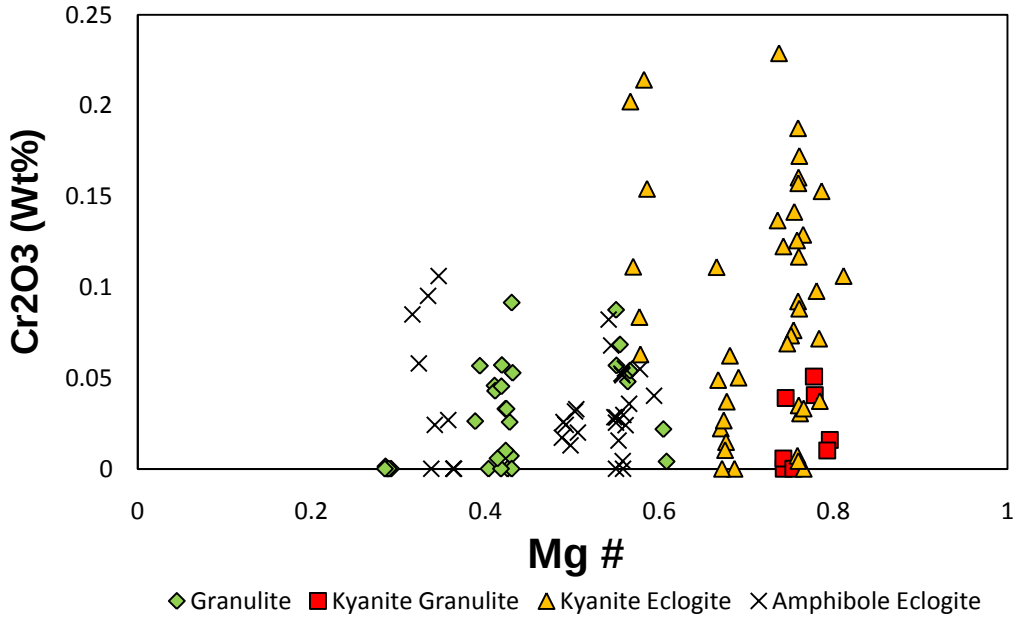

Figure 15

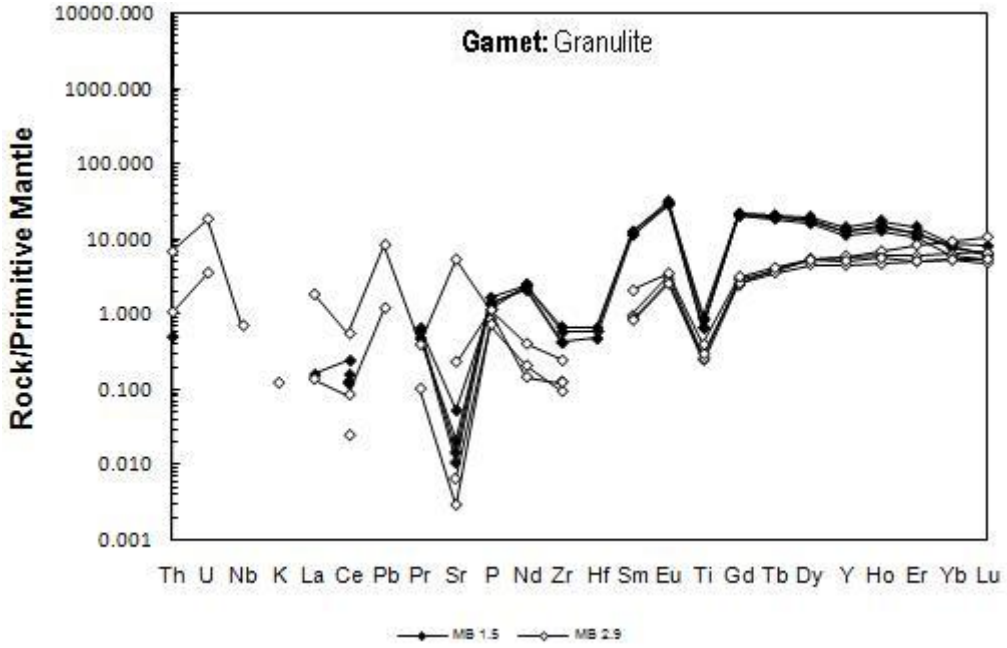

Figure 16

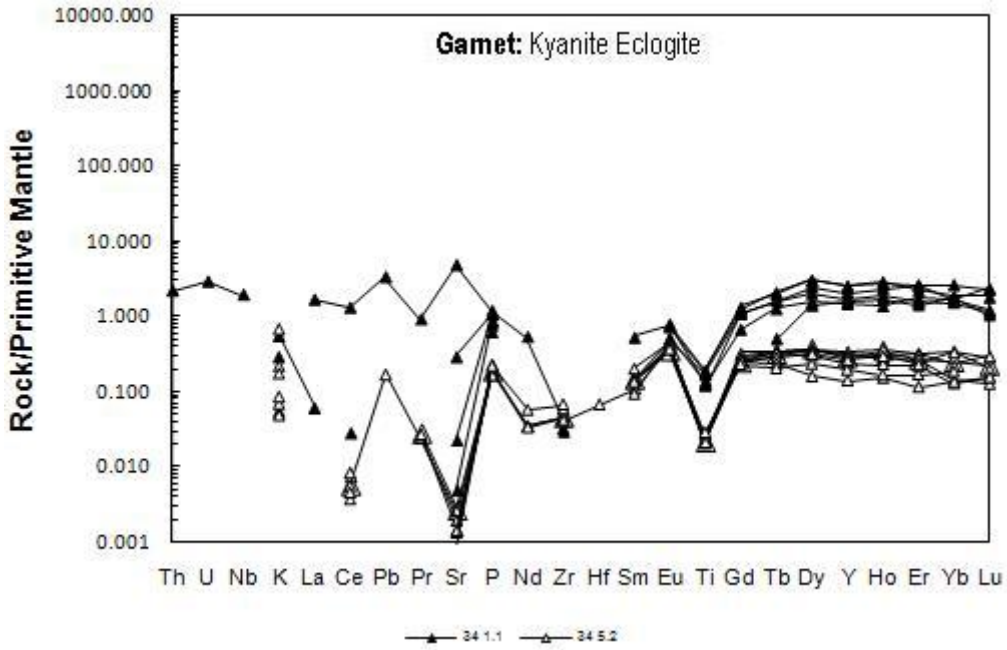

Figure 17

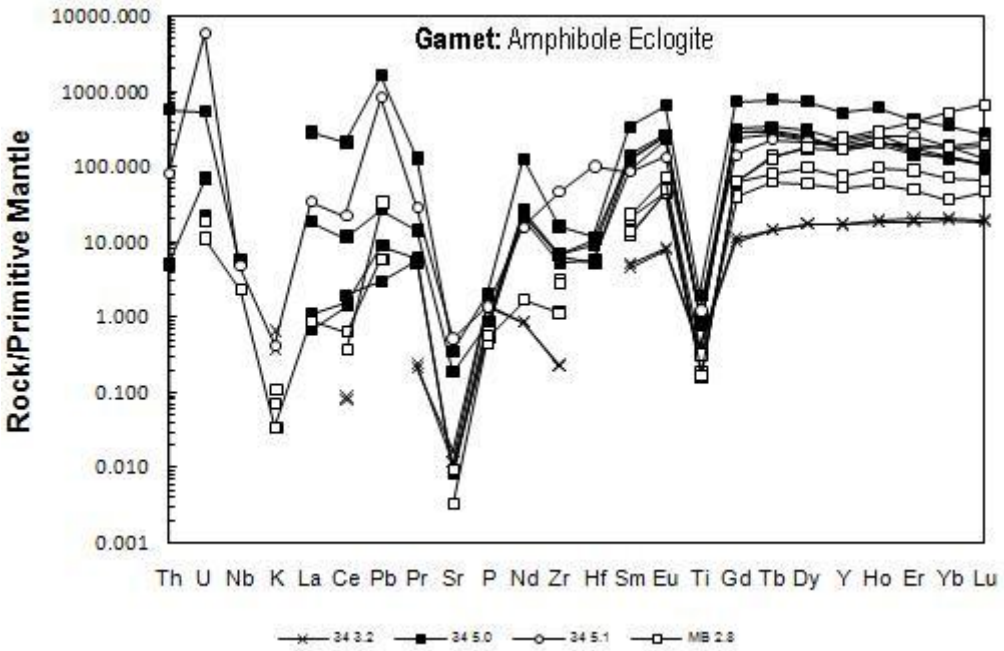

Figure 18

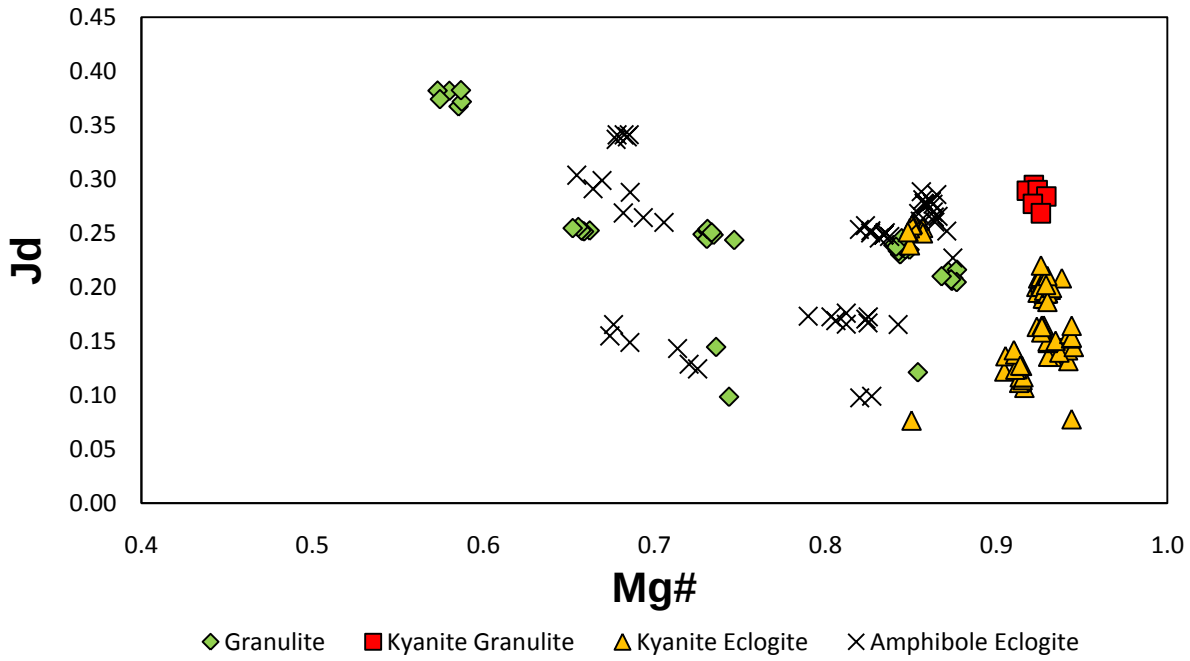

Figure 19

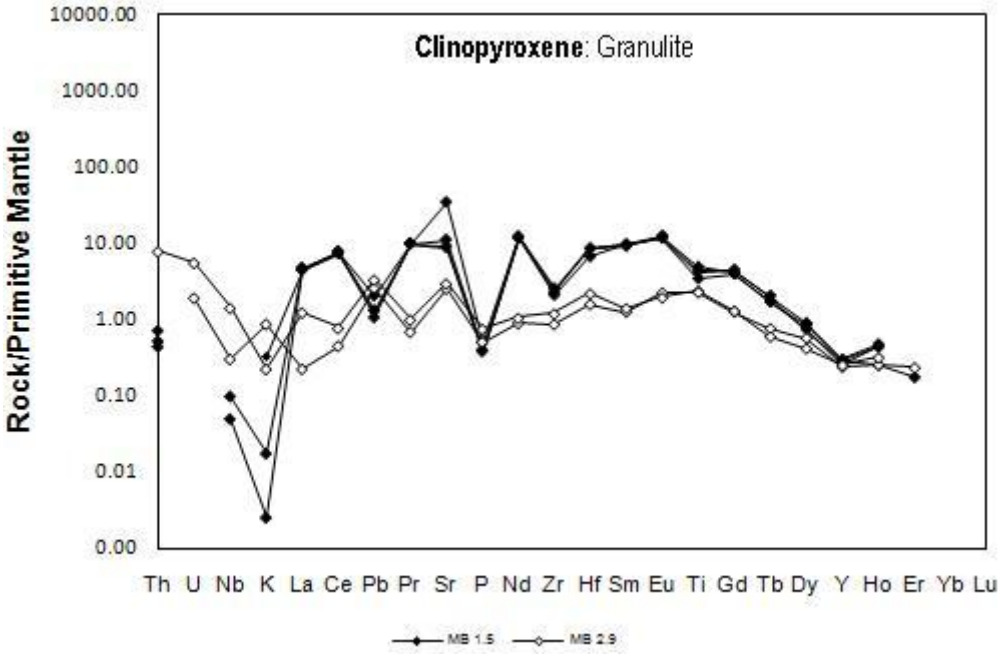

Figure 20

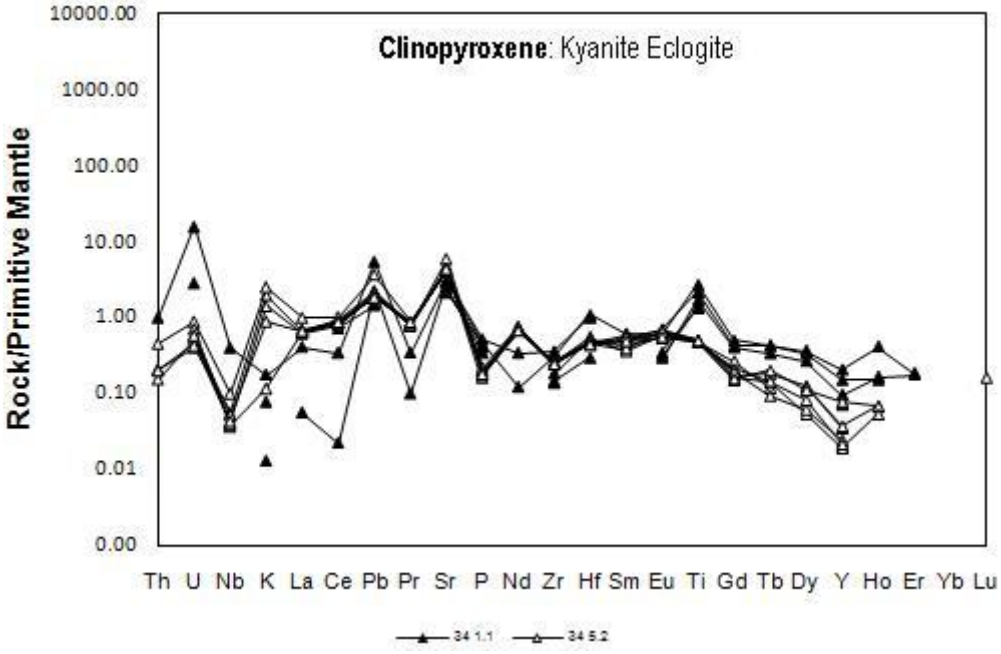

Figure 21

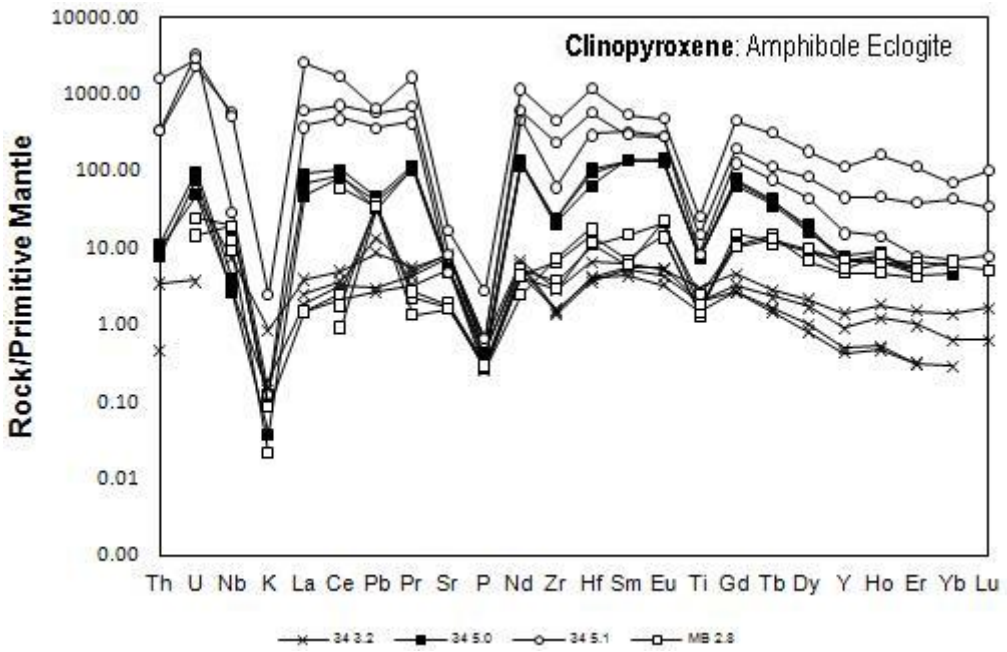

Figure 22

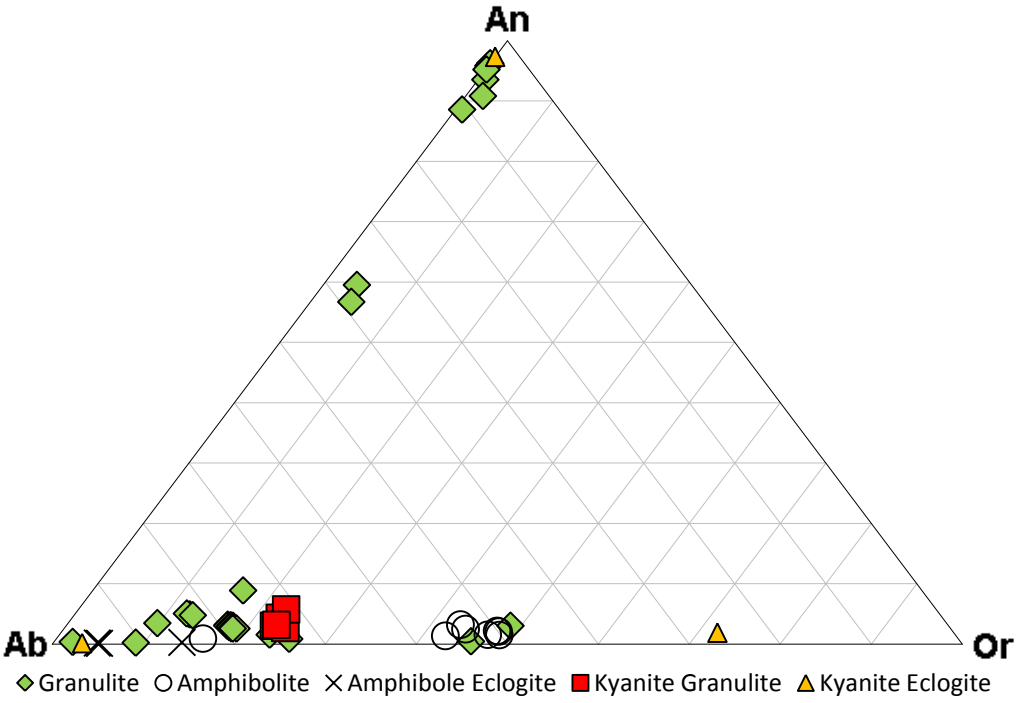

Figure 23

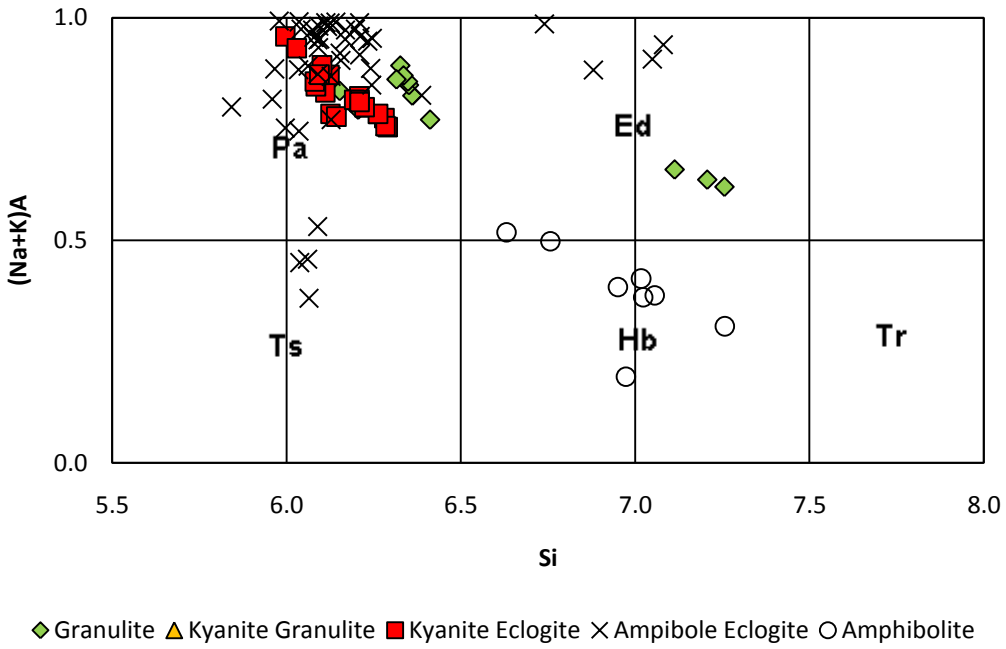

Figure 24

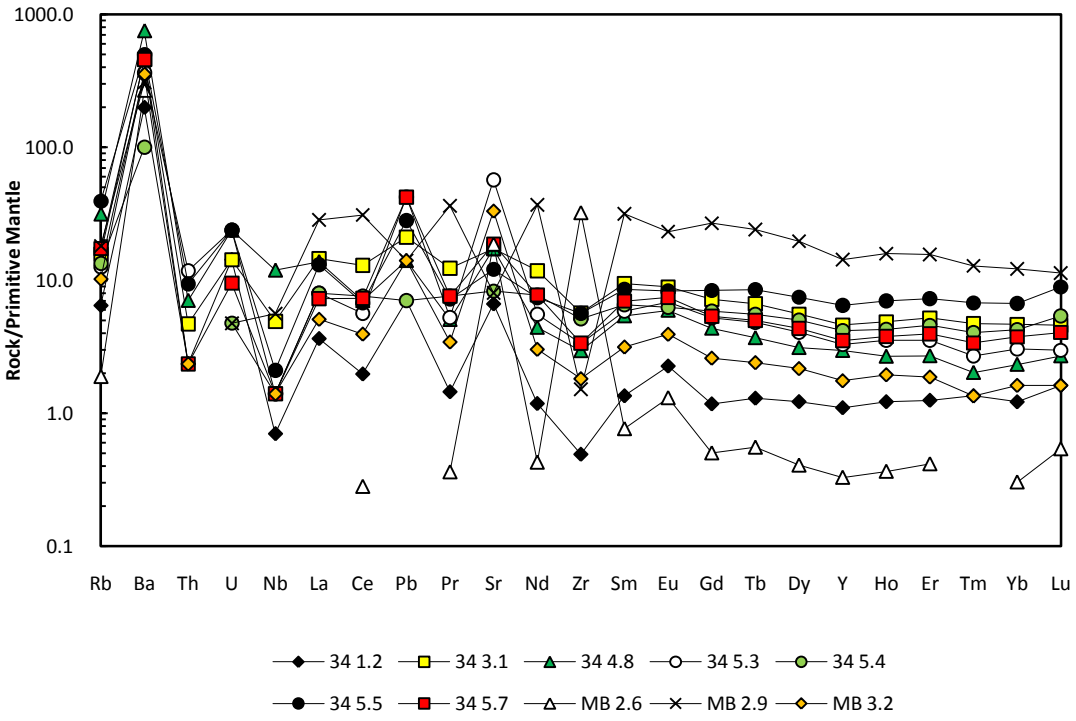

Figure 25

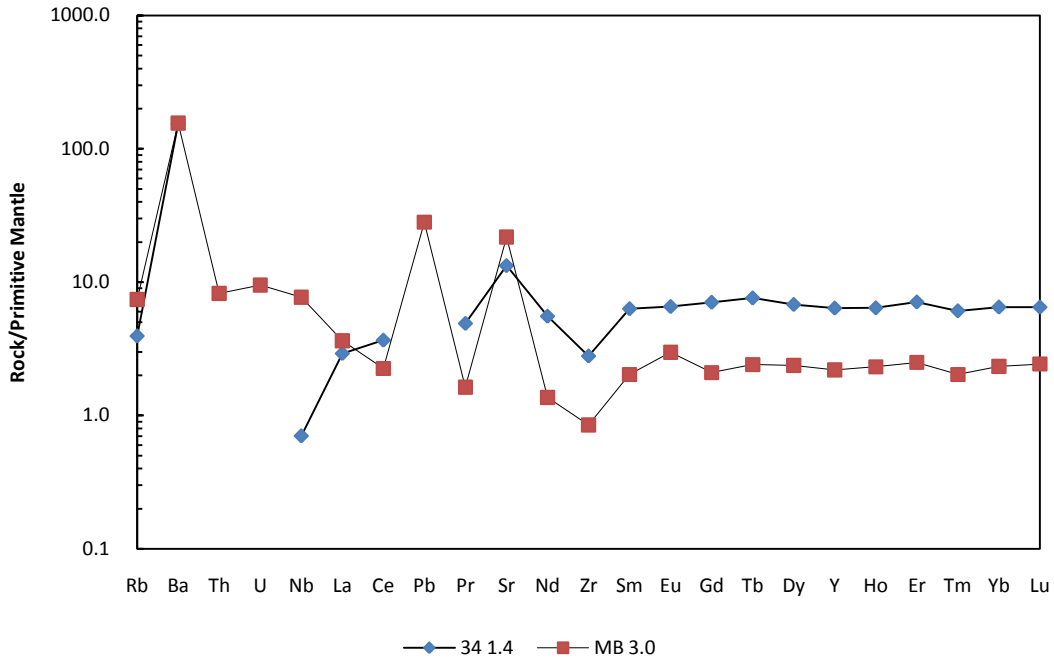

Figure 26

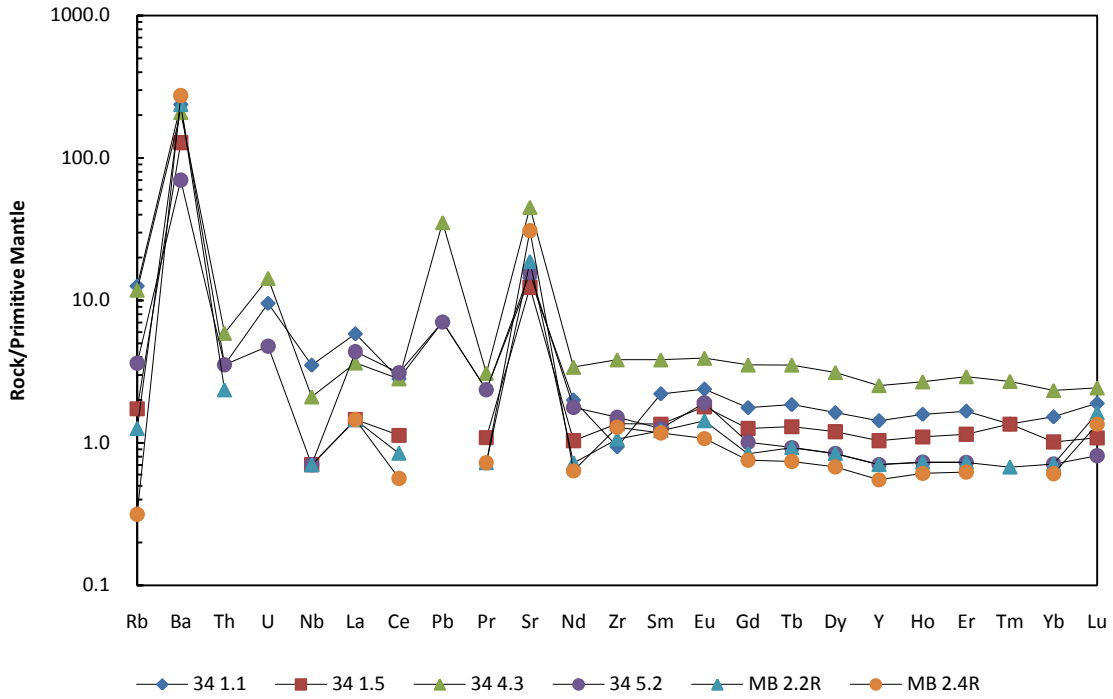

Figure 27

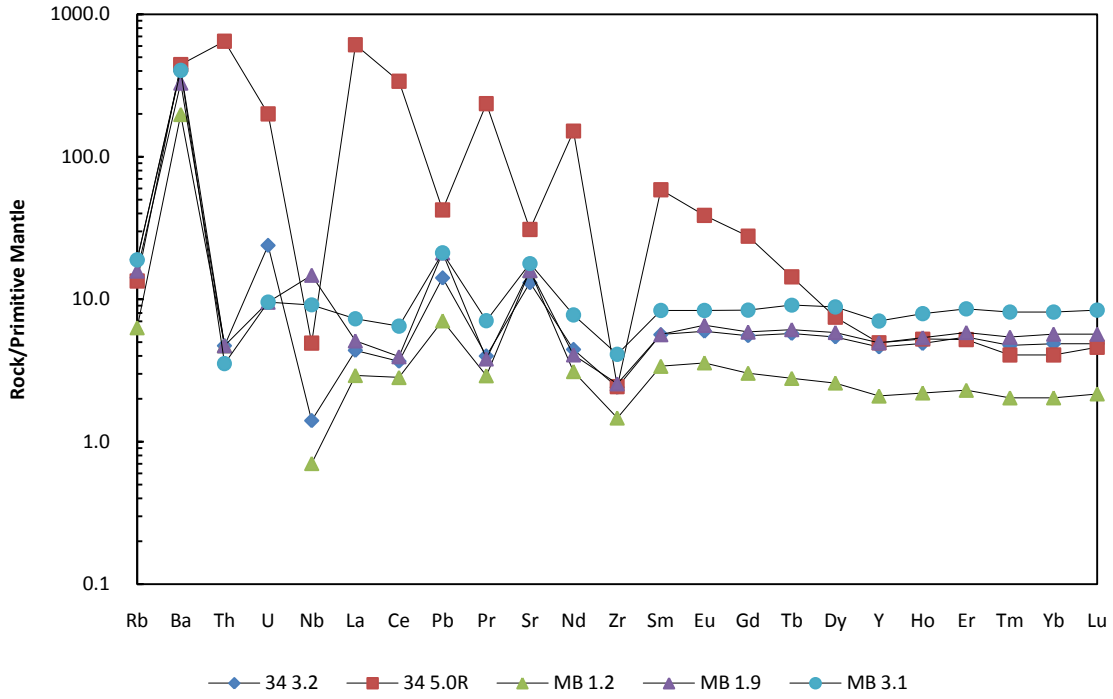

Figure 28

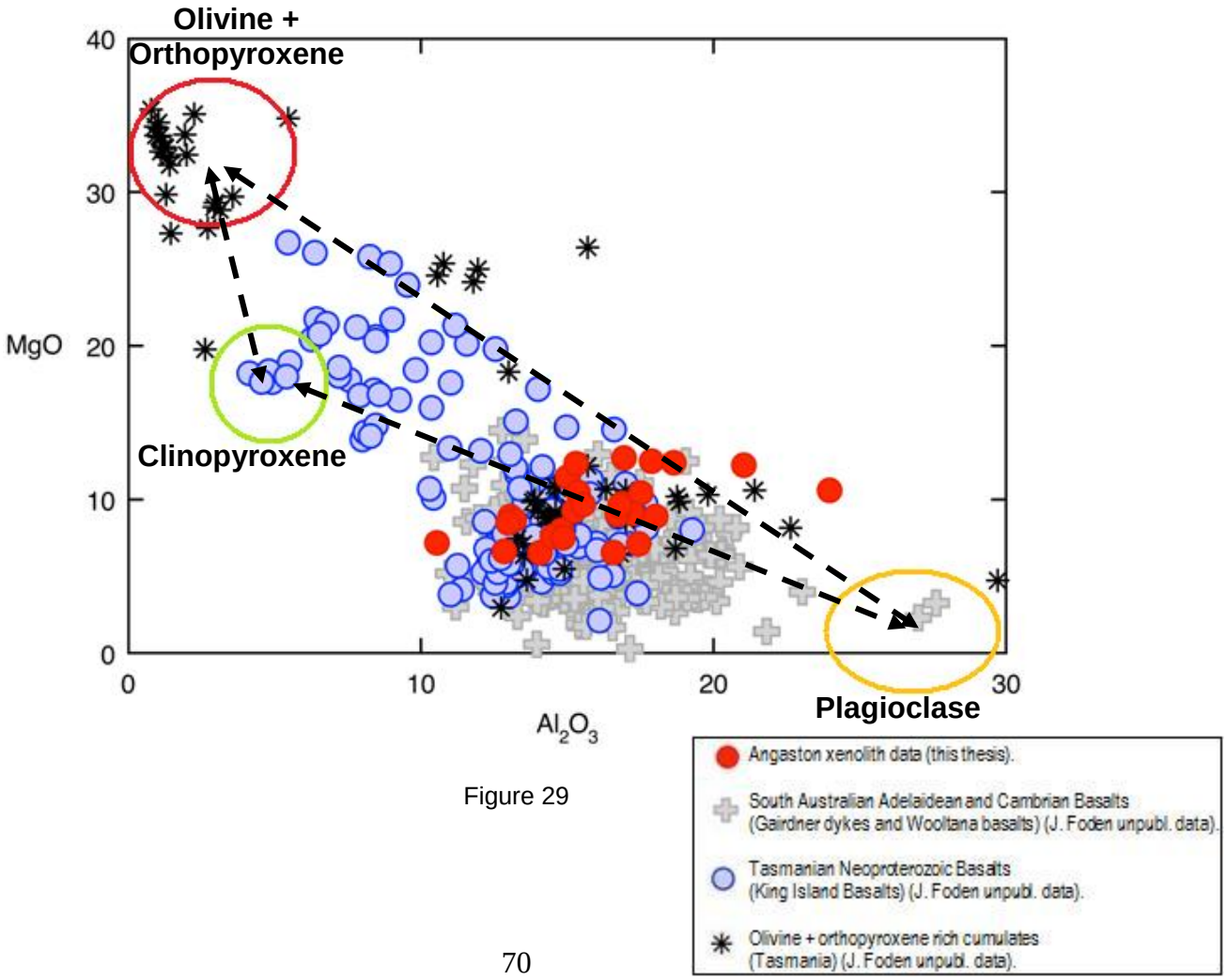

Figure 29

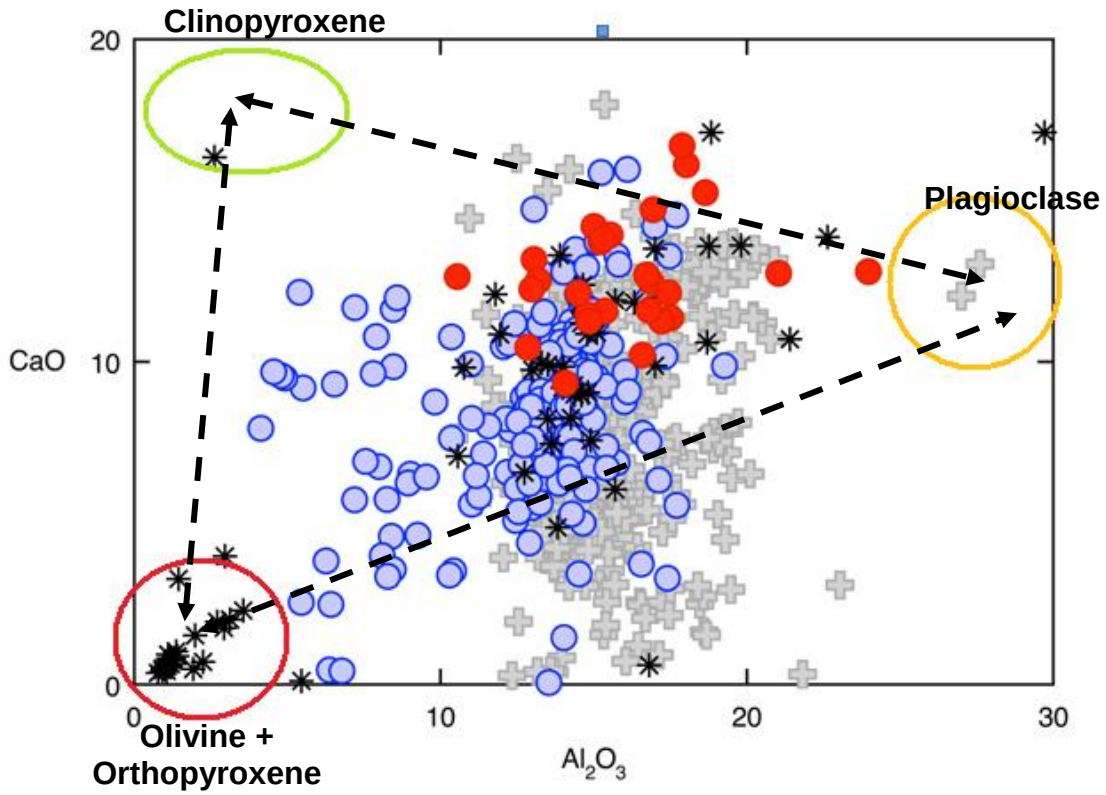

Figure 30

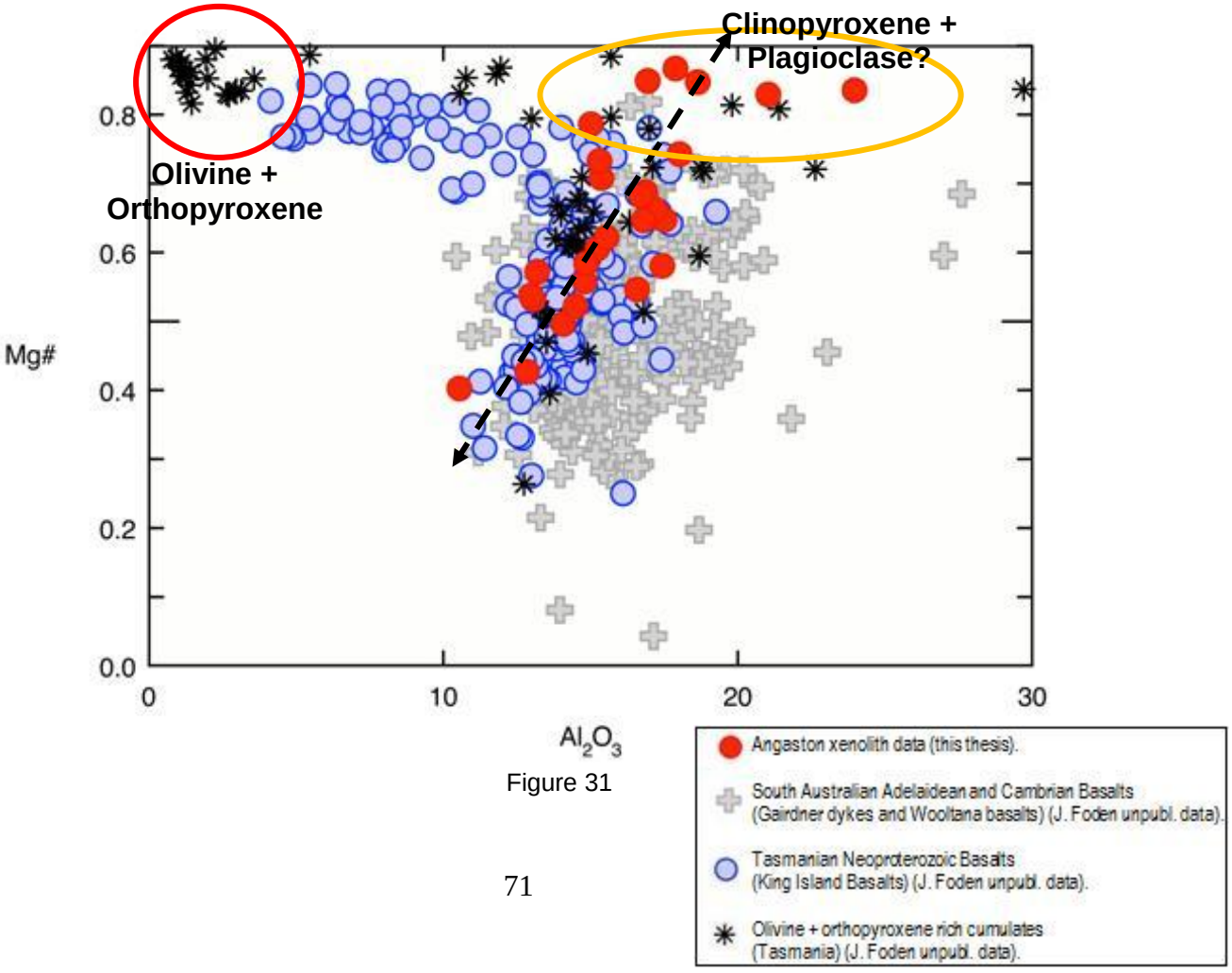

Figure 31

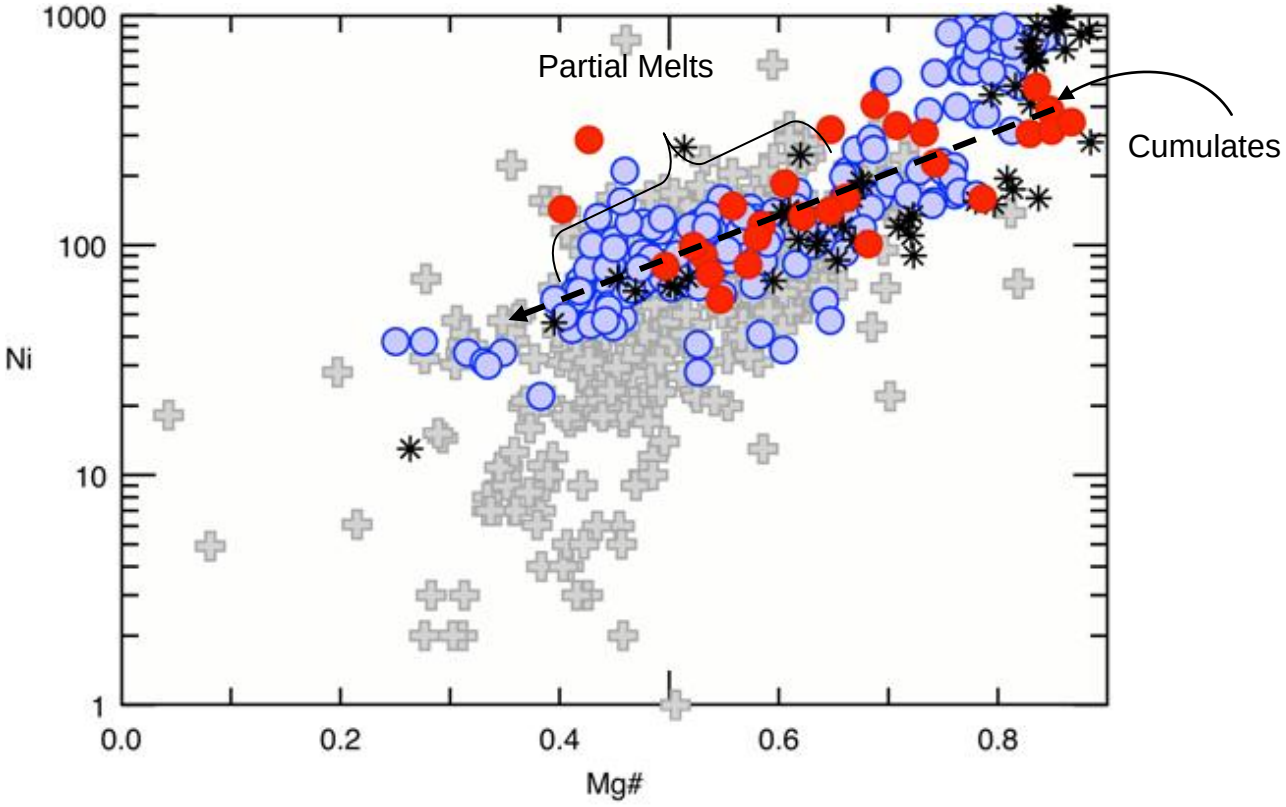

Figure 32

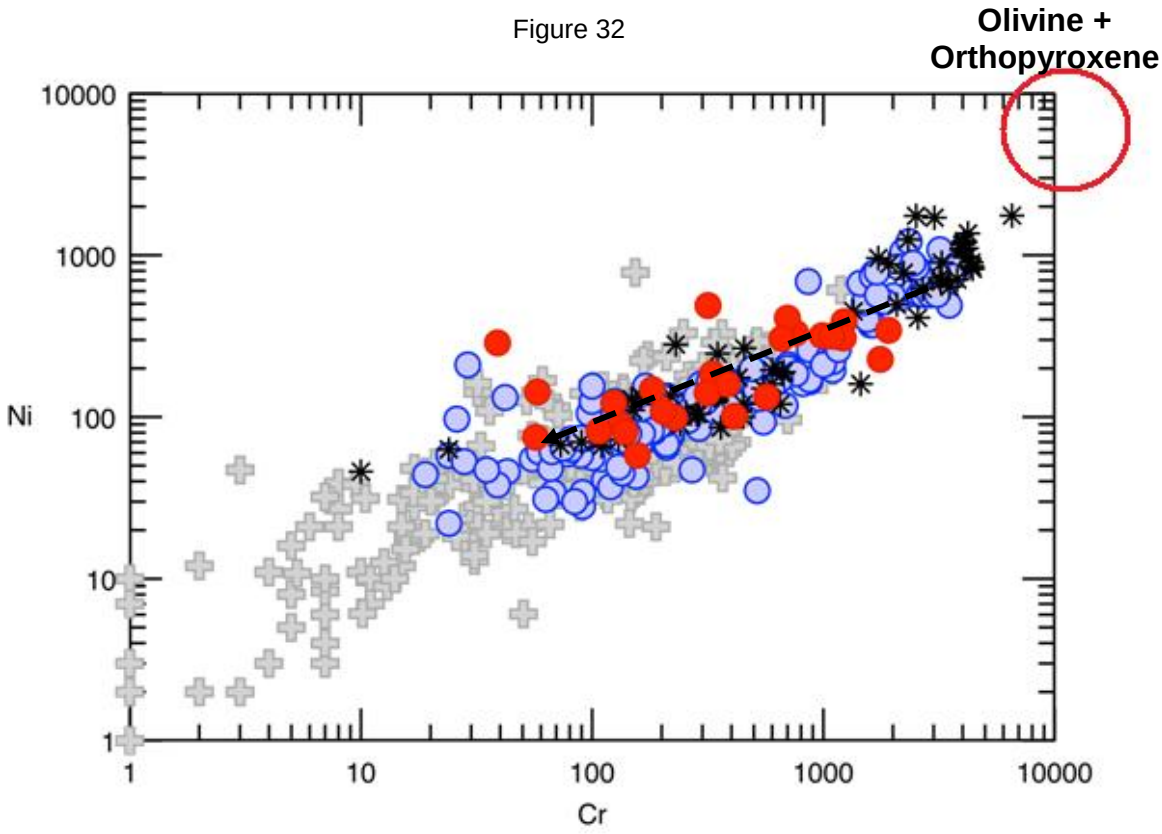

Figure 33

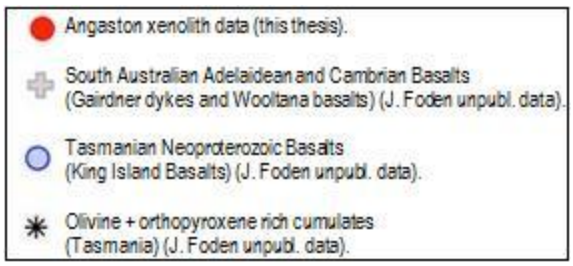

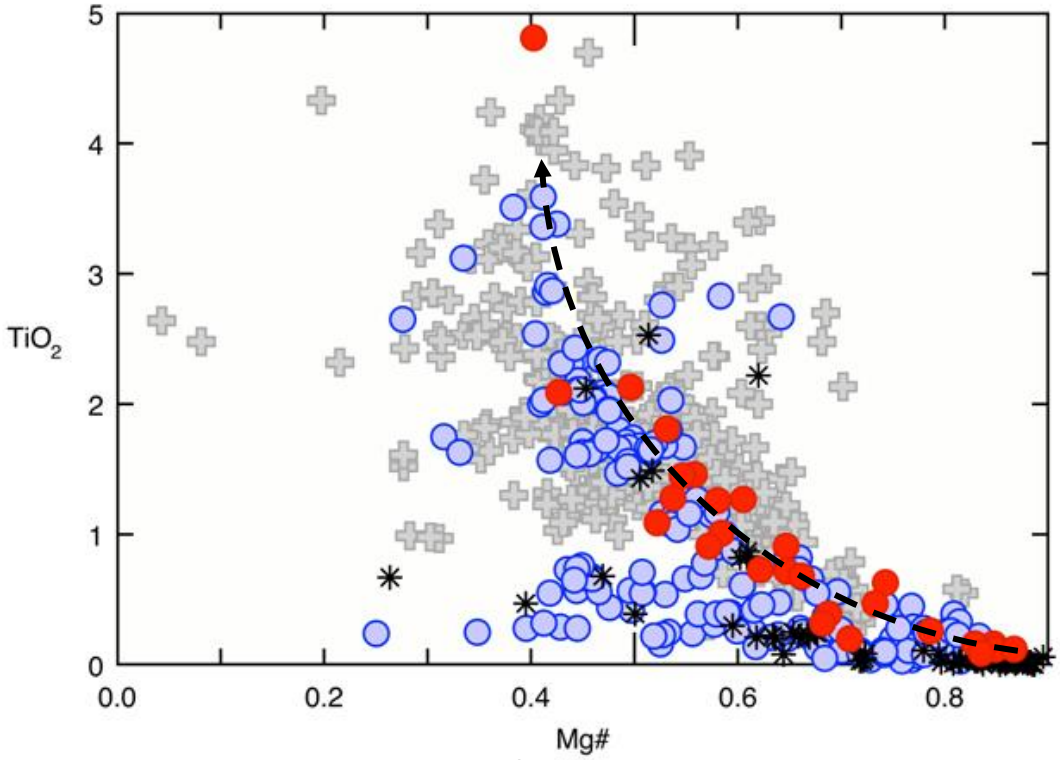
5
4
3
2
1
0
TiO2
0.0
0.2
0.4
0.6
0.8
Mg#

Figure 34

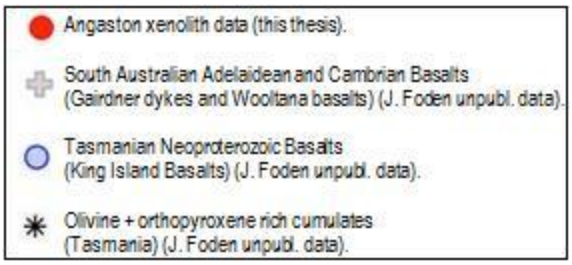
Angaston xenolith data (this thesis).
South Australian Adelaidean and Cambrian Basalts
(Gairdner dykes and Wooltana basalts) (J. Foden unpubl. data).
Tasmanian Neoproterozoic Basalts
(King Island Basalts) (J. Foden unpubl. data).
Olivine + orthopyroxene rich cumulates
(Tasmania) (J. Foden unpubl. data).

Figure 35

D.R. Segui

Angaston Kimberlite Xenolith Suite

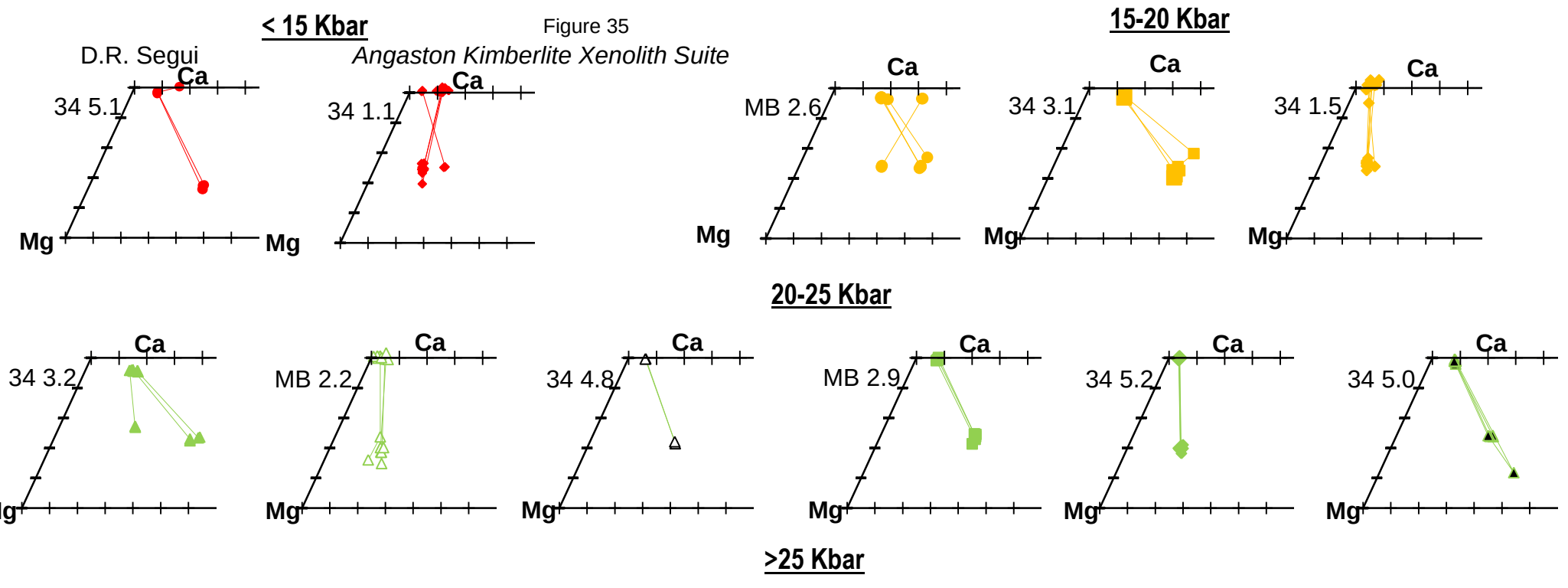

Figure 36

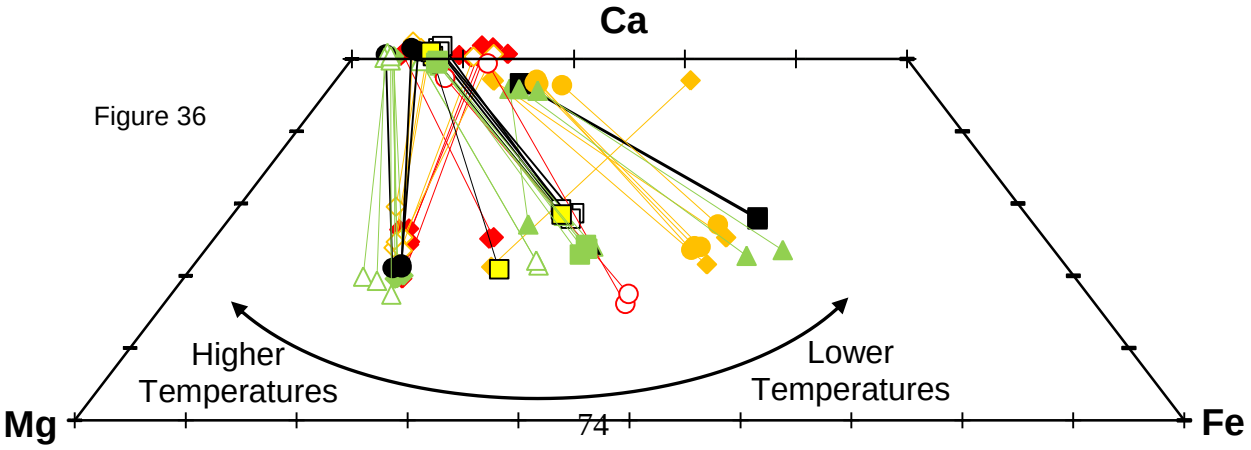

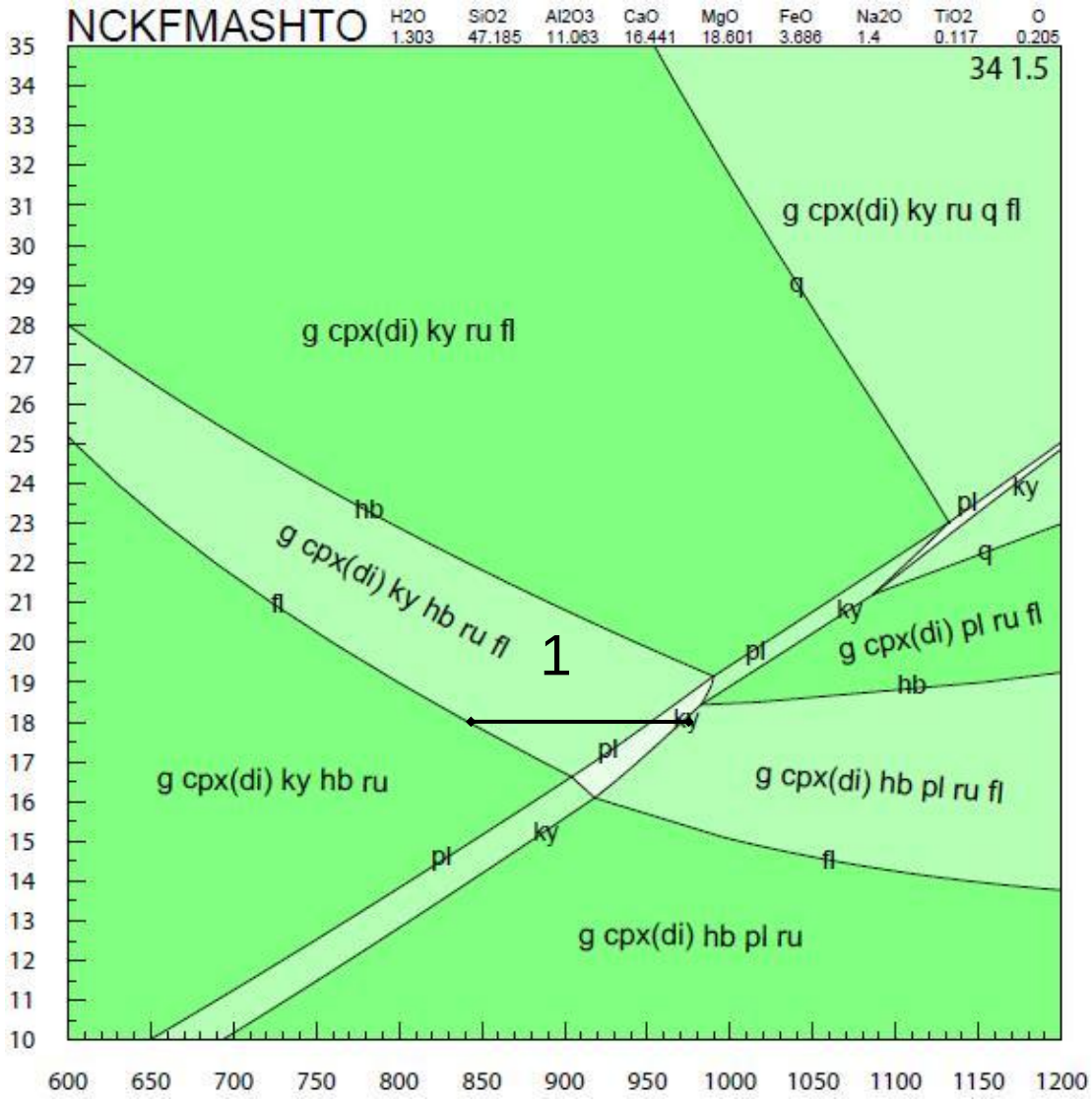
NCKFMASHTO
H2O 1.303
SiO2 47.185
Al2O3 11.063
CaO 16.441
MgO 18.601
FeO 3.686
Na2O 1.4
TiO2 0.117
O 0.205
34 1.5
g cpx(di) ky ru q fl
q
g cpx(di) ky ru fl
hb
g cpx(di) ky hb ru fl
fl
1
pl
ky
q
g cpx(di) pl ru fl
hb
g cpx(di) ky hb ru
g cpx(di) hb pl ru fl
g cpx(di) hb pl ru
35 34 33 32 31 30 29 28 27 26 25 24 23 22 21 20 19 18 17 16 15 14 13 12 11 10
600 650 700 750 800 850 900 950 1000 1050 1100 1150 1200

Figure 37

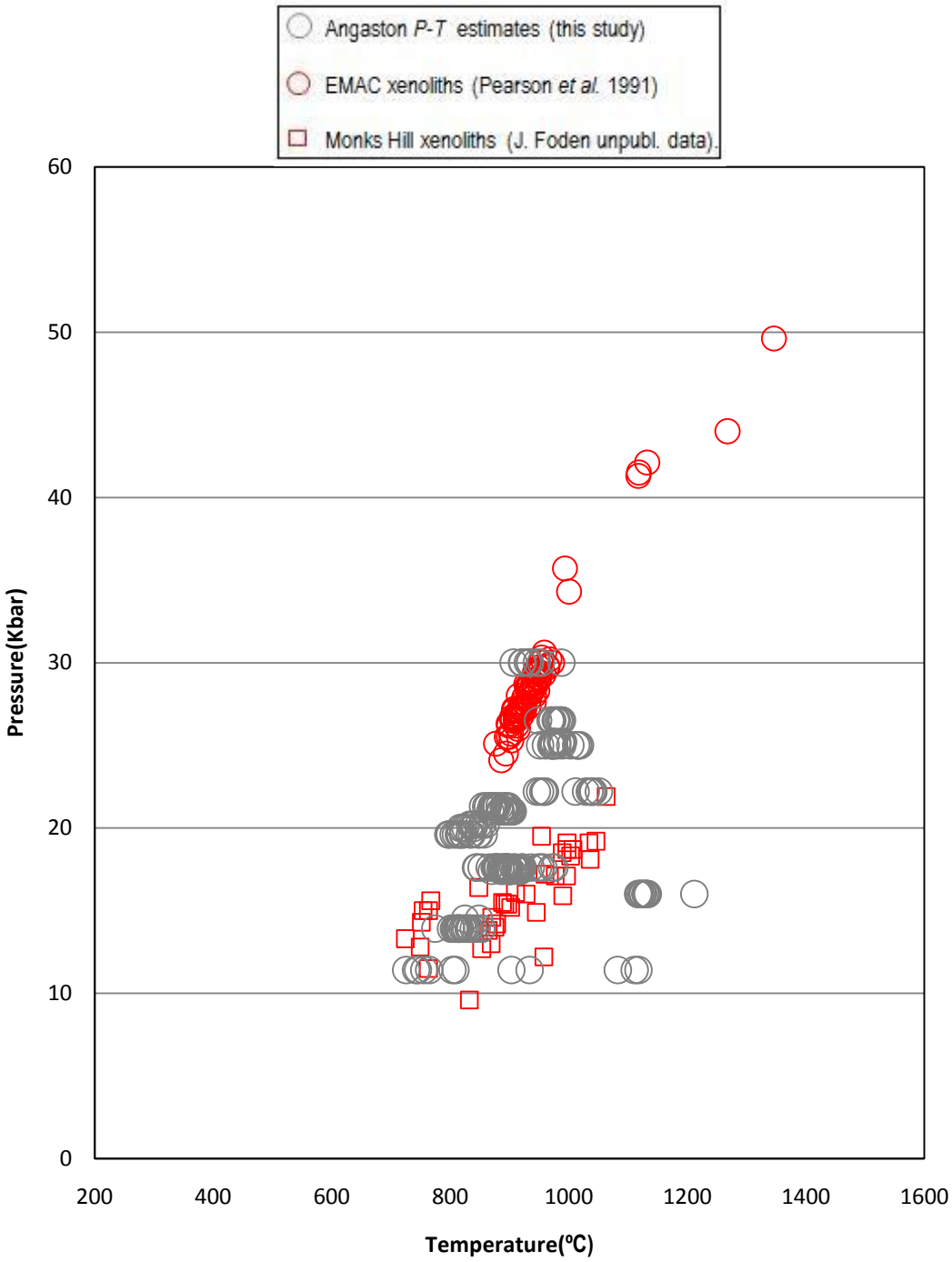
Angaston *P-T* estimates (this study)
EMAC xenoliths (Pearson *et al.* 1991)
Monks Hill xenoliths (J. Foden unpubl. data).
Pressure(Kbar)
60
50
40
30
20
10
0
200
400
600
800
1000
1200
1400
1600
Temperature(°C)

Figure 38

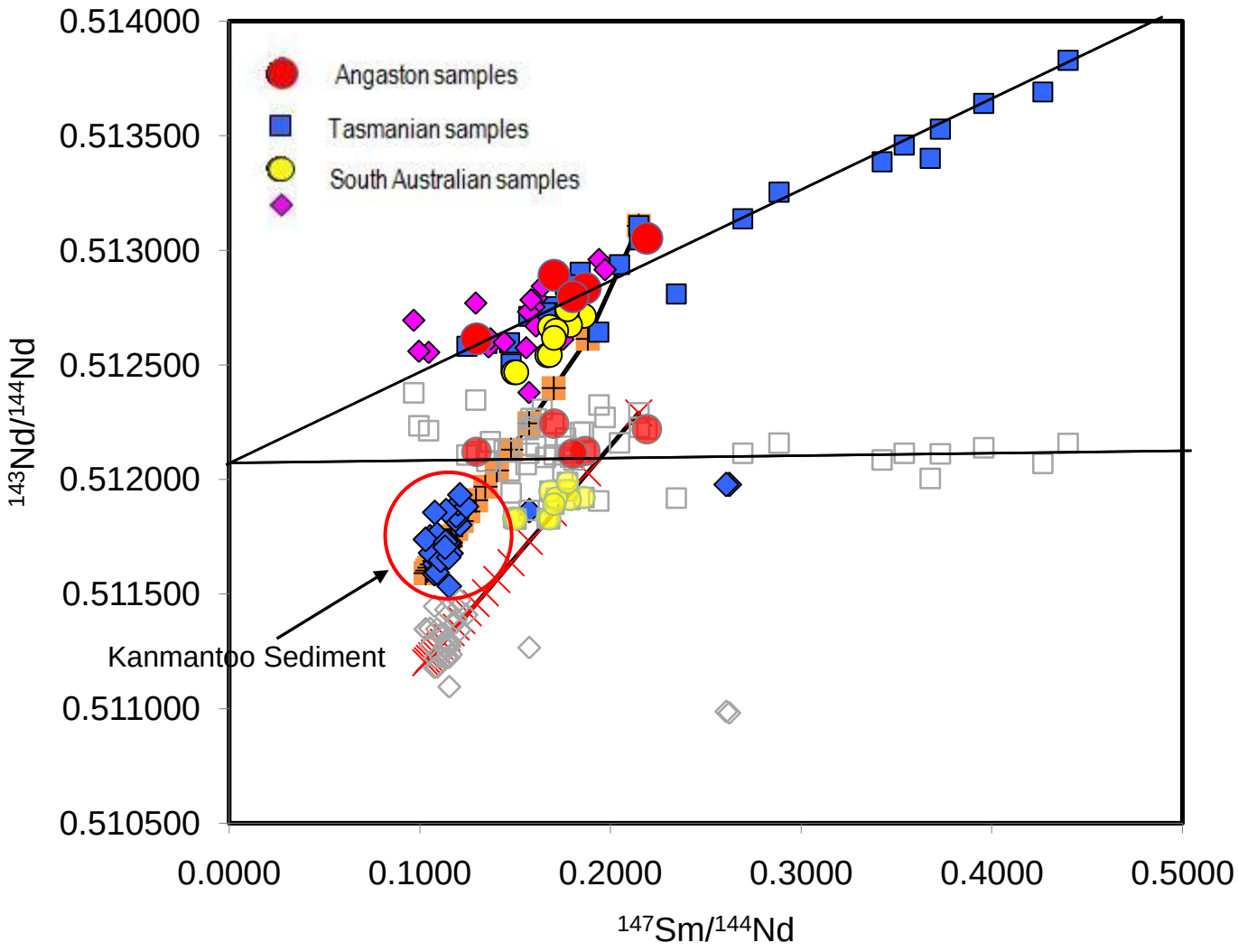
0.514000
0.513500
0.513000
0.512500
0.512000
0.511500
0.511000
0.510500
143Nd/144Nd
0.0000
0.1000
0.2000
0.3000
0.4000
0.5000
147Sm/144Nd
Angaston samples
Tasmanian samples
South Australian samples
Kanmantoo Sediment

Figure 39

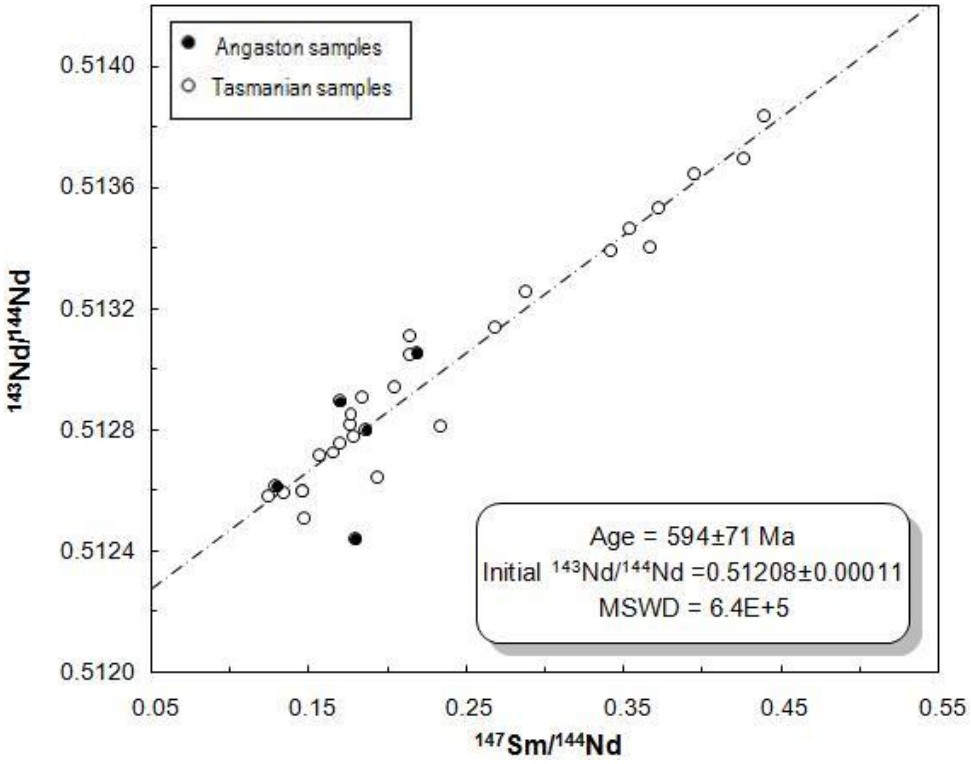

Figure 40

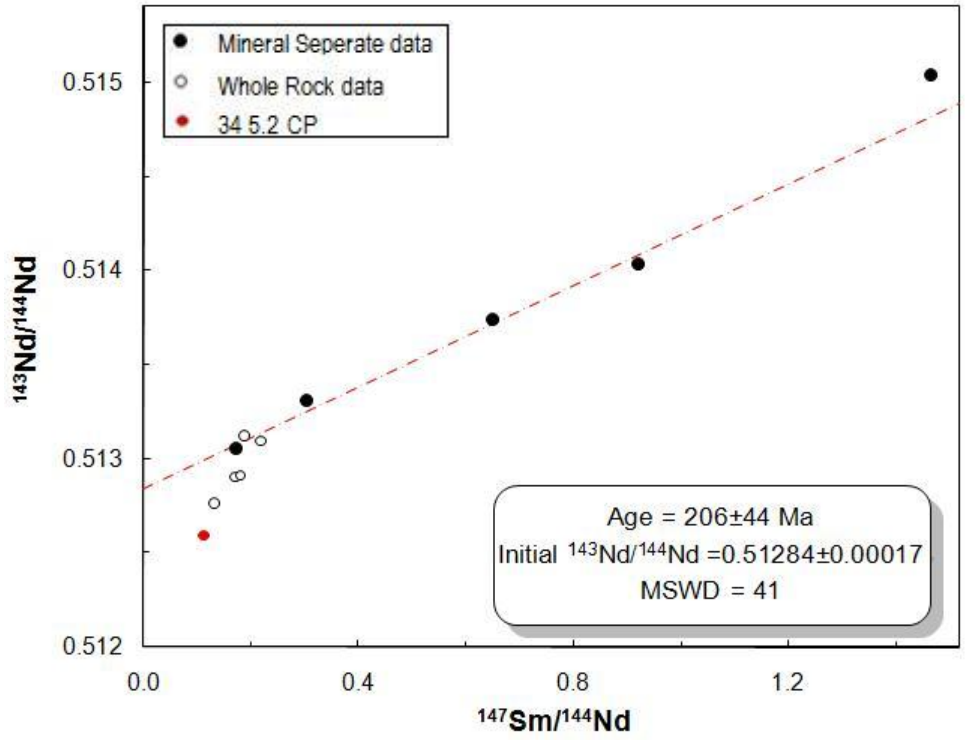

Figure 41

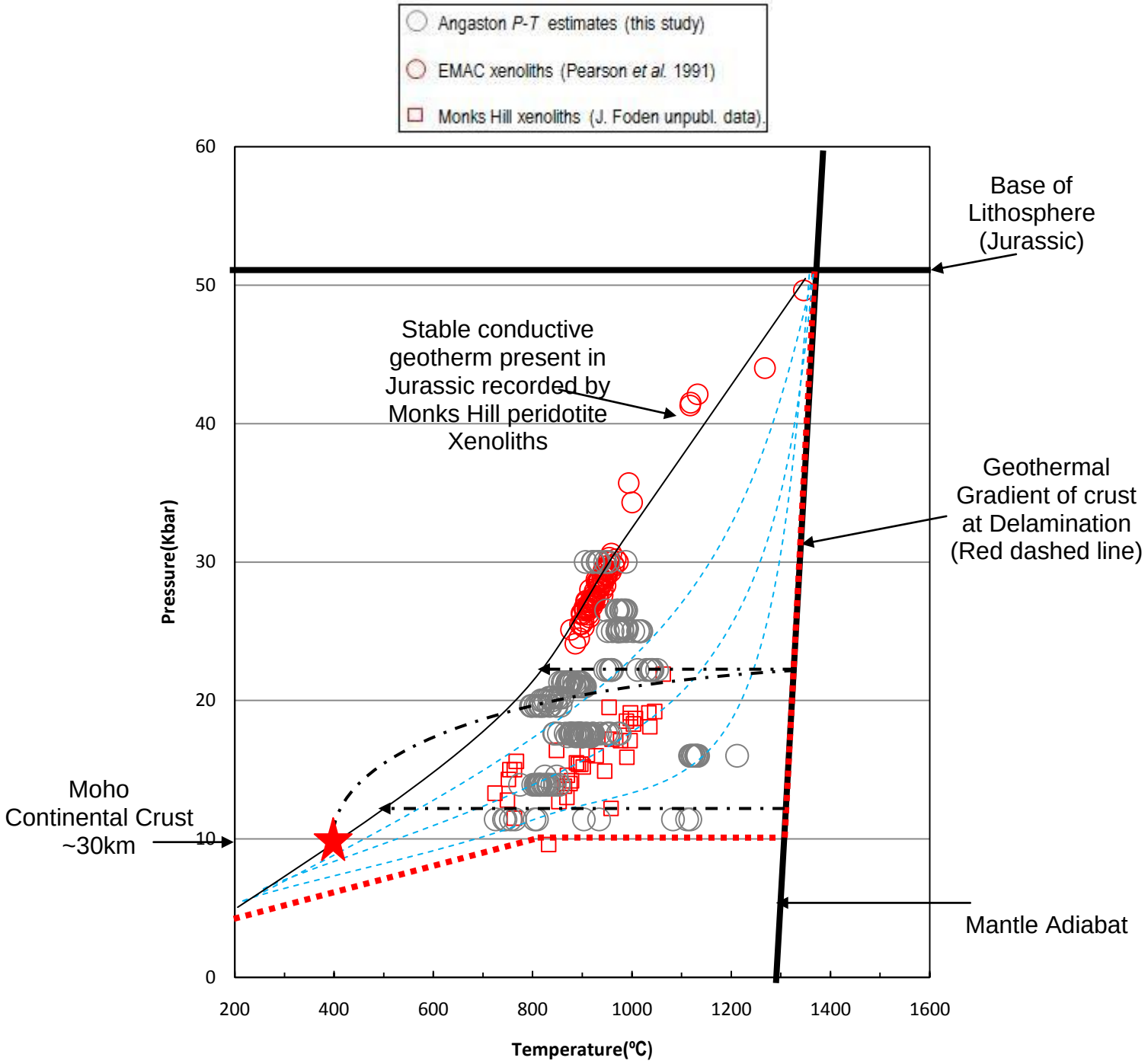
Angaston P-T estimates (this study)
EMAC xenoliths (Pearson et al. 1991)
Monks Hill xenoliths (J. Foden unpubl. data).
Base of Lithosphere (Jurassic)
Stable conductive geotherm present in Jurassic recorded by Monks Hill peridotite Xenoliths
Geothermal Gradient of crust at Delamination (Red dashed line)
Moho Continental Crust ~30km
Mantle Adiabat
Pressure(Kbar)
Temperature(°C)
0
10
20
30
40
50
60
200
400
600
800
1000
1200
1400
1600

Figure 42